

PERFORMANCE AND EMISSIONS ANALYSIS OF A
SYNCHRONOUS CHARGE TRAPPED TWO-STROKE ENGINE

A Thesis

Presented in Partial Fulfillment of the Requirements for the

Degree of Master of Science

with a

Major in Mechanical Engineering

in the

College of Graduate Studies

University of Idaho

by

Austin L. Welch

May 2012

Major Professor: Karen DenBraven, Ph.D.

AUTHORIZATION TO SUBMIT THESIS

This thesis of Austin Welch, submitted for the degree of Master of Science with a major in Mechanical Engineering and titled “PERFORMANCE AND EMISSIONS ANALYSIS OF A SYNCHRONOUS CHARGE TRAPPED TWO-STROKE ENGINE,” has been reviewed in final form. Permission, as indicated by the signatures and dates given below, is now granted to submit final copies to the College of Graduate Studies for approval.

Major Professor _____ Date _____
Karen DenBraven, Ph.D.

Committee Member _____ Date _____
Steven Beyerlein, Ph.D.

Committee Member _____ Date _____
David McIlroy, Ph.D.

Department Administrator _____ Date _____
John Crepeau, Ph.D.

Discipline's College Dean _____ Date _____
Larry Stauffer, Ph.D.

Final Approval and Acceptance by the College of Graduate Studies

_____ Date _____
Jie Chen, Ph.D.

ABSTRACT

This research covers the design, manufacturing, and testing of a Direct Injected Parallel Rotary Synchronous Charge Trapped (PR-SCT) engine. The advantages of this system over a reciprocating style system are explored, as well as the benefits of a direct injection fuel delivery strategy. Two distinct engine mapping processes are implemented. The first method, implementing a wide band oxygen sensor, proves to be quicker to implement for developing a base engine map, deviating 10% or less from optimum fuel injection angles for lowest brake specific fuel consumption (BSFC). An emission based method of holding the carbon monoxide percentage in the exhaust stream constant, leads to overall lower emissions and greater efficiencies at the expense of tuning time due to the slow reaction times of the emissions measurement equipment.

The PR- SCT system showed improvements in torque over all tested engine speeds and throttle positions. For the best BSFC, the charge trapping valve position becomes a function of engine speed and load. Optimum valve positions for the PR-SCT engine were found for the range of engine speeds and load conditions presented. A valve position map has been suggested for use in further research. Emissions from the PR-SCT engine did show reductions in both unburned hydrocarbon (UHC) and oxides of nitrogen (NO_x) production but not in carbon monoxide (CO) emissions.

ACKNOWLEDGEMENTS

I would like to thank the National Institute for Advanced Transportation Technology (NIATT) for funding this research. I would also like to thank my major professor Dr. Karen DenBraven for her help in reviewing this thesis as well as her devotion to the Clean Snowmobile Team and its members. I would like to thank my committee members Dr. Steve Beyerlein and Dr. David McIlroy for reviewing this work. A big thank you to Dr. Dan Cordon without whose help and insight this work would not have been possible. Russ Porter also deserves thanks for his help and guidance during the manufacturing of components for this work. I would also like to thank Dylan Dixon, Drew Hooper, Alex Fuhrman, Neil Miller, Jeremy Nichols, David Erickson and members of the Clean Snowmobile Team 2010-2012 for your help in designing, manufacturing, and testing various components used throughout this work. Finally, I would like to thank my mother and father, Otto and Tammy Welch, and other family and friends who have supported and encouraged me to continue to pursue a higher education.

TABLE OF CONTENTS

AUTHORIZATION TO SUBMIT THESIS.....	ii
ABSTRACT.....	iii
ACKNOWLEDGEMENTS.....	iv
TABLE OF CONTENTS.....	v
LIST OF FIGURES	vii
LIST OF TABLES.....	ix
LIST OF EQUATIONS	x
DEFINITION OF TERMS	xi
1.0 INTRODUCTION	1
1.1 CLEAN SNOWMOBILE CHALLENGE	1
1.2 RESEARCH GOALS.....	3
2.0 TWO-STROKE ENGINE.....	4
2.1 OPERATION	4
2.2 TUNED EXHAUST SYSTEM.....	10
2.3 POWER VALVES	10
2.4 FUEL DELIVERY	11
3.0 SYNCHRONUS CHARGE TRAPPING	14
3.1 PREVIOUS DEVELOPMENT.....	15
4.0 CLEAN SNOWMOBILE CHALLENGE DESIGNS	17
4.1 RECIPROACTING VALVE SCT	17
4.1.1 RESULTS.....	18
4.1.2 MALFUNCTIONS.....	19
4.2 PARALLEL ROTARY SCT.....	20
4.2.1 MANUFACTURING.....	22

4.2.2 MODIFICATIONS.....	24
5.0 TESTING.....	27
5.1 ENGINE CONFIGURATIONS.....	27
5.2 EQUIPMENT.....	28
5.3 DATA COLLECTION.....	29
5.4 TEST PLAN.....	30
5.5 COMPARISONS.....	31
6.0 ENGINE MAPPING.....	31
6.1 TUNING STRATEGY.....	36
7.0 RESULTS OF EMISSIONS TUNING.....	36
8.0 RESULTS OF PR-SCT.....	39
8.1 EMISSIONS OF PR-SCT.....	45
8.2 EMISSIONS ERROR PROPAGATION.....	45
8.3 UHC FORMATION AND RESULTS.....	46
8.4 CO FORMATION AND RESULTS.....	49
8.5 NO _x FORMATION AND RESULTS.....	51
9.0 CONCLUSIONS.....	54
9.1 ENGINE MAPPING CONCLUSIONS.....	54
9.2 PR-SCT CONCLUSIONS.....	55
10.0 FUTURE WORK.....	56
APPENDIX A: PR-SCT DRAWING PACKAGE.....	60
APPENDIX B: PR-SCT MODIFICATIONS.....	83
APPENDIX C: ERROR PROPAGATION BSFC.....	84
APPENDIX D: ERROR PROPAGATION EMISSIONS.....	86

LIST OF FIGURES

Figure 1: Four-Stroke Engine Operation	5
Figure 2: Two-Stroke Engine Configuration and Port Duration and Timing.....	6
Figure 3: Intake Stroke.....	7
Figure 4: Power Stroke	8
Figure 5: End of Power Stroke and Beginning of Blowdown	8
Figure 6: Beginning of Scavenging Process	9
Figure 7: Fresh Charge Displaced Into Cylinder After Scavenging Process.....	9
Figure 8: Power Valves on a Rotax 600cc E-TEC	11
Figure 9: Semi-Direct Injection System	12
Figure 10: Stratified vs. Homogenous Charge Combustion	13
Figure 11: Pressure vs. Volume for SCT and Stock Engine.....	15
Figure 12: Lotus Omnivore [®] Engine Cutaway	16
Figure 13: Previous Synchronous Charge Trapping Engine Design.	17
Figure 14: Reciprocating Valve Motion	18
Figure 15: Percent Throttle vs. BSFC at 3500 RPM	19
Figure 16: Shaft Torque vs. Engine Speed for 45° of Reciprocating Motion	20
Figure 17: Pulley System PR-SCT Valve.....	21
Figure 18: Valve Adjustment.....	22
Figure 19: Machined Cylinders and Inserts for PR-SCT system.....	22
Figure 20: Milling of the Cylinder to Accept PR-SCT System.....	23
Figure 21: Valves and Counter Balances.....	24
Figure 22: Exploded View Pulley System	25
Figure 23: Idler Pulley with Offset Bearing	26
Figure 24: Idler Pulley with Double Bearings	26
Figure 25: Exploded View Modified Pulley System	27
Figure 26: Detection of Knock with Pressure Transducer.....	29
Figure 27: Charge Trapping Valve Location 0° Degree.....	31
Figure 28: Exhaust Emissions as a Function of Equivalence Ratio.....	33
Figure 29: BSFC vs. Injection Angle.....	34
Figure 30: BSFC vs. Lambda.....	35

Figure 31: Torque and BSFC vs. Injection Angle Constant Lambda	37
Figure 32: Torque and BSFC vs. Injection Angle Constant Percent CO	38
Figure 33: Emissions vs. Injection Angle	39
Figure 34: Torque vs. Engine Speed at 200 TC and Varying Valve Positions.....	40
Figure 35: Brake Specific Fuel Consumption vs. Engine Speed	41
Figure 36: Torque vs. Engine Load Varying Valve Positions	43
Figure 37: BSFC vs. Engine Load at 4500 RPM.....	44
Figure 38: UHC Formation Due to Crevice Volume Filling and Flame Quenching.....	47
Figure 39: Brake Specific Hydrocarbon Emissions vs. Engine Speed	48
Figure 40: Injection Angle vs. Engine Speed for Emissions Comparison.....	49
Figure 41: Carbon Monoxide Formation vs. Equivalence Ratio for Propane	50
Figure 42: Carbon Monoxide Emissions vs. Engine Speed.....	51
Figure 43: Nitric Oxide Concentration vs. Percent EGR at Varying Equivalence Ratios	52
Figure 44: Oxides of Nitrogen Formation vs. Engine Speed.....	53

LIST OF TABLES

Table 1: Three-Phase Exhaust Emissions Reduction Strategy	2
Table 2: Five Mode Emissions Test.....	3
Table 3: Percent Error of Emissions Analyzer Associated with Measured Species.....	45
Table 4: Brake Specific Emissions Error for Various Species	46
Table 5: Valve Position for Maximizing Torque and Minimizing BSFC	55

LIST OF EQUATIONS

Equation 1: EPA Emission Score (E-Score).....	3
Equation 2: Pressure Resultant Equation.....	15
Equation 3: Calculating AFR and Lambda Values.....	32
Equation 4: Brake Specific Fuel Consumption Calculation	33
Equation 5: Error Propagation in Brake Specific Fuel Consumption.....	42
Equation 6: Error Propagation in Brake Specific Emissions	46

DEFINITION OF TERMS

After Bottom Dead Center	ABDC
After Top Dead Center	ATDC
Best Available Technology	BAT
Before Bottom Dead Center	BBDC
Bottom Dead Center	BDC
Brake Mean Effective Pressure	BMEP
Brake Specific Fuel Consumption	BSFC
Before Top Dead Center	BTDC
Carbon Monoxide	CO
Clean Snowmobile Challenge	CSC
Charge Trapping Valve	CTV
Direct Injection	DI
Exhaust Port Close	EC
Exhaust Gas Residuals	EGR
Exhaust Port Open	EO
Environmental Protection Agency	EPA
Homogenous Charge Compression Ignition	HCCI
Injection Angle	IA
Intake Port Close	IC
Intake Port Open	IO
Injection Quantity	IQ
Oxides of Nitrogen	NO _x
National Park Service	NPS
Parallel Rotary Synchronous Charge Trapping	PR-SCT
Power Take Off	PTO
Society of Automotive Engineers	SAE
Synchronous Charge Trapping	SCT
Semi-Direct Injection	SDI
Spark Ignition	SI

Throttle Counts	TC
Top Dead Center	TDC
Throttle Position	TP
Unburned Hydrocarbons	UHC
Variable Compression Ratio	VCR
Valve Position	VP
Yamaha Power Valve System	YPVS

1.0 INTRODUCTION

The University of Idaho's motivation for developing snowmobiles to meet and exceed the standards placed on manufacturers comes from a long history of innovative design strategies that maintain the performance many customers demand while improving exhaust emissions, noise, and efficiency to meet the challenges of the Clean Snowmobile Challenge (CSC). The University of Idaho has developed several unique strategies ranging from Direct Injection (DI) systems to combat exhaust emissions, mufflers designed to reduce noise emissions, and rear drive systems designed to improve efficiency and handling [1] [2] [3].

Originally developed as a means of transportation along snow and ice covered terrain, snowmobiles have become a favorite winter recreational vehicle for many people across the world. Throughout much of Alaska and Canada, snowmobiles are still used as a major mode of transportation during the winter months and their continued development has shown no sign of slowing, representing an almost 30 billion dollar per year industry [4]. Although snowmobile use varies greatly by location, many popular destinations include National Parks throughout North America. Snowmobile use in many of these parks, such as Yellowstone and Glacier National Park, has been closely monitored since early 2000 when their use was deemed to cause an adverse environmental impact. The Clean Snowmobile Challenge was formed as the threat of losing access to national parks became imminent.

1.1 CLEAN SNOWMOBILE CHALLENGE

Even before the introduction of the Environmental Protection Agency's (EPA) and National Park Service's (NPS) regulations limiting air emissions from non-road engines in early 2002, including those dealing with snowmobiles, the Society of Automotive Engineers (SAE) and others developed a collegiate design competition in which teams design and build snowmobiles to meet the increasingly stringent emission and sound standards [5]. This event was initiated due to concerns about environmental harm to many of the national parks in the U.S. Because of the negative impact on wildlife and habitat in environmentally sensitive areas, the EPA implemented a three-phase emissions

reduction schedule for snowmobiles in 2002. The average snowmobile at the time these regulations were introduced emitted as many unburned hydrocarbons (UHC) in one hour as the then current automobile emitted in over 24,000 miles of driving, with 30 times the amount of carbon monoxide (CO) emissions [5]. The reduction schedule consisted of three key reduction years in which manufacturers would have to meet the outlined standards. Table 1 shows how the EPA three-phase emission reduction strategy has been implemented.

YEAR	CARBON MONOXIDE	% REDUCTION	UNBURNED HYDROCARBON	% REDUCTION
2002	397		150	
2006	275	31 %	100	33 %
2010	275	31 %	75	50 %
2012	200	50 %	75	50 %

Table 1: Three-Phase Exhaust Emissions Reduction Strategy

The NPS decided that these regulations were not stringent enough for snowmobiles entering national parks; therefore, a stricter standard was placed on these snowmobiles commonly referred to the Best Available Technology (BAT). This CSC competition, which began in 2000, tests the ingenuity of students across the nation to develop clean, quiet, and efficient snowmobiles for use in environmentally sensitive areas.

Manufacturers are now required to pass several emissions tests for both pollution and noise. The first is the EPA's five mode emission test which was originally developed by the Southwest Research Institute and later adopted by the EPA [6]. This test is designed to simulate the emission production of a snowmobile through different operating modes of the engine. Each mode is then weighted based on the amount of time the snowmobile is expected to spend in a particular mode. Table 2 shows the five mode points as well as each mode's weighting.

Mode Point	Speed [% Rated]	Torque [% Rated]	Weighting [%]
1	100	100	12
2	85	51	27
3	75	33	25
4	65	19	31
5	Idle	N/A	5

Table 2: Five Mode Emissions Test

These weighted emissions are then combined to form an Emission Score (E-Score) given by the following Equation.

$$E = \left[1 - \frac{(\text{HC} + \text{NO}_x) - 15}{150} \right] * 100 + \left[1 - \frac{\text{CO}}{400} \right] * 100$$

Equation 1: EPA Emission Score (E-Score)

The EPA emissions score for snowmobiles requires that a score of 100 or greater and limits for total emissions production in each individual category must be achieved. Because of the more stringent regulations imposed by the NPS, a score of 170 points and an even further reduction in individual category emissions must be achieved to comply with BAT.

The University of Idaho has been attending the CSC competition since its inception in early 2000. Over the years the University of Idaho CSC team snowmobile has gone through many changes.

1.2 RESEARCH GOALS

Since the feasibility of charge trapping engines has already been established, the major goal of this research is the continued development of a Parallel Rotary Synchronous Charge Trapped (PR-SCT) Two-Stroke engine for potential use in snowmobiling applications [7]. A PR-SCT system has been developed and the baseline performance and emissions must be established. In this thesis the design of the parallel rotary system will be discussed, including its advantages over other reciprocating style Synchronous

Charge Trapping (SCT) systems, and results from dynamometer and emissions testing. A comparison of two distinct tuning strategies will also be discussed.

2.0 TWO-STROKE ENGINE

The versatility of the two-stroke engine comes from its simplicity. A simple two-stroke engine has in essence only three moving parts: the crankshaft, the connecting rod, and the piston. It is also able to complete a power stroke every revolution of the crankshaft, leading to an engine that has a very high power density. Power density, or volume specific power, refers to an engine that packages a considerable amount of power into a relatively small platform. This comes from the rough factor of two increase in power a two-stroke engine is able to achieve because of the increased number of power strokes over a similarly sized four-stroke engine. These advantages make it the ideal engine for many low cost high power applications. However, the simplicity of this engine can lead to issues with poor emissions and fuel economy if improperly implemented.

The University of Idaho has been working with the two-stroke engine platform since 2005. In 2007 the university won the CSC competition with a direct injected (DI) two-stroke snowmobile running on E10 fuel. [8] These results proved that a two-stroke powered snowmobile is still a viable option in today's market where performance is as important as an engine's emissions and efficiency. Although the DI two-stroke engine was a great advancement, there are still shortcomings that need to be addressed.

2.1 OPERATION

Every internal combustion engine must go through four distinct steps in order to produce power. These steps are intake, compression, power, and exhaust. A reciprocating four-stroke engine separates each step into a separate "stroke", or linear movement of the piston. A power stroke is initiated every fourth stroke, or two complete revolutions of the crankshaft. This separation of the processes is accomplished through a series of valves in the combustion chamber that control when each process begins and ends. These valves are controlled through an extensive valve train that consists of the valves themselves, a series of springs, cams, chains, and other components depending on the engine

configuration. This valve train adds complexity, weight, and cost to even a simple single cylinder four-stroke engines. A simple four-stroke cycle operation is given in Figure 1.

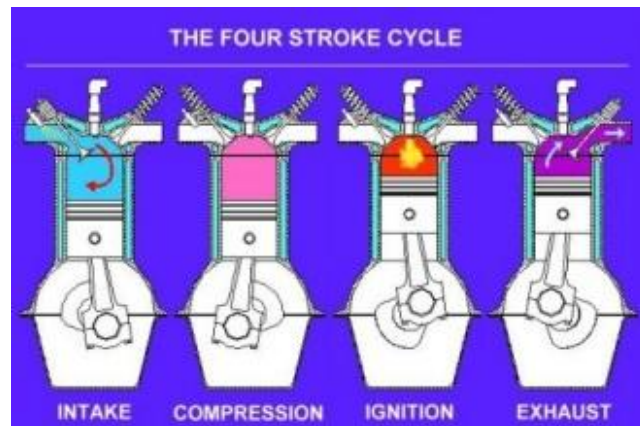


Figure 1: Four-Stroke Engine Operation

A two-stroke engine's ability to complete many of these steps simultaneously leads to its high power output from a relatively small package, with far less mechanical complexity. However, because of the simultaneous processes, there is a very complex gas exchange process. This process is controlled by the piston location in the cylinder relative to the location of the intake and exhaust ports. A simple two-stroke engine is shown in Figure 2a, the location of the intake and exhaust ports are labeled for clarification. Figure 2b shows the port timing and duration of a two-stroke engine. This diagram will be considered to in the next section.

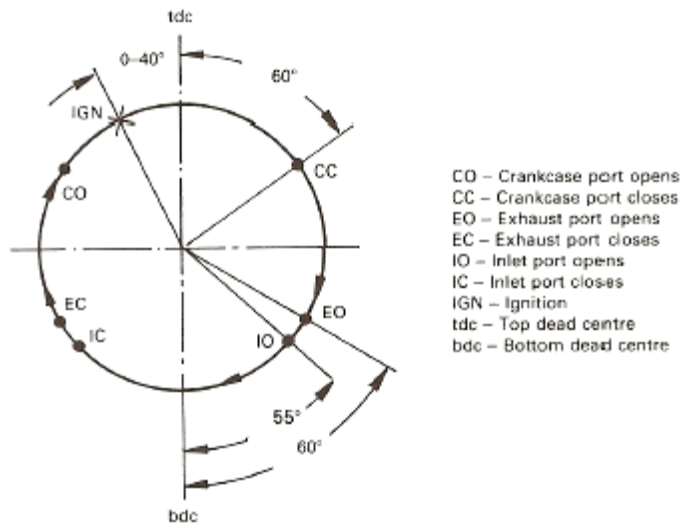
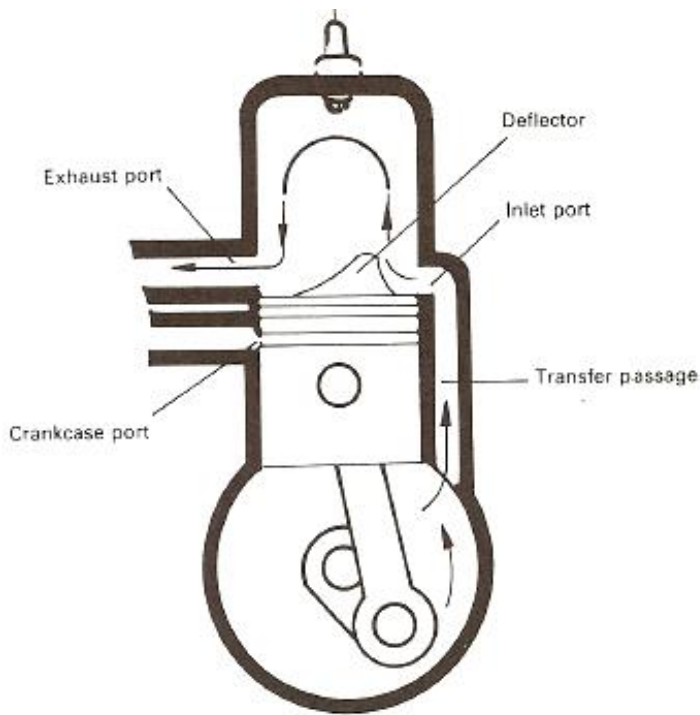


Figure 2: Two-Stroke Engine Configuration and Port Duration and Timing

To further explain a two-stroke engine's gas exchange process, a cycle-by-cycle overview will be given by following an air charge through one complete cycle. The cycle described is a carbureted crankcase inducted single cylinder engine with tuned exhaust. The cycle begins with the intake process in which the piston moves up in the cylinder

until a low enough pressure is reached in the crankcase for fresh air to be drawn past the throttle plates where it is then mixed with fuel. The fuel/air mixture commonly referred to as fresh or intake charge is drawn past the reed valves into the crankcase below the piston. These reed valves are placed in-line so that no intake charge may escape the crankcase back through the intake system when it is pressurized in a later step. This can be seen in Figure 3. The necessary components are labeled but will not be labeled in the future. Refer to Figure 3 as needed.

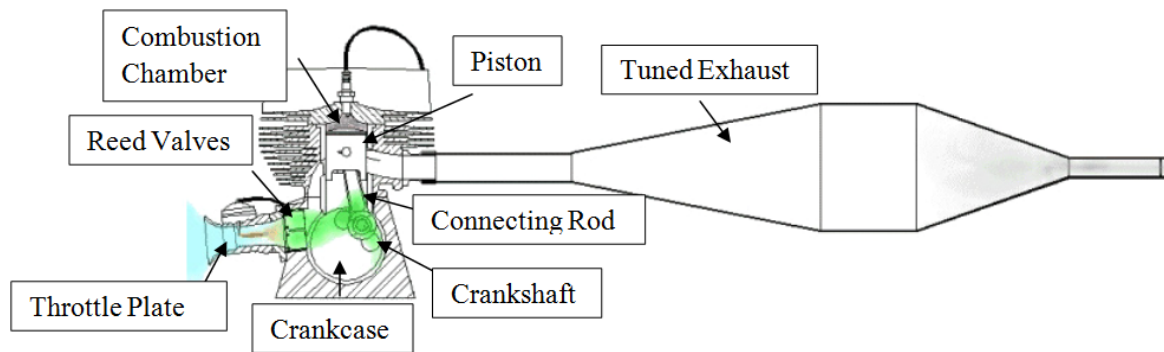


Figure 3: Intake Stroke

The piston then passes Top Dead Center (TDC) and begins moving down, compressing the fuel/air mixture in the crankcase. This compression process continues until the intake port opens (IO) at which point the fuel/air mixture moves from the crankcase to the combustion chamber. The piston again begins to move toward TDC closing the intake port (IC) at the same time the next fresh intake charge is being drawn into the crankcase. As the piston continues to move up inside the cylinder, the exhaust port is closed (EC). The compression process now begins. As the piston approaches TDC the spark plug discharges, igniting the intake charge and beginning the power stroke. This combustion event causes the piston to travel down the cylinder and compresses the previously inducted intake charge in the crankcase below. This can be seen in Figure 4.

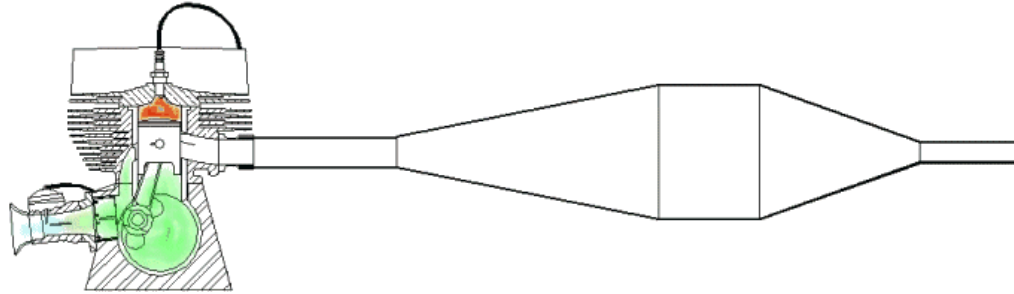


Figure 4: Power Stroke

As the piston moves down inside the cylinder, the exhaust port is uncovered (EO) shortly after combustion and blowdown begins. Blowdown is the process in which the spent exhaust gases are evacuated from the cylinder due to the increased pressure in the combustion chamber. These high pressure exhaust gases create a pressure wave that begins to travel down the length of the exhaust system. This can be seen in Figure 5. The pressure waves are labeled with arrows in the exhaust system.

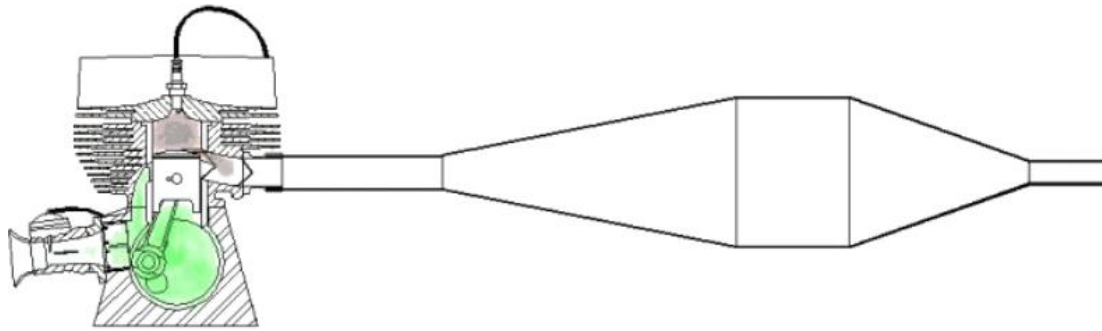


Figure 5: End of Power Stroke and Beginning of Blowdown

Blowdown continues as the piston moves towards Bottom Dead Center (BDC) until the pressure in the cylinder is equal to that of the exhaust system at which point inertial effects of the gases can cause a negative pressure in the cylinder. Next, the intake port opens (IO) and scavenging begins. Scavenging refers to the simultaneous exchange of fresh intake charge with spent exhaust gases in the combustion chamber of a two-stroke engine [9]. This can be seen in Figure 6.

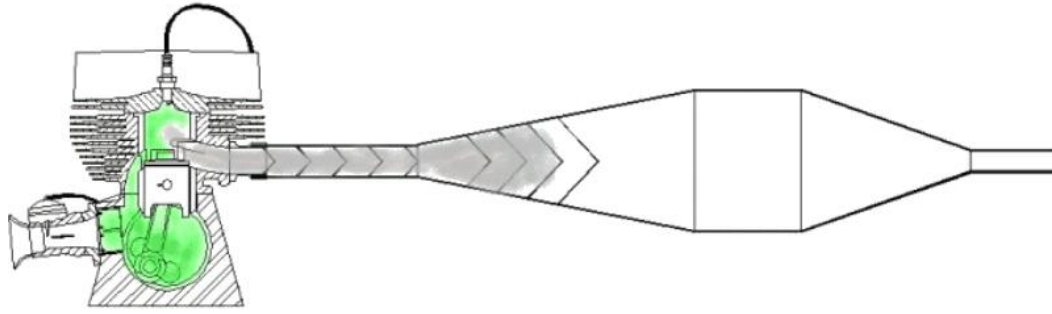


Figure 6: Beginning of Scavenging Process

The intake of fresh charge can continue until the intake ports close (IC) at which point the scavenging pressure, or pressure inside the cylinder at the conclusion of the scavenging phase, is greater than the pressure in the exhaust system. However, there is still a certain degree of crankshaft rotation that must take place in order for the compression process to begin again. This can result in fresh charge, approximately equal to the volume displaced during the IC to EC portion of crankshaft rotation, being pushed into the exhaust system. This can be seen in Figure 7. This charge is lost, and does not contribute to the combustion process. It is common to refer to losing this charge as “short-circuiting”. Short-circuiting is the largest contributor to the formation of unburned hydrocarbons in a two-stroke engine [10]. In order to eliminate short-circuiting, tuned exhaust systems, commonly referred to as a “tuned pipe”, are used to recover the lost charge. This will be explained in greater detail in the next section. Once the exhaust port is closed compression can begin and the cycle repeats.

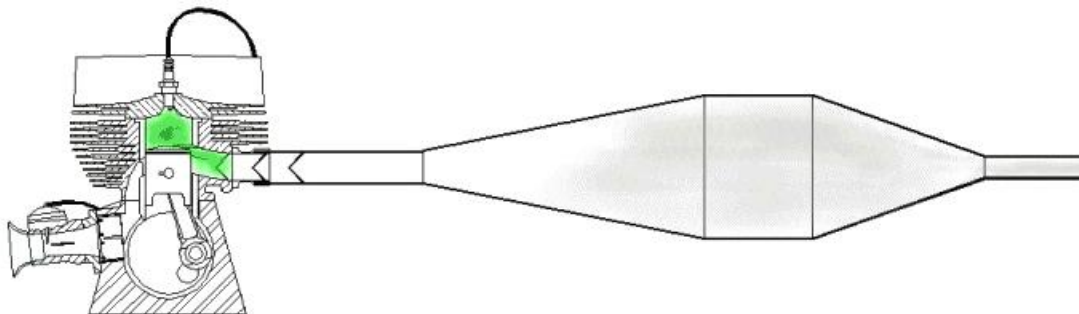


Figure 7: Fresh Charge Displaced Into Cylinder After Scavenging Process

2.2 TUNED EXHAUST SYSTEM

One method of combating some of the negative side effects of a two-stroke engine's gas exchange process is with the use of a tuned pipe. The tuned pipe is made of two distinct sections that help to not only reduce and potentially eliminate short-circuiting during a desired operating range but can also greatly increase power output due to the dynamic supercharging effect. A tuned pipe is broken into diverging and converging sections that have two distinct purposes.

The diverging section of the tuned pipe creates an expansion wave as a result of the increasing area change that travels back towards the combustion chamber, helping to pull residual exhaust gases out of the cylinder as well as pull fresh charge into the cylinder. It is timed such that it arrives in the cylinder at the same time as the scavenging process is underway. This helps lead to a greater scavenging efficiency, which is defined as the fraction of exhaust gases residual (EGR) replaced with fresh charge in the cylinder [9]. If the expansion wave has a large enough magnitude, fresh charge can continue to be pulled into the exhaust system which dictates the need for the converging section of the tuned pipe. The converging section of the tuned pipe creates a pressure wave, as a result of the decreasing area change, that travels towards the combustion chamber pushing most of the fresh charge in the exhaust system back into the cylinder. This results in a greater trapping efficiency which is defined as the amount of fresh charge retained compared to the amount of fresh charge delivered [9].

A tuned exhaust system is designed to work over a particular band of engine speeds in which the engine is expected to spend the majority of its operating time. At locations outside of this band, the amount of short-circuiting increases dramatically, due to the decrease in the trapping and scavenging efficiencies. Operating outside the effective range of the tuned pipe causes the pressure and expansion waves to return at the wrong time, displacing fresh charge into the exhaust system.

2.3 POWER VALVES

Another method of alleviating the short-circuiting effect and off-tune points in the exhaust system that occur when operating outside the design range of the tuned pipe is

the use of power valves. Power valves have been in use since the early 1970s [11]. Power valves effectively broaden the operating range of an engine by changing the port height based on engine conditions. By changing the port height, the expansion portion of the combustion cycle is increased. This results in a greater power output, as well as closing the exhaust before the mistimed pressure and expansion waves can displace any of the fresh charge. This results in higher trapping efficiencies. The Yamaha Power Valve System (YPVS) was one of the first commercially available systems, and created a 20% increase in horsepower over previous engine designs [12]. Currently, power valves are used by a variety of manufacturers with several types in production. The most common type of power valve is a guillotine-style valve with multiple positions allowing for a very broad power band. The guillotine-style valve can be seen in Figure 8 on a Rotax 600cc Skidoo E-TEC engine, which is the base engine for this research. For further information on power valve technology refer to the thesis of Dylan Dixon [11]

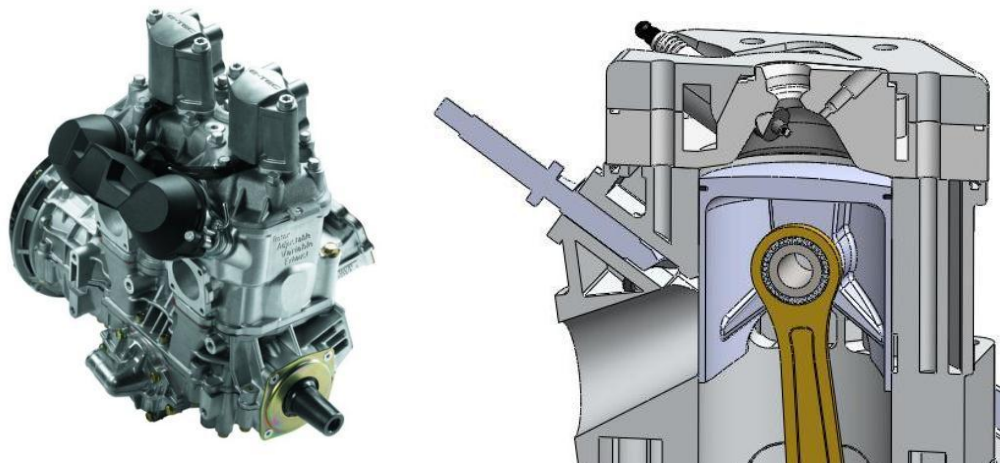


Figure 8: Power Valves on a Rotax 600cc E-TEC

2.4 FUEL DELIVERY

Traditionally, two-stroke engines have been carbureted for simplicity and cost. However, with increasing emission standards on off-highway vehicles, fuel injection systems are becoming the norm rather than the exception on the majority of two-stroke engines. There are three main types of fuel injection strategies which vary based on the location of the injector and the tuning strategy. Throttle body injection is the simplest and cheapest

form of fuel injection to implement. This is a single point injection scheme where a single (or multiple injectors depending on fuel flows needed) is placed directly after the throttle body. This allows a precise amount of fuel to be sprayed into the incoming air stream. This was a very common method of fuel injection in automobiles during the 1980's, replacing carburetors [13]. In order to meet the first phase of the EPA's emission reduction strategy, snowmobile manufacturers developed another form of fuel injection in which the injector is placed in the boost port. This type of system is known as a semi-direct injection (SDI) system and can be seen in Figure 9. Skidoo was the first manufacturer to develop this type of system, which was called the 2-TEC[®], in 2004. Polaris followed shortly after with its version, called the Cleanfire[®], in 2006. These systems showed an approximately 50% reduction in UHC emissions, while significantly increasing fuel economy from 6.9 mpg to 19.1 mpg [9]. These results are directly related to a reduction in the amount of fuel that is short circuited. However, because SDI engines must be operated fuel rich for reliability, the reduction in CO emissions was not as significant at 30%. Because a SDI system still delivers a fuel/air mixture, scavenging flows and mixing of EGR still affect the performance of a SDI system.

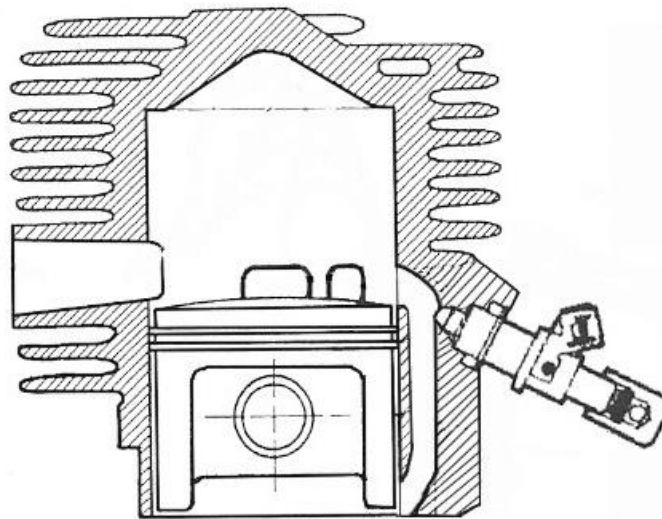


Figure 9: Semi-Direct Injection System

Although the SDI system was a step in the right direction, this type of system could not meet NPS emissions standards with a two-stroke platform. The next step in fuel injection

technology came in the form of direct-injection systems. Direct-injection (DI) systems have been in use for almost a century in diesel engines, and have only recently transitioned to gasoline engines. A DI system works by spraying fuel directly into the combustion chamber at a specific time in order to facilitate combustion. DI style injectors must have the ability to precisely meter the amount of fuel being delivered as well as the time at which it is delivered. This makes them more expensive than many other types of injectors being manufactured today. However, if implemented correctly the benefits of a DI system can greatly outweigh the added cost and complexity of the system. Unlike any other type of fuel injection scheme, DI systems have the ability to run two different modes of operation. Because the fuel is not mixed with the air before it enters the combustion chamber as it is in a throttle body or SDI style system, a DI system can run both in homogeneous and stratified modes of operation [14]. These modes refer to how well the fuel is mixed with the surrounding air during combustion. See Figure 10.

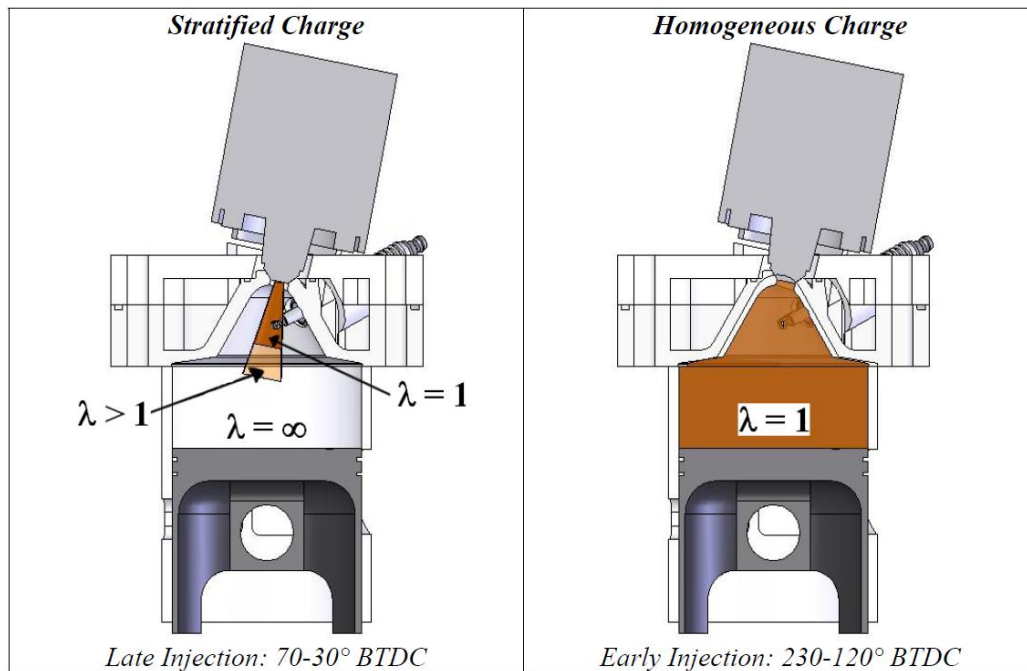


Figure 10: Stratified vs. Homogeneous Charge Combustion

A stratified charge is the result of late injection, and results in a globally lean mixture in much of the combustion chamber with a stoichiometric mixture very near the sparkplug to facilitate combustion. A stratified charge results in dramatic decrease in the amount of

fuel being injected. This strategy is generally used in low speed/low load situations. A homogenous mixture is the result of early injection and causes a mixture of fuel and air that is thoroughly mixed throughout the combustion chamber. For a more detailed review of DI technology and homogenous vs. stratified operation refer to the theses of Nathan Bradbury [10] and Justin Johnson [15] respectively. A DI system was selected for fuel delivery for this research.

3.0 SYNCHRONUS CHARGE TRAPPING

The next step in potentially improving emissions from two-stroke engines is synchronous charge trapping. The goal of a Synchronous Charge Trapping (SCT) engine is to eliminate or reduce the amount of fuel that is lost to short-circuiting. The valves in a SCT engine act similarly to power valves in a typical two-stroke engine. However, instead of remaining in a fixed position, they are synchronized with the crank and are therefore continually moving. After Top Dead Center (ATDC) the valve begins moving out of the exhaust port so that when the exhaust port opens blowdown can begin and scavenging efficiency can be maintained. After Bottom Dead Center (ABDC), as the piston begins moving up in the cylinder, the SCT valve effectively lowers the exhaust port height resulting in a higher trapped volume and a greater trapping efficiency.

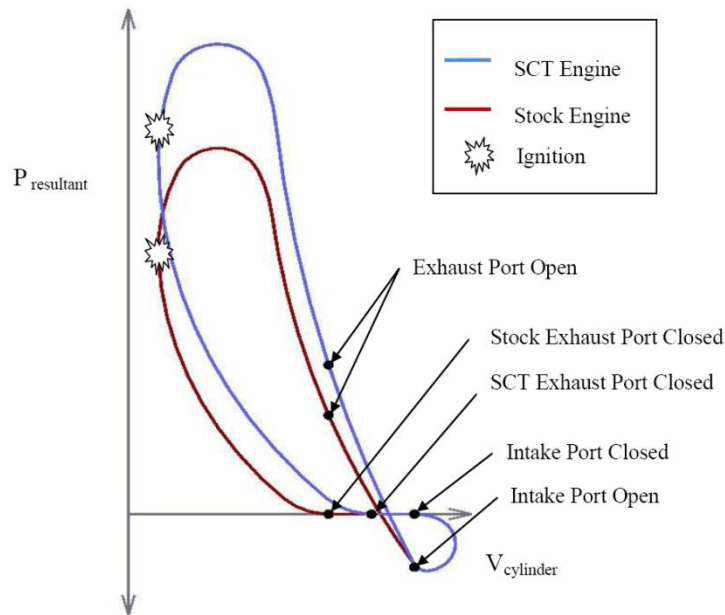


Figure 11: Pressure vs. Volume for SCT and Stock Engine

This can be seen on the theoretical pressure volume diagram in Figure 11. This figure shows the resultant pressure as a function of in-cylinder volume. The resultant pressure described by Equation 2 is the result of including the force under the piston generated by pressure in the crankcase and the force on top of the piston generated by combustion.

$$P_{resultant} = P_{cylinder} - P_{case}$$

Equation 2: Pressure Resultant Equation

By closing the exhaust port earlier, the compression process can begin sooner, resulting in higher in-cylinder pressures before combustion. This leads to greater work over the same expansion stroke.

3.1 PREVIOUS DEVELOPMENT

A variety of manufacturers, most notably Boyesen and Lotus, have been developing SCT engines for the past decade. Because Boyesen's development has halted in recent years and up to date information is not available, a brief overview of only Lotus' use of charge trapping valves will be given.

The Lotus Omnivore[®] research engine branches out into several areas of interest in modern engine technology. The Omnivore[®] is a Variable Compression Ratio (VCR) Homogenous Charge Compression Ignition (HCCI) Direct Injected Engine with Variable Charge Trapping Valves (CTV). Figure 12 shows a cutaway of the Omnivore[®] with highlighted components [16].

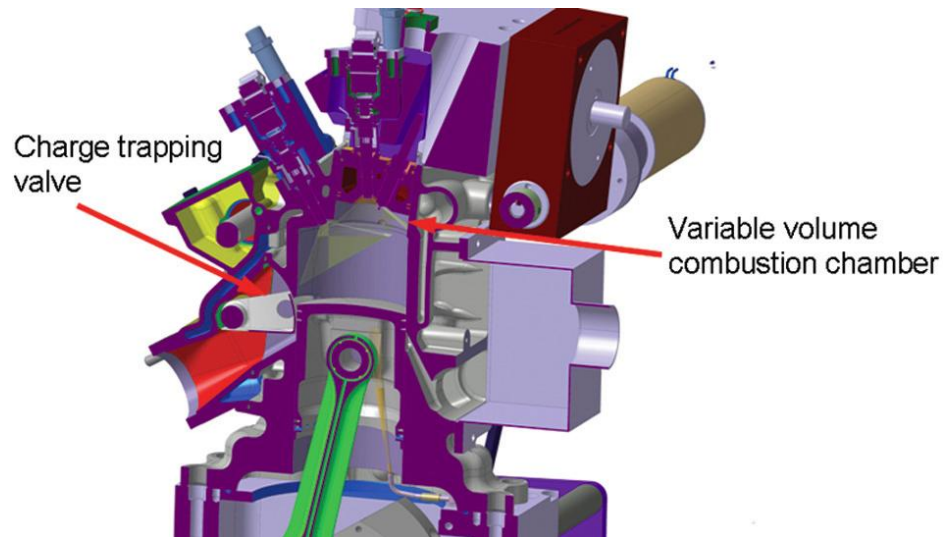


Figure 12: Lotus Omnivore[®] Engine Cutaway

The use of CTVs in the Omnivore[®] engine is designed to trap Exhaust Gas Residuals (EGR) in order to control the auto-ignition sequence along with the VCR during the HCCI modes of operation. HCCI is a mode of combustion in which the fuel/air mixture is compressed to the point of auto-ignition, resulting in higher burn rate and greater heat release when compared to a spark ignition (SI) engine [17]. This is because an auto-igniting mixture generally has several locations that begin the combustion process simultaneously instead of a single point with a flame front that moves out such as in a SI engine. Lotus' design uses reciprocating valves driven from an eccentric shaft that rotates at the same speed as the crankshaft. The stroke of the valve is determined by an articulating link between the eccentric shaft and the valve linkage [7].

4.0 CLEAN SNOWMOBILE CHALLENGE DESIGNS

The University of Idaho has been developing a SCT engine for the past four years and is now on its second iteration. The original design proved that SCT technology was a viable option to pursue to improve fuel efficiency. However, an emission analysis was never performed and is therefore one of the focuses of this thesis.

4.1 RECIPROACTING VALVE SCT

The University of Idaho's original SCT engine was a reciprocating valve design similar to the designs of Lotus and Boyesen. A Rotax 600cc E-TEC engine was modified to accept the SCT valves and linkage. The initial design can be seen in Figure 13 with non-factory parts labeled.

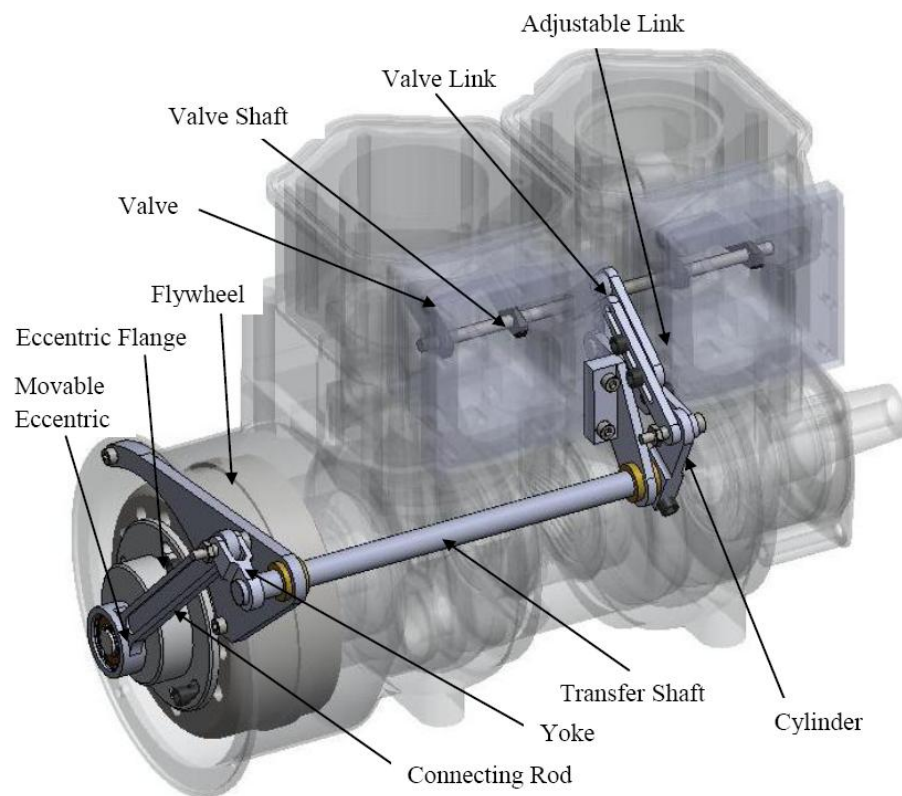


Figure 13: Previous Synchronous Charge Trapping Engine Design.

An eccentric flange was bolted directly to the flywheel. The slots allow the flange to be rotated with respect to the crank, which then passes through a moveable eccentric in the lower portion of the connecting rod labeled above. This connecting rod transmits

movement to the yoke and through the transfer shaft. The transfer shaft rides on brass bushings to help eliminate binding. Movement is then transferred along an adjustable linkage that controls the stroke of the valve. For the entire manufacturing and design process refer to the thesis of Peter Britanyak [7]. Figure 14 shows the reciprocating valve movement in the previous SCT design.

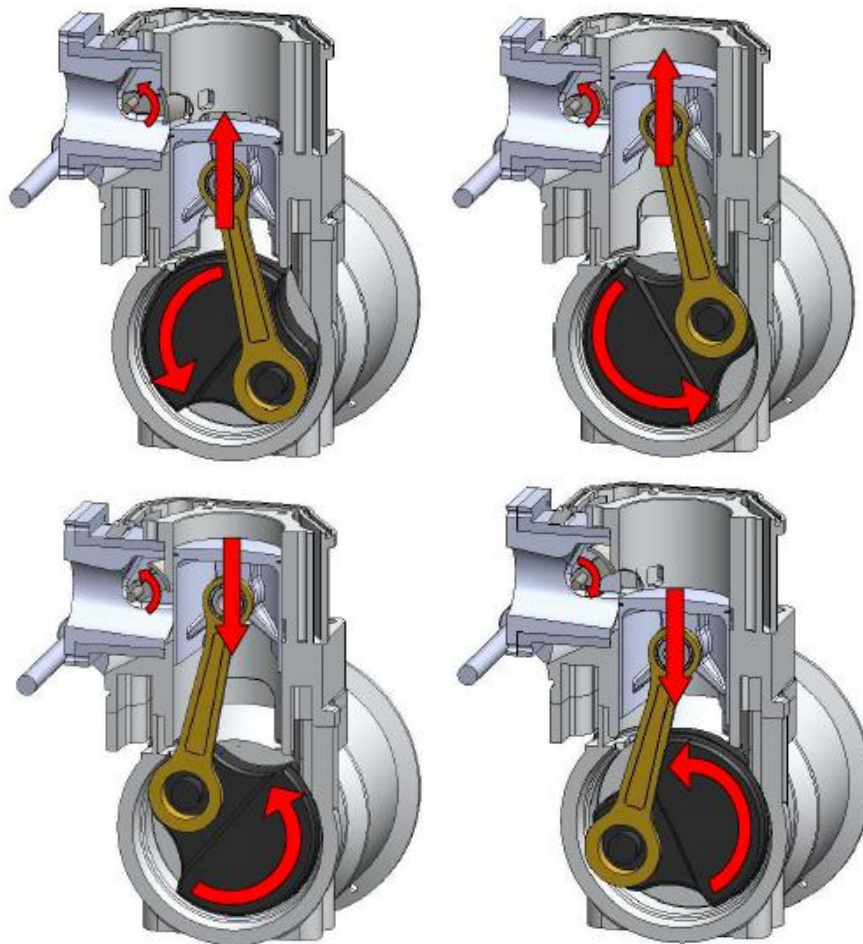


Figure 14: Reciprocating Valve Motion

4.1.1 RESULTS

The results of the first generation SCT engine showed improvements in both Brake Specific Fuel Consumption (BSFC) and peak torque, especially at low engine speeds. This was to be expected due to the larger trapped volume leading to greater potentials for work to be extracted. These results can be seen in Figure 14. The average percent decrease in BSFC was 10% in the 3500 RPM range. Because of several malfunctions

which will be detailed in the next section, very little data were available. However, the results that were found proved that Synchronous Charge Trapping engines were a viable research area.

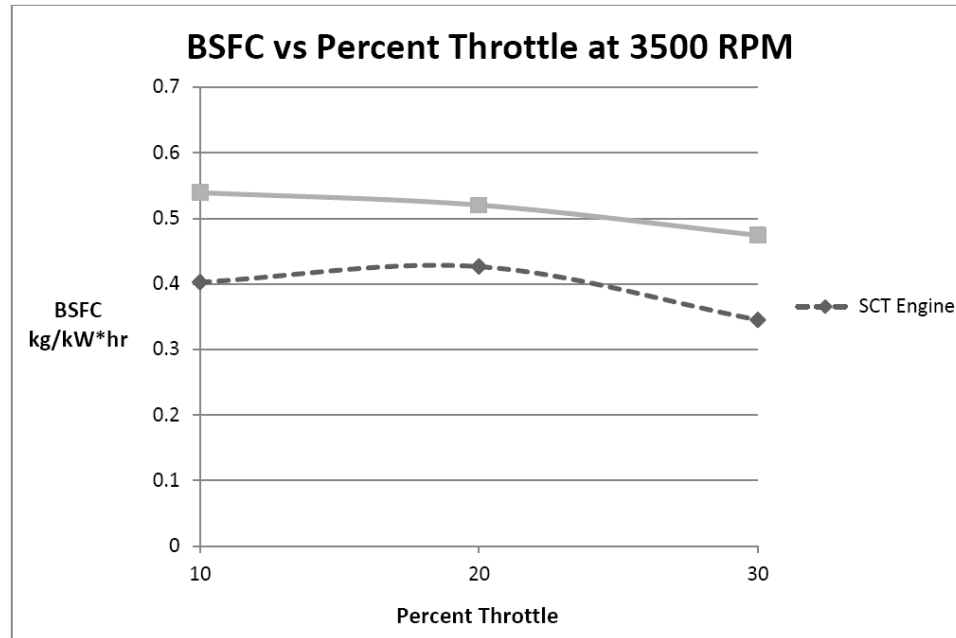


Figure 15: Percent Throttle vs. BSFC at 3500 RPM

4.1.2 MALFUNCTIONS

Although the results were promising, there were some crucial flaws in the first generation SCT system. The largest flaw was that the reciprocating motion of the valves would lead to premature valve shaft failure at anything over 4000 RPM. The maximum allowable torque the valve shaft was able to see is a function of the center of mass of the valve in relation to the center of the shaft and the acceleration that the valve undergoes. Even though the center of mass of the valve is relatively small, it is located a significant distance away from the valve shaft. This, combined with the large acceleration due to the reciprocating motion of the system, led to shaft failure. In order to overcome shaft failure, several different types of materials and manufacturing processes were investigated to redesign the first generation SCT system. Figure 15 shows the results from using three different types of material including billet stainless steel, sheet stainless steel, and sheet titanium. The sheet metals would have been used with a metal spinning

manufacturing process to create extremely light valves. However, even with the reduced weight, valve shaft failure was still imminent in the test engine operating ranges. These results led to an entire redesign of the SCT system.

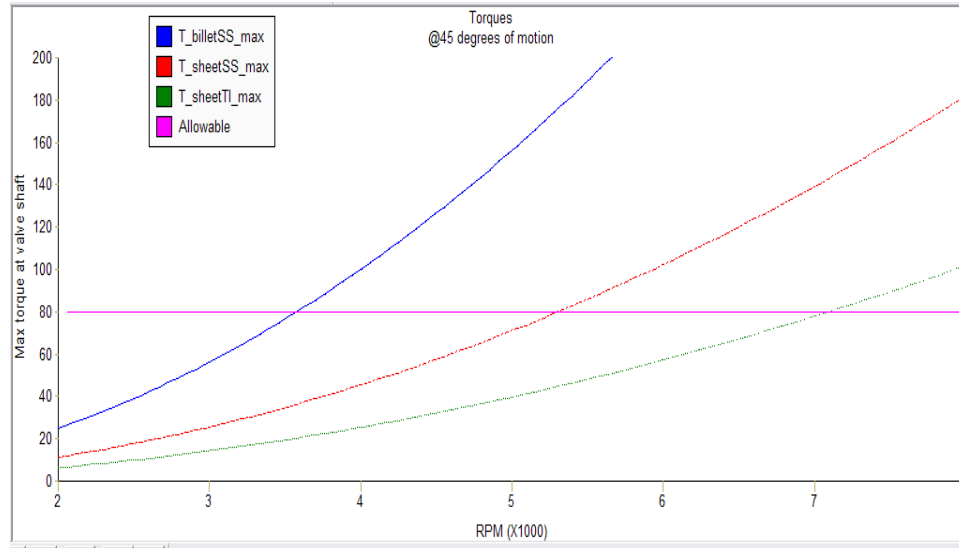


Figure 16: Shaft Torque vs. Engine Speed for 45° of Reciprocating Motion

4.2 PARALLEL ROTARY SCT

In 2010 the University of Idaho began development of a Parallel Rotary Synchronous Charge Trapped (PR-SCT) two-stroke engine. This was decided as a result of the malfunctions with the reciprocating system. To eliminate the reciprocating motion, the valves were fixed to a shaft that runs parallel to the engine crankshaft. A system of pulleys transmits the rotational motion from the crankshaft to the valve shaft. The drive pulley is attached to the engine flywheel for convenient power take off (PTO). The valve and pulley system are seen in Figure 16. The crankcase and cylinders have been made transparent so that the valve system can be more easily seen.

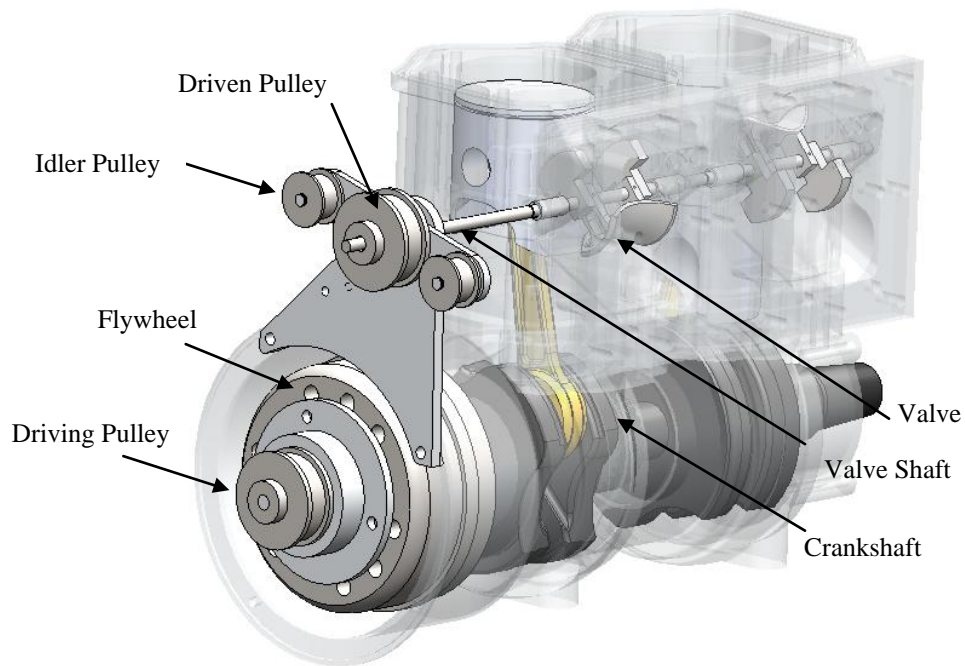


Figure 17: Pulley System PR-SCT Valve

The phase of the valves can be adjusted by changing the location of the idler pulleys with respect to the driving and driven pulley. Rotating the idler pulley bar counter clockwise will advance the valve in relation to the crank and close the exhaust port sooner increasing the trapped volume. This is seen in Figure 17. Belt routing allows the valve shaft to rotate in the opposite direction as the crankshaft, resulting in proper exhaust port closure.

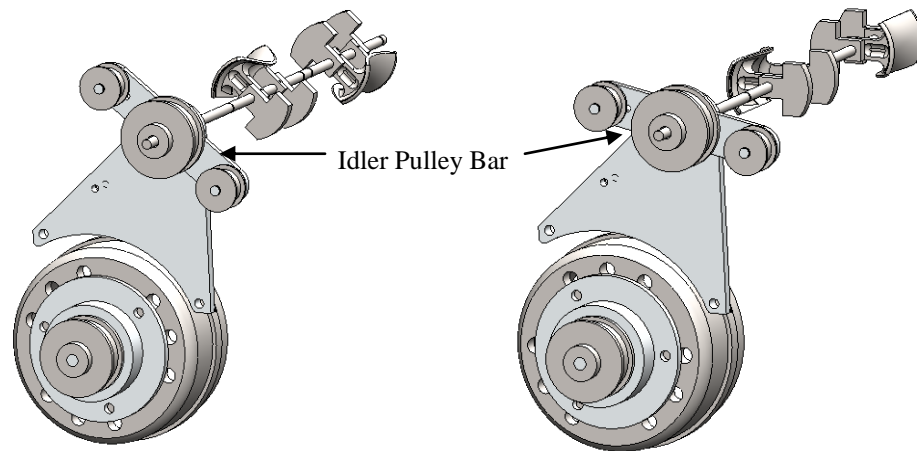


Figure 18: Valve Adjustment

4.2.1 MANUFACTURING

Machining of the PR-SCT system began by modifying a stock Ski-Doo 600 cc Rotax engine to accept the PR-SCT valve assembly. In order to secure the valve assembly, and make it easily serviceable, two inserts were manufactured that merged with a modified factory cylinder. These inserts along with the modified cylinder can be seen in Figure 18.

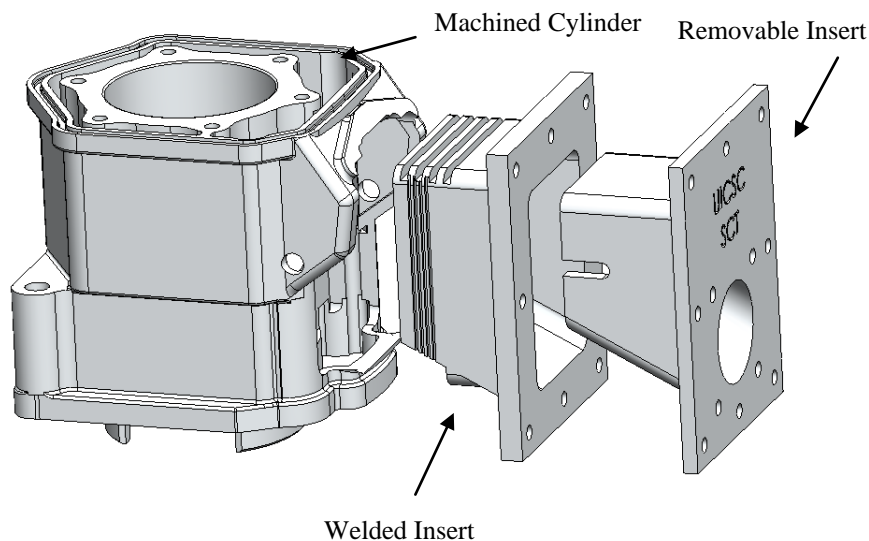


Figure 19: Machined Cylinders and Inserts for PR-SCT system

The factory cylinders were the first parts to be modified. The RAVE 2 exhaust valve system needed to be removed from the factory cylinders. Therefore, a pocket was machined that allowed for the permanent insert to be welded into the machined cylinder. The machining was done on a HAAS 4-Axis milling machine and can be seen in Figure 19.

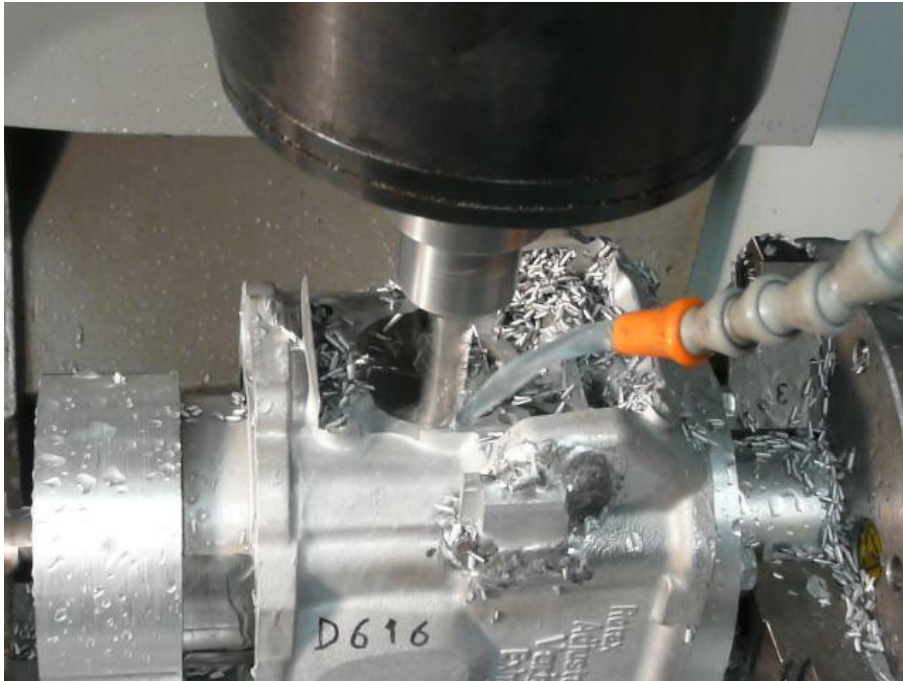


Figure 20: Milling of the Cylinder to Accept PR-SCT System

Next, the welded insert was machined and welded into the modified cylinders. To regain some of the cooling capacity lost by machining a pocket into the coolant passages of the cylinder, fins were added to the welded insert. This would help to increase heat transfer to the cooling system. Because of the potential for warpage, a final machining of the welded insert was done after it was welded to the modified cylinder to remove any imperfections that the welding process may have caused. This allowed for a proper mating between the modified cylinders and the removable inserts. RTV sealant was also used between the welded insert and the modified cylinder to help seal the water passages and prevent leaks into the exhaust system. Finally the removable insert was machined such that the exhaust path matched closely to the factory exhaust opening so proper exhaust flows were maintained.

The exhaust valves were manufactured to reflect the geometry of the cylinder. This helped to maintain tight clearances between the valve face and piston, creating a seal so that trapping could occur. Counter balances were also machined to reduce centripetal forces on the shaft as much as possible. The final valve design with counter balances can be seen in Figure 20.

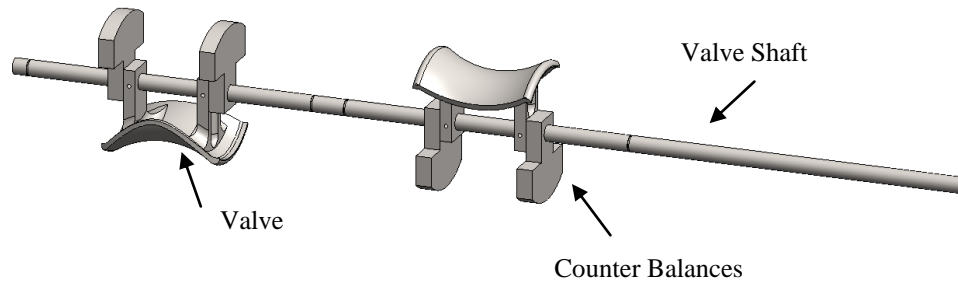


Figure 21: Valves and Counter Balances

4.2.2 MODIFICATIONS

During testing several problems were noticed with the PR-SCT valve adjustment mechanism that reduced system reliability. An exploded view of the valve adjustment and pulley system is shown in Figure 21. The first issue that arose was the vibration of the idler pulley bracket. A brass bushing was press fit onto the idler bracket and slip fit to the pulley bracket. This was done to allow movement between both brackets and maintain valve adjustability. However, issues arose during continued use and adjustment of the valve. The brass bushing would wear against the pulley bracket. This caused a poor fit in the bushing which caused the idler bracket to back off the pulley bracket. The bushing would then rub against the driven pulley causing further wear. Eventually the bushing would become worn enough that the idler bracket would wobble uncontrollably.

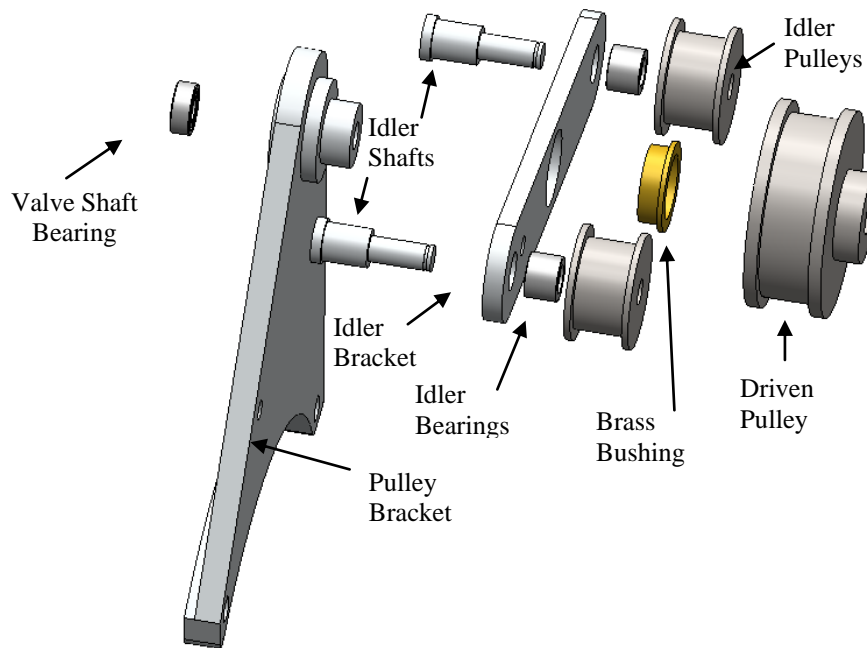


Figure 22: Exploded View Pulley System

A new idler bracket adjustment system was designed to alleviate this problem. The new system replaced the brass bushing with a ball bearing. The ball bearing was pressed both onto the idler and pulley brackets. This resulted in little to no lateral movement, while still allowing the idler bracket to rotate freely with respect to the pulley bracket.

The next area that needed attention was the idler shafts and bearings. The idler pulleys were originally machined to accept a single needle bearing that rode on the idler shaft. Under continued operation these shafts continued to wear, causing the idler pulleys to shake violently, breaking the external snap rings that retained them to the shaft and causing engine malfunctions. This was first attributed to material selection. It was determined that a harder material such as stainless steel would not wear as quickly and would prolong the life of the shafts. Although this did prolong the life of the shafts, idler shaft failures were still common. It was then determined that shaft failures were not caused by material selection as much as bearing selection and manufacturing of the idler pulleys. In Figure 22 is a cutaway view of the original bearing and pulley assembly.

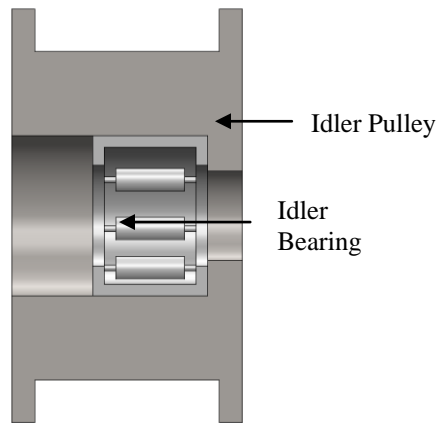


Figure 23: Idler Pulley with Offset Bearing

The original manufacturing plans call for the idler bearings to be offset to one side of the pulley in order to properly align the system. When the timing belt was tensioned, the pulley became unstable while rotating. By offsetting the bearing, the load is not distributed evenly across the bearing surface. Premature wear of the idler shafts and bearing failures were the result. In order to alleviate this problem, a wider bearing surface was incorporated to more evenly distribute the load. Since a wider bearing in the diameter necessary was not commercially available, two smaller bearings were placed side by side. This can be seen in Figure 23.

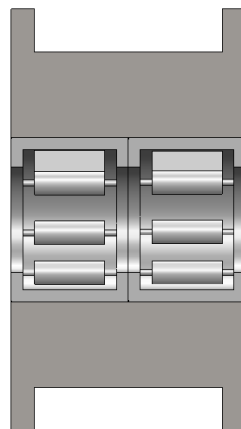


Figure 24: Idler Pulley with Double Bearings

The final modification made to the original PR-SCT system included an accurate measurement system for valve position. By machining an indexing ring that pressed onto the pulley bracket, repeatable and accurate measurements of valve position could be maintained. An exploded view of the final pulley system is shown in Figure 24.

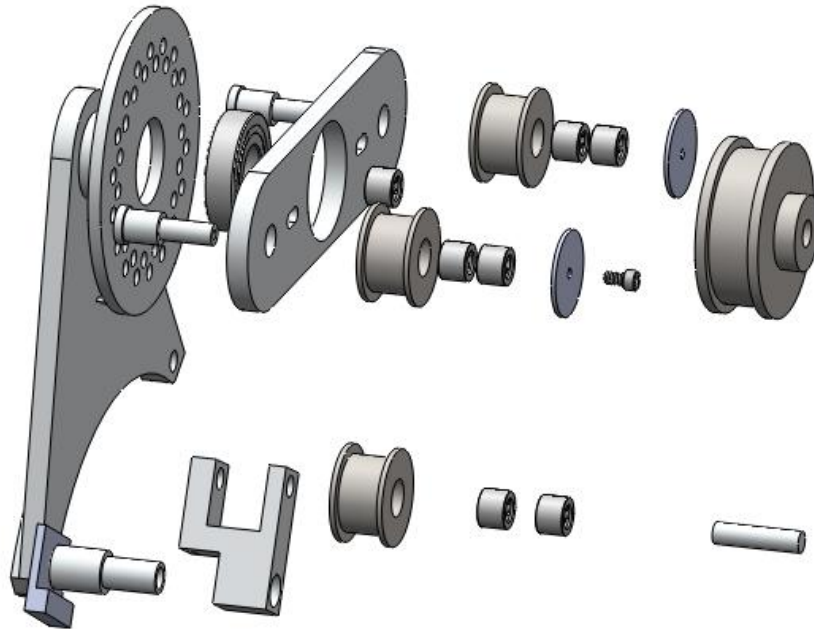


Figure 25: Exploded View Modified Pulley System

5.0 TESTING

The following procedure was used to test the PR-SCT engine and determine Injection Angle (IA), Injection Quantity (IQ), and Valve Position (VP). The data that was collected included torque, power, fuel flow, unburned hydrocarbons (UHC), carbon monoxide (CO), and oxides of nitrogen (NO_x). The variables manipulated included throttle position (TP), engine speed (RPM), VP, IA, and IQ. The baseline engines that were used for comparison are the factory Rotax 593 cc engine with tuned exhaust system and the Parallel Rotary SCT engine with the charge trapping valves removed.

5.1 ENGINE CONFIGURATIONS

The factory Rotax 593 cc engine with tuned exhaust was chosen for a baseline, and will be referred to as baseline 1 from this point forward. This enables a comparison to be made of the Parallel Rotary SCT engines performance to a commercially available engine. Although the focus of this thesis is the development of a Parallel Rotary SCT engine for use in snowmobiling applications, many other powersports industries could benefit from these findings. The factory Rotax 593 cc engine consisted of all factory components available from the manufacturer.

The Parallel Rotary SCT with charge trapping valves removed was chosen as a second baseline, and will be referred to as baseline 2 from this point forward. This eliminates the possibility that the manufacturing of the SCT system would have an effect on engine performance without the inclusion of the valve. Baseline 2 consists of the remanufactured SCT Cylinders on a factory Rotax 593cc engine bottom end with factory E-TEC cylinder head. The charge trapping valve will be removed but the pulley and valve shaft system will be installed to eliminate exhaust leaks. The factory y-pipe and a straight piece of stainless steel exhaust will be used to eliminate the tuned exhaust system. A factory engine map was used initially to begin testing. Remapping will be done according to the engine mapping procedure outlined below.

The test engine that will be used consisted of the SCT cylinders on a Rotax 593cc engine bottom end, and E-TEC cylinder head and injection system. The entire valve and pulley system will be included in this engine. The initial engine map will be the one developed for the SCT Engine with no valve. Remapping will again be done based on the engine mapping procedure mentioned below.

5.2 EQUIPMENT

Torque and power measurements were made using a Borghi and Saveri[®] eddy current dynamometer model FE-260-S. Fuel flow measurements will be made using a Max Machinery fuel measurement system model 710. Emissions measurements will be made using a Horiba[®] portable emissions analyzer model MEXA-584L. In-cylinder pressure measurements will be made using a Kistler[®] in-cylinder pressure transducer model 6052C. The in-cylinder pressure measurements are used during tuning to combat engine

knock. Engine knock is caused when the unburnt gas mixture is ignited spontaneously after combustion was initiated by the spark plug due to the increased temperature and pressure inside the combustion chamber [18]. The distinctive knocking sound is a result of the flame fronts, one from the location of the spark plug and one from the unburnt gases, colliding and resonating in the combustion chamber. Knock can severely damage an engine and must be monitored carefully. Figure 25 shows normal and abnormal combustion as detected using a pressure transducer and oscilloscope. The left figure represents a normal combustion event. Slight knock and intense knock are represented by the middle and right figure, respectively. The intensity of engine knock can be seen directly by the intensity of the resonance frequency superimposed on the normal combustion pressure trace.

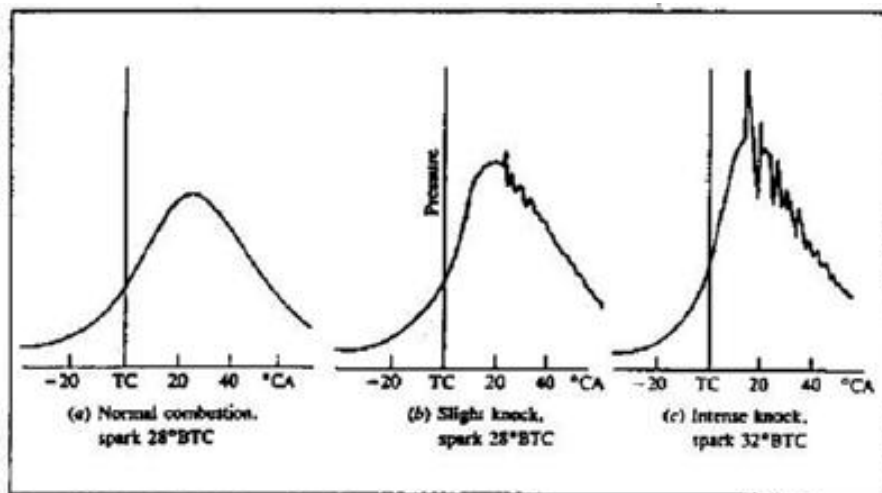


Figure 26: Detection of Knock with Pressure Transducer

5.3 DATA COLLECTION

The data that was collected and analyzed included torque, power, brake specific fuel consumption (BSFC), brake mean effective pressure (BMEP), as well UHC, CO, and NO_x emissions. Torque and BSFC data were taken to form a direct comparison between the test engine and baseline engines from 3500 – 5500 RPM and 20%-60% throttle. BSFC is a measure of an engine's fuel mass flow rate per unit power, and is a measure of how efficiently an engine is converting chemical energy to mechanical power. BMEP data can be calculated from the recorded torque at the dynamometer and the swept

volume of the engine. BMEP is a measure of an engine's power output and will be used to directly compare the SCT engine to the baselines. Finally, emissions data was taken not only to compare to baseline, but to help with engine tuning as outlined in the engine mapping procedure later. The emissions data will also be used to estimate the engine's trapping efficiency. Trapping efficiency is a measure of the percentage of the air/fuel mixture delivered that is retained in the cylinder and used for combustion.

5.4 TEST PLAN

Stock Engine – The stock engine was tested gathering the required data at engine speeds ranging from 3500-5500 at 1000 RPM increments. Throttle position was varied from 20% to 60% in 20% increments. This resulted in nine data collection points for comparison.

SCT Baseline – For baseline 2, the same RPM was used for data collection but based on two possible comparisons. If possible, baseline 2 was tuned to minimize BSFC and match stock torque at a given RPM. If this could not be done, baseline 2 was tuned for maximum torque at a given throttle position and RPM and a comparison of BSFC was made. Data was collected for this baseline and %CO was found for use in SCT valve testing.

Test Engine – The SCT test engine used the same RPM and data collection points but valve position was also varied. The initial engine map was from baseline 2. Tuning was again done to minimize BSFC and match stock torque at a given RPM or tune for maximum torque at a given throttle position and RPM and compare BSFC. Three valve positions were chosen. The three valve positions were 0°, 10°, and 20° degrees initially. The initial 0° valve setting is based on the valve closing the exhaust ports at the same moment the transfer ports close as shown in Figure 26. A numerically higher valve position refers to a retarding of the valve with respect to transfer port closure.

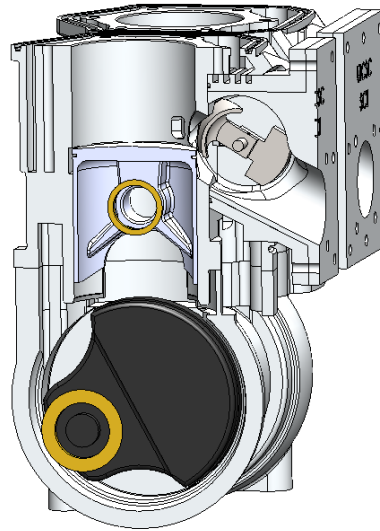


Figure 27: Charge Trapping Valve Location 0° Degree

These values could change, depending on in-cylinder pressure sensor data. The only foreseen problems with valve positions is that engine will not run if the valve closes too quickly, trapping a large portion of EGR in the cylinder and resulting in a noncombustible mixture. EGR could also be the result of the reduced scavenging efficiency from the use of a straight exhaust, but this should also be noticeable on the SCT baseline.

5.5 COMPARISONS

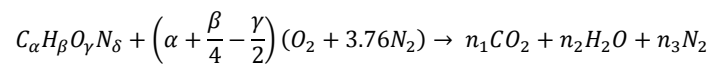
For comparison, an improvement in torque, BMEP, BSFC, and Trapping Efficiency and/or decrease in emissions over baseline 1 and baseline 2 at any valve position are sought. Once optimum valve positions are determined at the nine data collection points a valve position map can be recommended. It may result that the valve position does not need to be varied significantly and fixed valve timing will make the overall SCT system more robust.

6.0 ENGINE MAPPING

With the recent acquisition of engine exhaust emissions measurement equipment, it was proposed that a new means of engine tuning be implemented. Historically, DI engine

tuning at the University of Idaho has been accomplished using a lambda sensor, fuel flow measurements, engine torque, and engine power. Lambda is a ratio of the actual air/fuel ratio to the stoichiometric air/fuel ratio (AFR) for a given fuel. AFR is a ratio of the mass of air to the mass of fuel in a combustible mixture. Stoichiometric AFR values are found by assuming complete combustion and balancing the general chemical Equation for an arbitrary fuel as shown in Equation 3 [18].

$$\lambda = \frac{AFR_{actual}}{AFR_{stoich}}$$



$$AFR_{stoich} = \left(\alpha + \frac{\beta}{4} - \frac{\gamma}{2}\right)$$

Equation 3: Calculating AFR and Lambda Values

Engine mapping began by adjusting the IA while maintaining a constant lambda. The optimum lambda value varies as a function of engine speed and engine load. General rules of thumb have been established such that slightly lean mixtures are acceptable at low loads and/or low engine speeds while slightly rich mixtures are generally necessary at high loads and/or high engine speeds [10]. Rich mixtures are necessary to combat engine knock and keep exhaust gas temperatures (EGTs) at a reasonable level to prevent engine failure. Lean mixtures generally have fewer emissions as can be seen by the Figure 27 which shows the general relationship for a variety of harmful and non-harmful emissions species vs. equivalence ratio. [18].

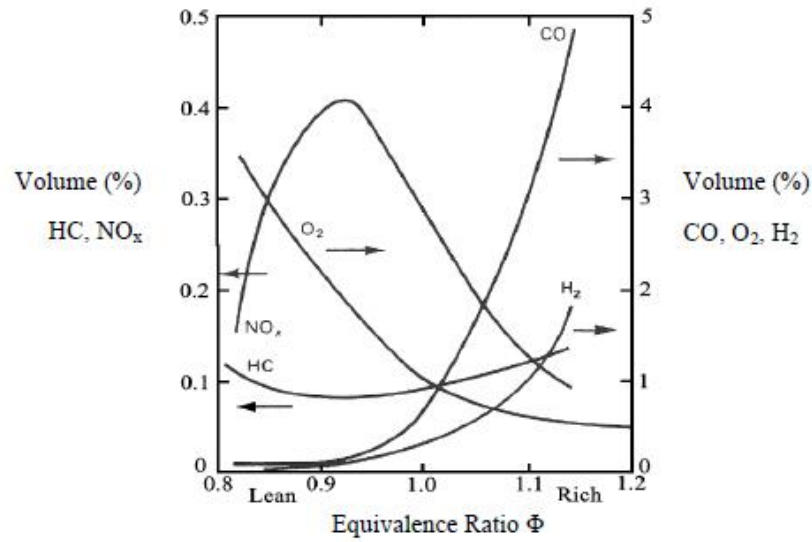


Figure 28: Exhaust Emissions as a Function of Equivalence Ratio

Equivalence ratio is the inverse of lambda and is the ratio of the actual fuel/air ratio to the stoichiometric fuel/air ratio [18]. An equivalence ratio greater than 1 corresponds to a rich mixture while an equivalence ratio less than one corresponds to a lean mixture. More information on the formation of exhaust emissions and combustion chemistry will be provided in a later section.

At every IA, engine torque, power, and fuel flow was recorded and a BSFC value was calculated using Equation 4. This allows an injection angle to be determined at which the engine is the most efficient at converting chemical energy to mechanical power. An example of an IA sweep is shown in Figure 28.

$$BSFC = \frac{\text{Fuel Flow}}{\text{Engine Power}}$$

Equation 4: Brake Specific Fuel Consumption Calculation

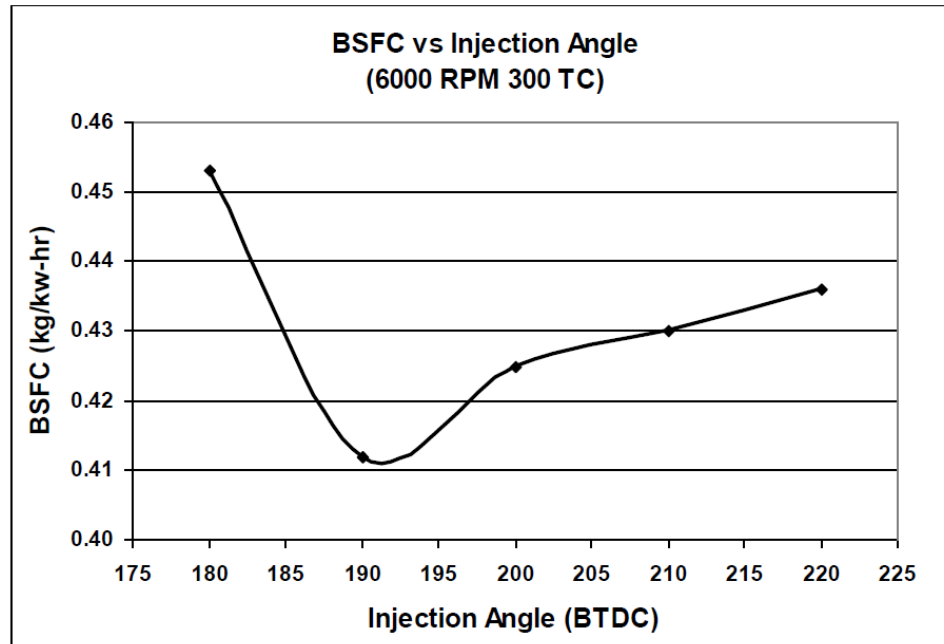


Figure 29: BSFC vs. Injection Angle

In Figure 28, it can be seen that the optimal IA corresponds to a value between 190° and 195° before top dead center (BTDC). Once this injection angle is established, a fuel sweep is run from the rich to lean limits of combustion. This produces a second graph shown in Figure 29. From Figure 29, an optimum lambda value can be determined to minimize BSFC at that specific operating condition. This process must be repeated throughout the operating range of the engine to develop a usable engine map.

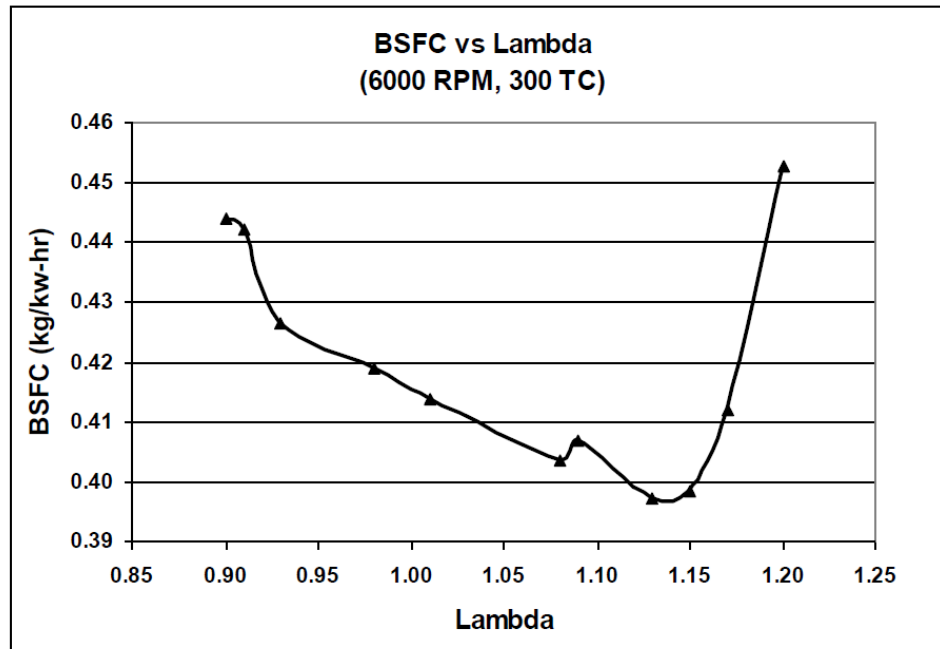


Figure 30: BSFC vs. Lambda

Several concerns have been expressed about this method of engine mapping. First, depending on the type of engine and method used to find lambda, in-cylinder lambda measurements can be very hard to obtain. In four-stroke engines, because there is a separation of the processes necessary for combustion, lambda measurements made in the exhaust system by a wide-band oxygen sensor can be accurate as long as there is not a large portion of valve overlap. A wide-band oxygen sensor works by measuring the difference in the partial pressures of oxygen in the exhaust stream and ambient air [18]. However, when used in a two-stroke engine a wideband oxygen sensor can give false readings due to the short-circuiting of fresh fuel and air as well as the return pulse from the tuned exhaust. This happens because the oxygen sensor can read the oxygen in the short-circuited mixture as a lean condition when the combusted mixture could be something entirely different. A more accurate tuning method has been proposed. An emissions analyzer can be used to measure the amount of CO in the exhaust products. By maintaining the same level of CO emissions, the combustible mixture is equivalent for every testing condition. This measurement is independent of the fuel/air mixture that may

be short-circuited and provides a more accurate measurement of actual combustion characteristics.

6.1 TUNING STRATEGY

1. For all test engines at each data point the injection angle will initially be set at 200° BTDC.
2. Injection quantity will then be varied to maximize torque.
3. CO% will then be measured and recorded for further tuning.
4. Injection angle will then be varied in 10 degree increments from 150 degrees to 200 degrees while maintaining the CO% found at maximum torque.
5. Injection angle will be recorded that gives maximum torque value.
6. Repeat steps 2-3 with new injection angle then proceed to step 7.
7. Injection angle, quantity, and CO% at maximum torque will now be known.
8. Next injection quantity will be varied to produce minimum BSFC.
9. CO% will then be measured and recorded for further tuning.
10. Fuel quantity and CO% at minimum BSFC will now be known.
11. Two maps will now have been developed: one producing maximum torque and one producing minimum BSFC for all throttle positions and RPMs

7.0 RESULTS OF EMISSIONS TUNING

Two methods of engine mapping were investigated during this work. Both methods manipulated the same variables in order to develop an engine map. However, the first method held lambda constant while the second held % CO in the exhaust stream constant. The advantage of using a wideband oxygen sensor and holding lambda constant is the response time of this type of system. Engine mapping can be accomplished quickly. Changes in IA and IQ are shown almost instantly and further adjustments can be made if necessary.

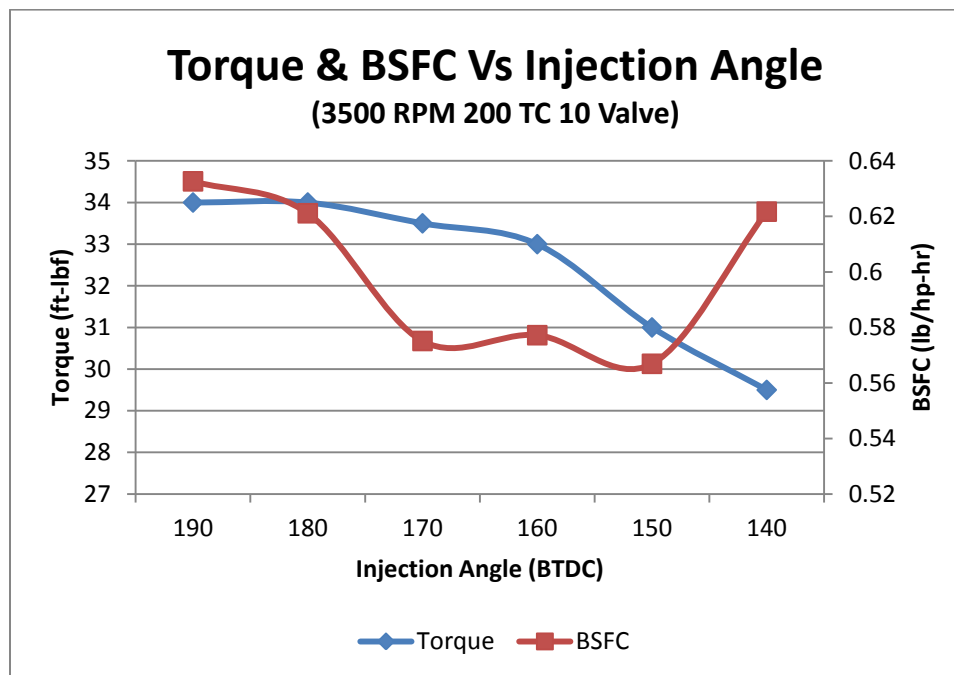


Figure 31: Torque and BSFC vs. Injection Angle Constant Lambda

Figure 30 shows the results of the IA sweep holding lambda constant at 3500 RPM 200 Throttle Counts (TC) and a 10° VP. TC is used to control engine load throughout this work and 10% throttle is equivalent to 100 TC. The minimum BSFC point was determined to be 150° BTDC. In Figure 31 the % CO in the exhaust stream was held constant and IA was again swept. By holding % CO constant, a clear minimum is established. The minimum BSFC occurs at an IA of between 150° and 140° BTDC. When compared to Figure 30 the percent difference is at most 6% if an IA of 140° is chosen to continue the mapping process. The main disadvantage of using the emissions analyzer to map the engine came in the response time. Because of the decreased reaction time of the MEXA-584L emissions analyzer, which has a maximum sampling rate of 1 Hz, and the increased time for the exhaust sample to move from the combustion chamber to the emission analyzer, the time necessary to fully map an engine increases dramatically.

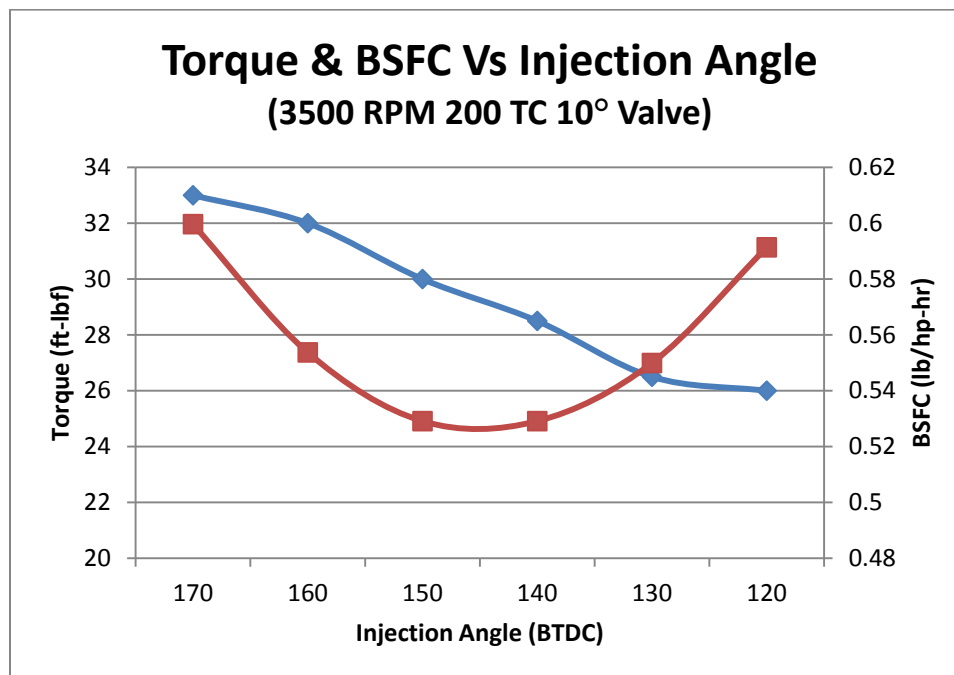


Figure 32: Torque and BSFC vs. Injection Angle Constant Percent CO

As a first approximation of IA, using a constant lambda value will increase the speed at which a base engine map is built. This becomes useful when time is more important than map quality. If emissions are of concern, a more in-depth mapping process can be implemented using an emission analyzer once a base map is built. When BSFC is combined with other emissions measurements, a clearer picture is introduced. Figure 32 shows emissions as a function of IA. UHC and NO_x emissions are reported in parts per million (PPM) and CO emissions are reported as a percent volume. By holding % CO constant a clear minimum in base emissions is established and corresponds to an IA of 140° BTDC. Although both the 150° and 140° BTDC IA have similar BSFC values in Figure 31, if an IA of 140° is selected a 19% decrease in UHC and 16% decrease in NO_x emissions is achieved while only dropping engine torque by 5%.

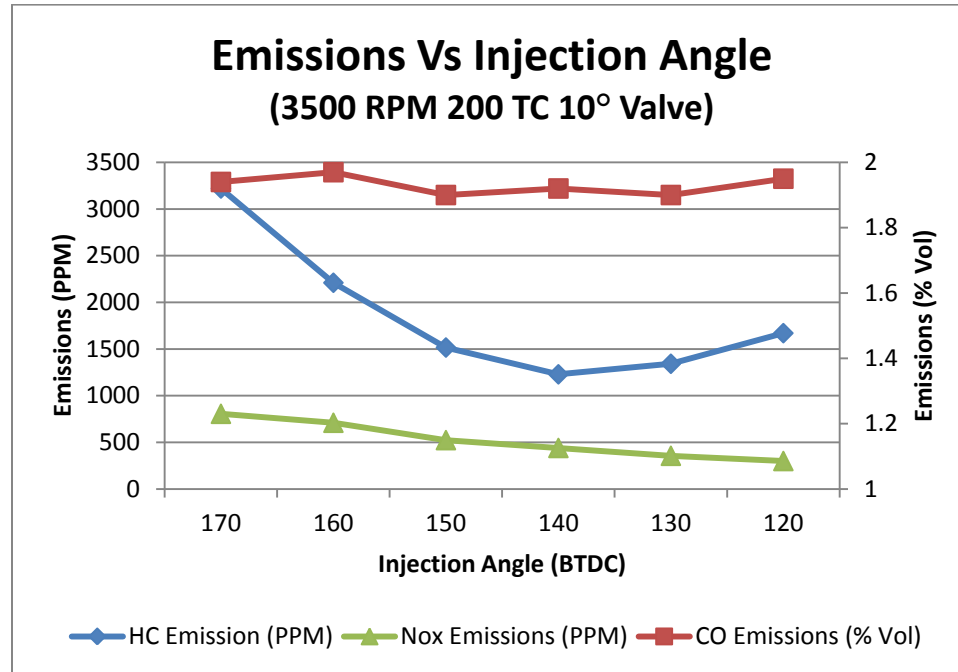


Figure 33: Emissions vs. Injection Angle

8.0 RESULTS OF PR-SCT

The main focus of this work was the further development of the University of Idaho's PR-SCT system. In Figure 33, torque as a function of engine speed at varying VPs is shown. At engine speeds of 4500 RPM and below, the PR-SCT engine makes more torque than baseline 1 and baseline 2 but above these RPMs the PR-SCT system falls below baseline 1 yet remains higher than baseline 2. The first conclusion that can be drawn from this is that the PR-SCT system should not be compared directly to baseline 1. By removing the tuned exhaust and RAVE 2 systems from both baseline 2 and the PR-SCT engines, the characteristics that the original engine had been designed around have changed dramatically. The base engine was designed with the intention of a tuned exhaust and power valve system being implemented. By eliminating these components, the scavenging and trapping efficiencies of the engine have changed.

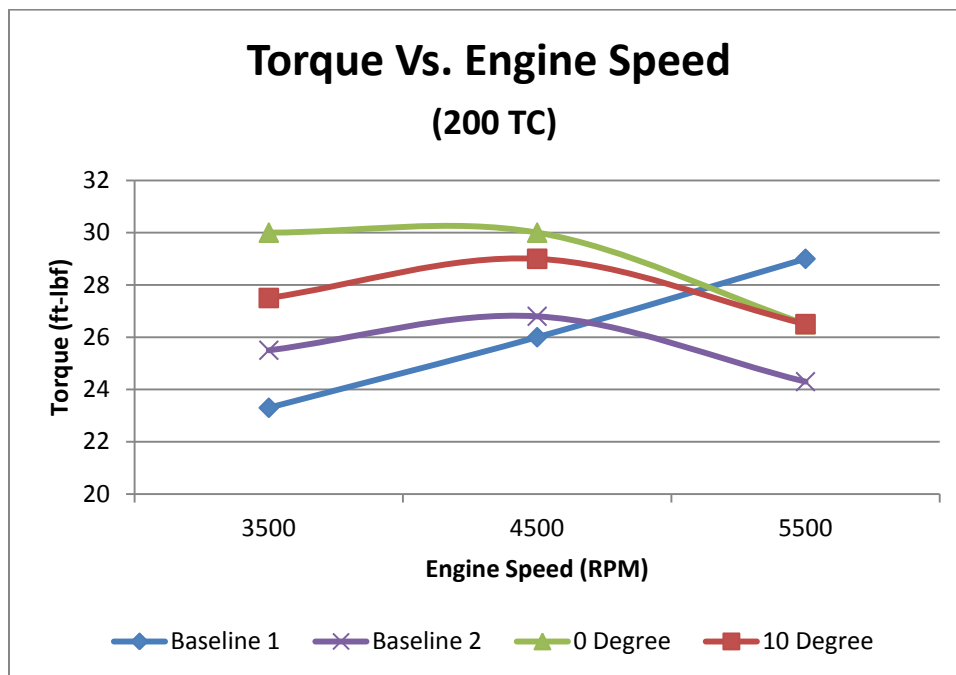


Figure 34: Torque vs. Engine Speed at 200 TC and Varying Valve Positions

Although, the tuned exhaust was not built for an operating speed of 5500 RPM it can still affect engine performance, especially when combined with a multi-position power valve system such as the RAVE 2. As discussed earlier, when operating below the design speed of the tuned pipe the negative and positive pressure pulses return too quickly. By implementing the RAVE 2 system, manufacturers were combating these mistimed pulses with lower exhaust port heights, regaining scavenging and trapping efficiencies. When compared to only baseline 2, the percent increase in torque of the PR-SCT engine at 3500 RPM and 200 TC was 18% and 8% at 0° VP and 10° VP respectively. When engine speed is increased, the percent increase drops to 12% and 9% at 4500 and 5500 RPM respectively. Although there is a slight difference in the 0° VP and 10° VP at 4500 RPM and 5500 RPM, it was neglected because of the relative error in the measurements. The relative error of the torque measurements are a function of the instability in the dynamometer equipment, the error in the dynamometer, and human interpretation. The instability in the dynamometer comes from its use of a proportional-integral-derivative controller (PID). This type of controller generally has minor oscillations around the desired set point. In the case of the dynamometer, this means that the torque applied is

constantly oscillating to maintain a desired engine speed. In most cases, on a well behaved engine, the oscillations are generally less than 2% of the average torque value. Because the dynamometer does not offer a simple interface for storing and manipulating data, such as averaging, the user generally records the engine torque and horsepower by hand which increases the possibility of human error. To quantify the error in torque measurements the root-sum-square (RSS) method was used. Human error was left out of the error analysis because quantifying human error for an experiment such as this was not part of this research. Therefore the relative error is a function of the dynamometer error and the error related to the instability of the system. The dynamometer error is 0.05% of the recorded torque and the error due to the instability is approximated as 2% of recorded torque.

Another measure of efficiency is engine BSFC. As discussed earlier, BSFC is a measure of how efficiently chemical energy is converted to mechanical power. Figure 34 shows a comparison of BSFC measurements for different engine speeds and VPs. Baseline 1 will not be included.

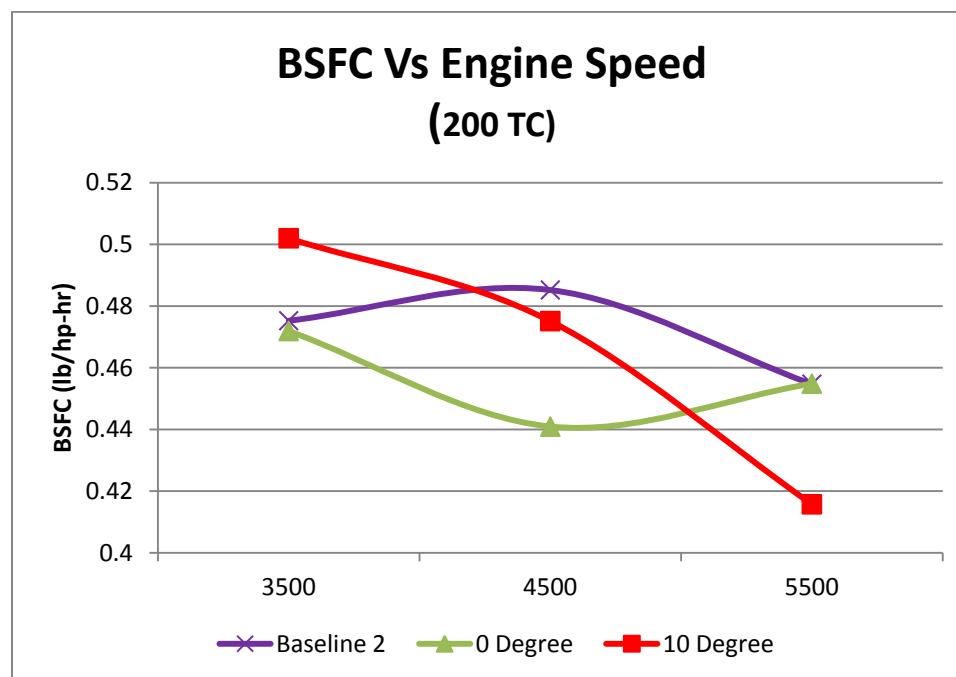


Figure 35: Brake Specific Fuel Consumption vs. Engine Speed

At an engine speed of 3500 RPM 200 TC, the BSFC of the PR-SCT engine at 0° VP decreased by 0.6% which, when the error is taken into account, the difference is negligible. The error on the BSFC measurement is calculated using an error propagation technique following Equation 5 [19].

$$error_{BSFC} = \sqrt{\left(error_{Fuel} \left(\frac{dBSFC}{dfuel} \right) \right)^2 + \left(error_{power} \left(\frac{dBSFC}{dpower} \right) \right)^2}$$

$$BSFC = \frac{fuel}{power}$$

$$\frac{dBSFC}{dfuel} = \frac{1}{Power}$$

$$\frac{dBSFC}{dpower} = -\frac{fuel}{power^2}$$

Equation 5: Error Propagation in Brake Specific Fuel Consumption

The error on the fuel flow measurement is 0.75% or better for gasoline [20]. However, as is the case for the dynamometer, there is no data logging function built into the fuel flow meter. Therefore, a total fuel flow measurement is recorded using a handheld stopwatch over a 30 second period and then fuel flow rates are calculated. Again the human error was not taken into account but must be mentioned. There is also an error associated with the fuel used that was not taken into account but must again be mentioned. The fuel used for this research was not from a certified source. Therefore, inconsistencies in fuel quality and ethanol content can result in variations in fuel flow requirements that were not included. The error associated with the BSFC calculation disregarding human error and fuel inconsistencies is less than 0.1% at most. This error is not included in the Figures containing BSFC because the error is very small relative to the difference between measured values.

At the 10° VP 3500 RPM 200 TC, the BSFC increased by almost 6%. This could be due to the reduced trapping efficiency at this valve position. However, since in-cylinder AFR is not known a trapping efficiency could not be measured. When the engine speed was increased from 3500 RPM to 4500 RPM both the 0° and 10° VP showed a decrease in

BSFC corresponding to 9% and 2% respectively. When engine speed was increased again, the BSFC decreased but the minimum BSFC corresponded to the 10° VP at a 6% decrease while the 0° VP showed a decrease of only 0.2% which is smaller than the error associated with the measurement. This reversal is thought to be the result of a large amount of EGR in the cylinder reducing engine power and efficiency. However, this cannot be proven with the emissions equipment currently available.

Next engine load was varied by changing the throttle position. Figure 35 shows engine torque as a function of engine load for varying VP. The baseline 2 engine was not able to run at higher engine loads. The decreased trapping efficiency, as a result of the removal of the RAVE 2 system and the tuned exhaust, caused engine instability and data could not be collected.

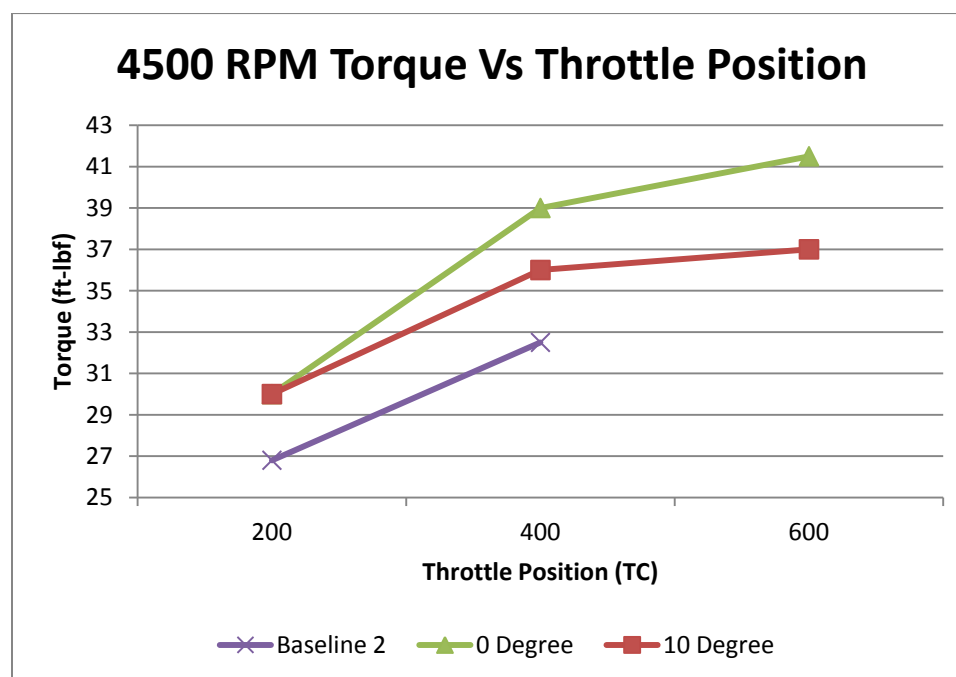


Figure 36: Torque vs. Engine Load Varying Valve Positions

Once the valve was included, higher load conditions were achieved and sustained. When compared to baseline 2, both the 0° and 10° VPs showed increases in torque. At 200 TC an increase of 11% was seen by both VPs but at higher TCs the 0° VP produced more

torque consistently than the 10° VP. A 9% increase and 12% increase over the 10° VP was seen at 400 TC and 600 TC respectively.

However, when comparing BSFC over the same operating range an interesting phenomenon occurs. As shown in Figure 36, an average of 6 % decrease in BSFC was seen at both valve positions at 200 TC with less than a 1 % difference between the two positions. At 400 TC, the BSFC decrease drops to an average of 3.5% but the difference between the 0° and 10° VP increases. This trend continues up to the 600 TC point. However, now the percent difference between the BSFC measurements is greater than the percent increase in torque seen in Figure 35 at a 12% increase in torque with an accompanying 18% increase in BSFC. This leads to the conclusion that although the 0° VP leads to a greater torque, the associated increase in BSFC negates the benefits of the increased torque. The optimum valve position becomes a function of both engine speed and load.

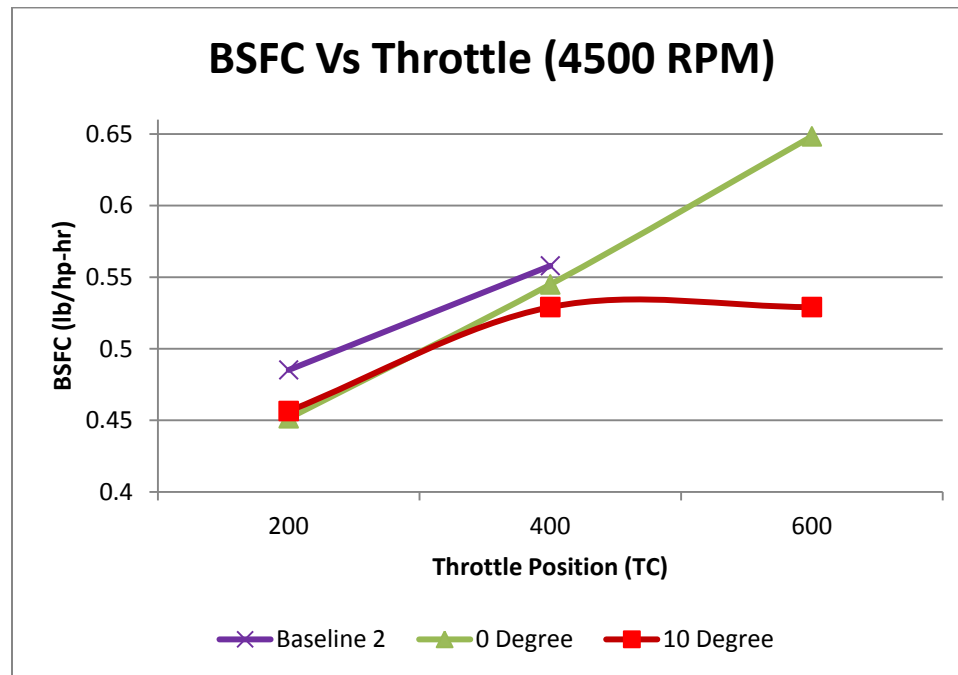


Figure 37: BSFC vs. Engine Load at 4500 RPM

8.1 EMISSIONS OF PR-SCT

With the ever increasing push for cleaner vehicles, it was necessary to investigate what effect the PR-SCT system had on exhaust emissions. The three main emissions products that are commonly considered are unburned hydrocarbons (UHC), carbon monoxide (CO), and oxides of nitrogen (NO_x).

8.2 EMISSIONS ERROR PROPAGATION

Errors in the emissions measurements that will be discussed in the next sections are a combination of three sources. The error associated with the particular emission being measured, the error associated with the fuel flow measurement needed to calculate the mass flow through the engine, and the error associated with the dynamometer. The same error propagation technique discussed earlier was used to calculate the error associated with each emissions measurement. The Horiba MEXA-584L 5 gas analyzer has the following error associated with each particular species being measured [11]. Although carbon dioxide (CO₂) is generally not considered a harmful emission when compared with the other byproducts its error is still needed due to the fact that the total carbon flow through the engine is needed to calculate brake specific emissions.

Component	CO, % of value	HC, % of value	NO _x , % of value	CO ₂ % of value
Measurement Error	3 %	5 %	5.6 %	5 %
Measured Unit	% volume	ppm	ppm	% volume

Table 3: Percent Error of Emissions Analyzer Associated with Measured Species

These errors combined with the errors associated with the dynamometer and the fuel flow measurements combine to form a total error using Equation 6. For a list of calculations see Appendix D.

$$\text{Brake Specific Emissions} = \frac{\text{Fuel Flow} (\% \text{ Emissions})}{\text{Total Carbon Power}}$$

$$\text{error}_{\text{emissions}} = \sqrt{\left(e_{\text{fuel}} \left(\frac{dBSE}{dfuel}\right)\right)^2 + \left(e_{\text{power}} \left(\frac{dBSE}{dpower}\right)\right)^2 + \left(e_{\text{emission}} \left(\frac{dBSE}{demissions}\right)\right)^2 + \left(e_{TC} \left(\frac{dBSE}{dTC}\right)\right)^2}$$

Equation 6: Error Propagation in Brake Specific Emissions

The final error associated with each measured species is shown in Table 4. These values are the average error associated with the brake specific emissions for the nine data points collected on each Figure to follow. Error bars were not included in the analysis because although the absolute value of the brake specific emission is not known to a high confidence, the repeatability of the measurements was generally high. This leads to the idea that the difference between data points is still valid. The main contributor to the error in these measurements was the fuel system and the emissions equipment. These will be discussed in further detail in a later section.

Component	CO, % of value	HC, % of value	NO _x , % of value
Measurement Error	164 %	103 %	182 %
Unit	$\frac{g}{kw * hr}$		

Table 4: Brake Specific Emissions Error for Various Species

8.3 UHC FORMATION AND RESULTS

In general the formation of UHCs comes from four main sources. In a two-stroke engine, a large amount of UHCs can be formed due to the short-circuiting of fresh charge into the exhaust system. This can happen as the result of operating outside the effective range of the tuned exhaust system. The PR-SCT system should be able to reduce this by trapping a larger amount of the fresh charge in the cylinder. The second mode of UHC formation is specific to DI fuel delivery systems. As shown previously in Figure 32, the IA plays a major factor in the amount of UHC produced. The later injection occurs, the less likely short-circuiting of the fresh charge will occur. This is true until fuel is injected so late in the process that mixing cannot occur and an incombustible mixture results. The third

mode of UHC formation is not dependent on engine type and is due to flame quenching and crevice volume filling. Flame quenching occurs when fuel adheres to the cylinder walls and combustion can only occur through evaporation and subsequent oxidation [10]. Crevice volume filling can occur when a propagating flame is extinguished when it reaches a narrow gap. In an engine this can happen in several places such as the threads of a spark plug or the groove of the piston ring [21]. This can be seen in Figure 37.

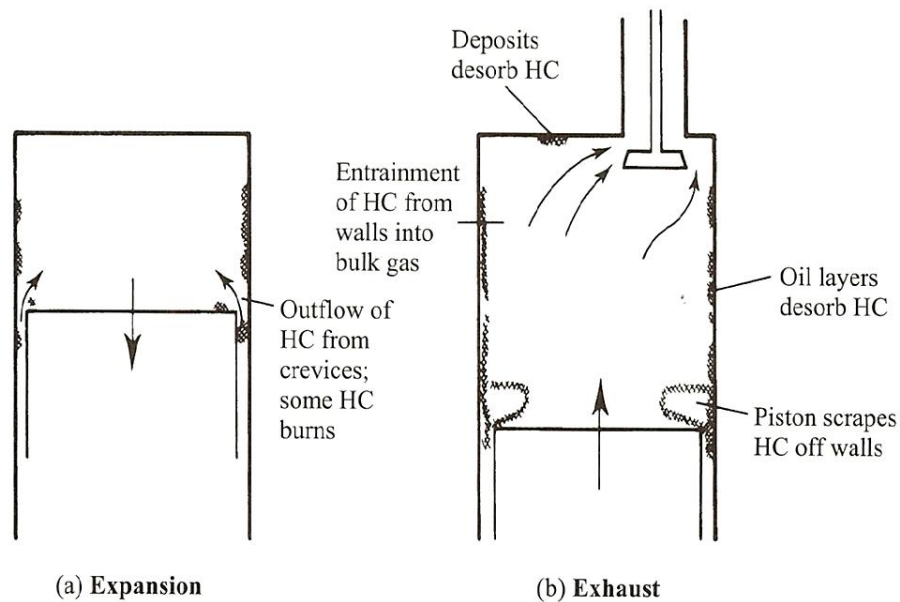


Figure 38: UHC Formation Due to Crevice Volume Filling and Flame Quenching

Once the flame is extinguished, the residual UHCs can be scraped into the scavenging flows and into the exhaust system. The final formation mechanism of UHCs comes from incomplete flame propagation [21]. If there is a large amount of EGR the combusting mixture may approach the flammability limit and there may be several cycles with little or no heat release. For more information on UHC formation in DI two- stroke engines refer to the thesis of Nathan Bradbury [10]. Figure 38 shows the brake specific hydrocarbon emissions (BSHC) vs. engine speed.

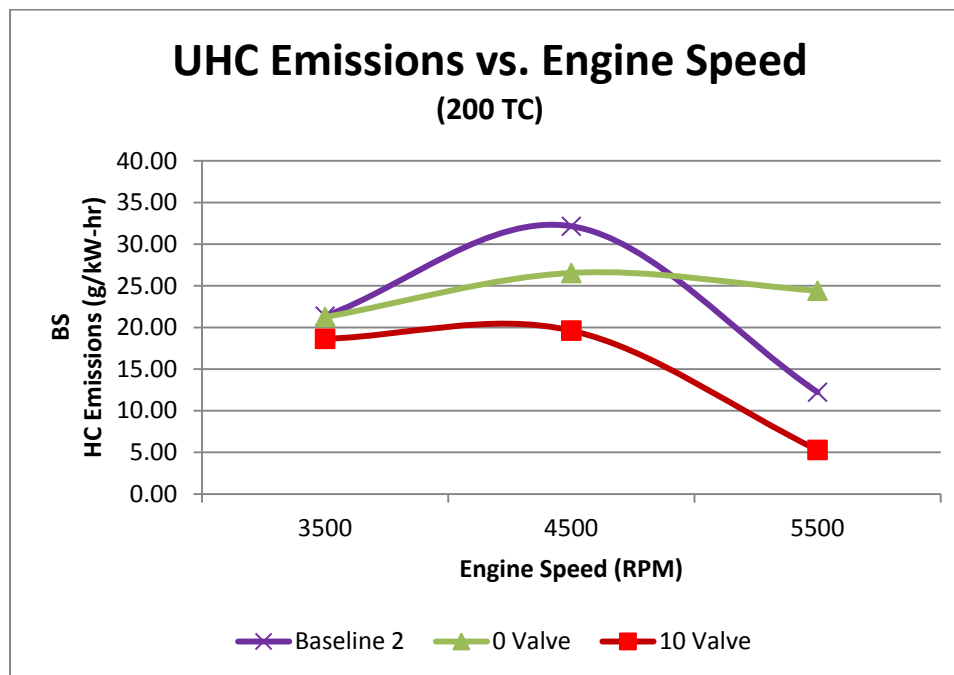


Figure 39: Brake Specific Hydrocarbon Emissions vs. Engine Speed

Brake specific emissions are used to describe the flow rate of a particular pollutant per unit power. It is often used to compare engines of different sizes and types. At 3500 RPM, the BSHC emissions are close enough that with the error associated with the measurements the difference between them is negligible. As the engine speed increases, the main factors that are contributing to UHC formation are a combination of IA and EGR. To what extent is unclear, as currently there is no way to measure EGR. This will be discussed further in the future work section below. At 4500 RPM, both the 0° and 10° VP have shown improvements in UHC emissions over baseline 2. Referring to Figure 38, the optimum IA for baseline 2 occurred at 170° BTDC. This was the earliest IA of the three calibration points and also corresponded to the largest BSHC. As engine speed increased to 5500 RPM, the 0° VP BSHC becomes the largest contributor potentially due to the increased IA as well as a larger percentage of EGR.

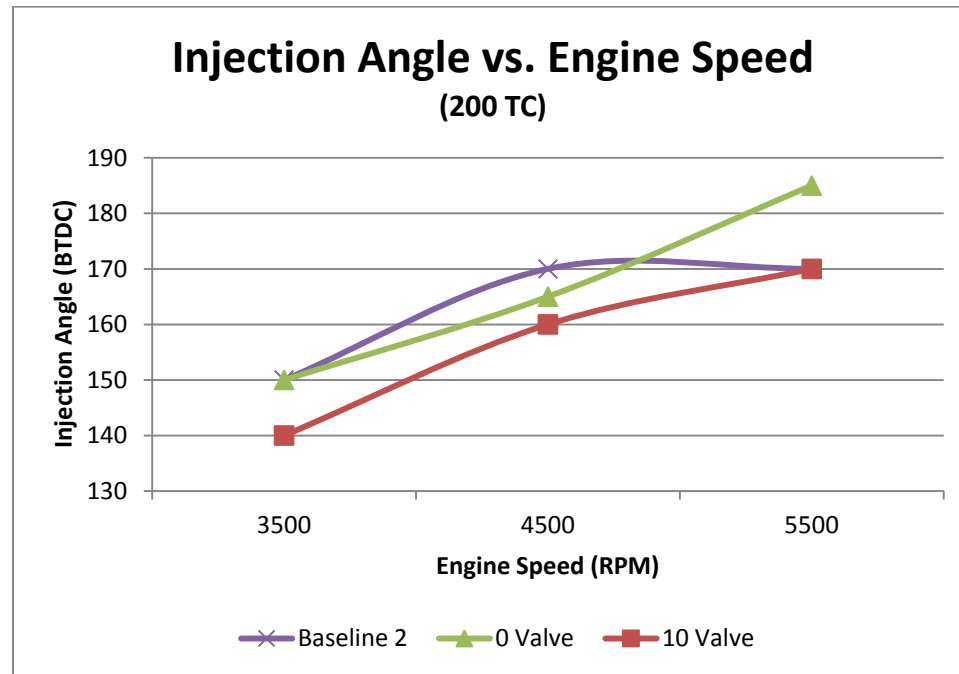


Figure 40: Injection Angle vs. Engine Speed for Emissions Comparison

8.4 CO FORMATION AND RESULTS

The formation of CO is similar in all SI engines. In general, CO formation occurs in an engine in a fuel rich condition. Operating with a lack of oxygen does not allow for the complete oxidation of the carbon in the fuel into carbon dioxide. There are three main reasons that a two-stroke engine may be operated fuel rich. The first is that excess fuel will cool the piston crown and prevent engine seizure. The second is that maximum power output occurs just rich of stoichiometric, and finally for rapid transient throttle response [10]. However, even if the engine is operated under fuel lean conditions CO is always present due to the dissociation of the carbon dioxide molecule. Dissociation is a process by which larger molecules are broken apart into smaller pieces.

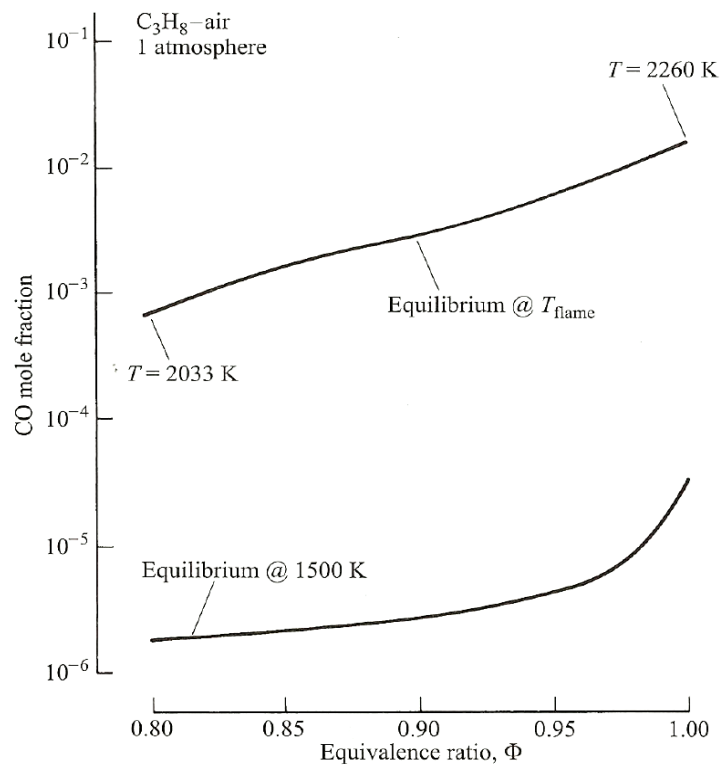


Figure 41: Carbon Monoxide Formation vs. Equivalence Ratio for Propane

This phenomenon is very strongly temperature dependent as can be seen in Figure 40 which shows the equilibrium CO levels vs. equivalence ratios for the combustion of propane at different temperatures [21]. Because temperatures after combustion fall very rapidly in a spark ignition engines, CO does not reach equilibrium at combustion temperatures and pressures but passes into the exhaust stream between equilibrium concentrations at peak combustion temperatures and pressures, and equilibrium concentrations at exhaust temperatures and pressures. For more information on the formation of CO refer to Turns [21]. In a DI fuel delivery system, IA again plays a significant role in CO formation. The larger the IA, the more time the mixture has to reach a homogeneous state, making for more complete combustion.

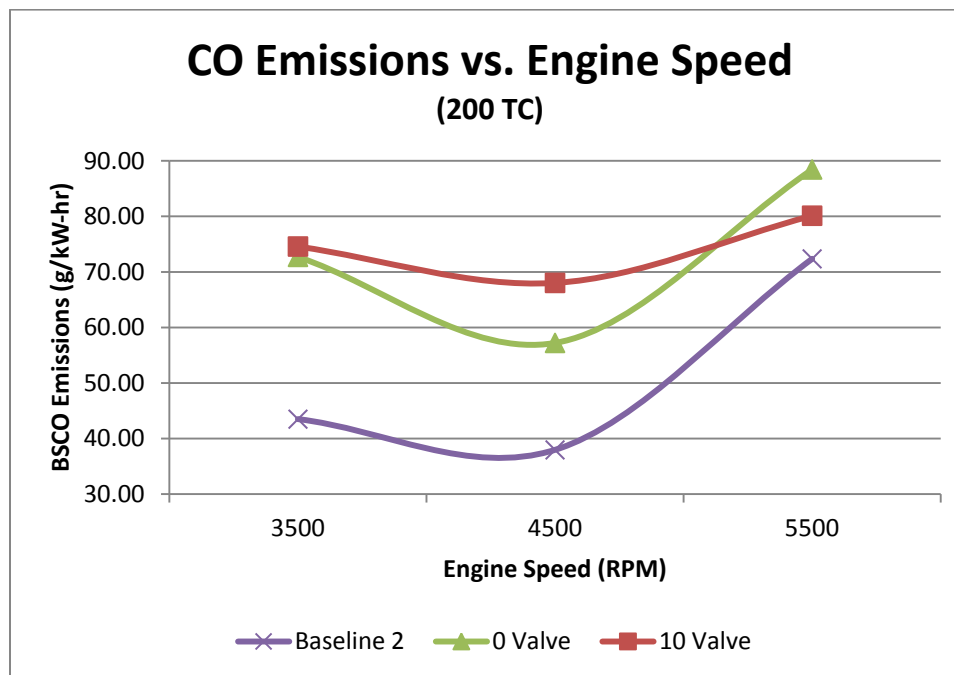


Figure 42: Carbon Monoxide Emissions vs. Engine Speed

Figure 41 above shows brake specific carbon monoxide (BSCO) emissions vs. engine speed. Baseline 2 has the lowest BSCO emissions across the entire operating range with an average 33% lower BSCO. This can be attributed to large IA providing adequate mixing time as well as low EGR from the removal of the charge trapping valve. At an engine speed of 3500 RPM, the 0° and 10° VP show no clear picture between because of the error associated with measurements. As engine speed increases to 4500 RPM, the highest BSCO corresponds to the lowest IA with increasing IA providing better BSCO for both the 0° and baseline 2 engine configurations. This leads to the conclusion that IA is playing more of a role in the formation of CO in the PR-SCT engine than any other factor.

8.5 NO_x FORMATION AND RESULTS

There are four main formation mechanisms of NO_x, assuming there is no nitrogen bonded to the fuel, including the Zeldovich mechanism, the Fenimore mechanism, the N₂O intermediate mechanism, and the NNH mechanism. The Zeldovich mechanism is also known as the thermal mechanism and is the primary means of formation. In order for the Zeldovich mechanism to progress, two things are necessary. First elevated temperatures

are necessary to begin the dissociation process and second there must be a sufficient supply of oxygen to dissociate and combine with the nitrogen molecules [10]. The other three mechanisms are used to describe the rapid formation of NO_x as a result of “super equilibrium” concentrations of oxygen and hydroxyl radicals. For more information regarding NO_x formation refer to Turns [21].

For combustion processes dominated by thermal NO_x formation, lowering the combustion temperature is the primary concern. Through the use of EGR, in cylinder temperatures, and subsequently NO_x formation, can be greatly reduced. This can be seen in Figure 42 in which exhaust nitric oxide concentrations are plotted against % EGR for varying equivalence ratios. The maximum NO_x formation occurs just lean of stoichiometric but decreases dramatically with the introduction of EGR. Unfortunately, in many practical devices operating just lean of stoichiometric provides the greatest efficiency.

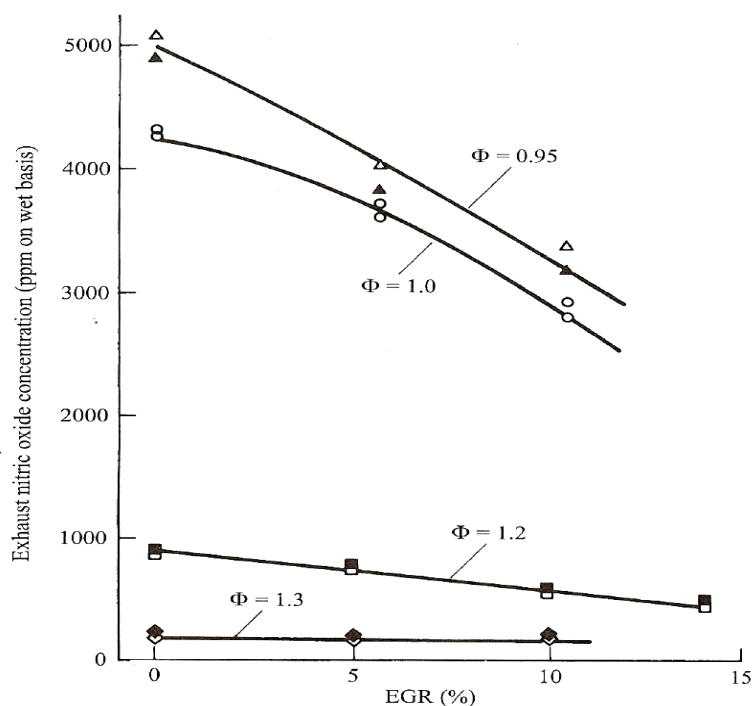


Figure 43: Nitric Oxide Concentration vs. Percent EGR at Varying Equivalence Ratios

The introduction of EGR decreases NO_x formation by increasing the heat capacity of the mixture for a given amount of heat release, resulting in lower combustion temperatures

[21]. Another way of decreasing NO_x formation in a SI engine is to retard the spark timing. By retarding the spark timing, the combustion event is shifted in such a way that the peak pressures occur well after TDC, resulting in lower pressures and temperatures.

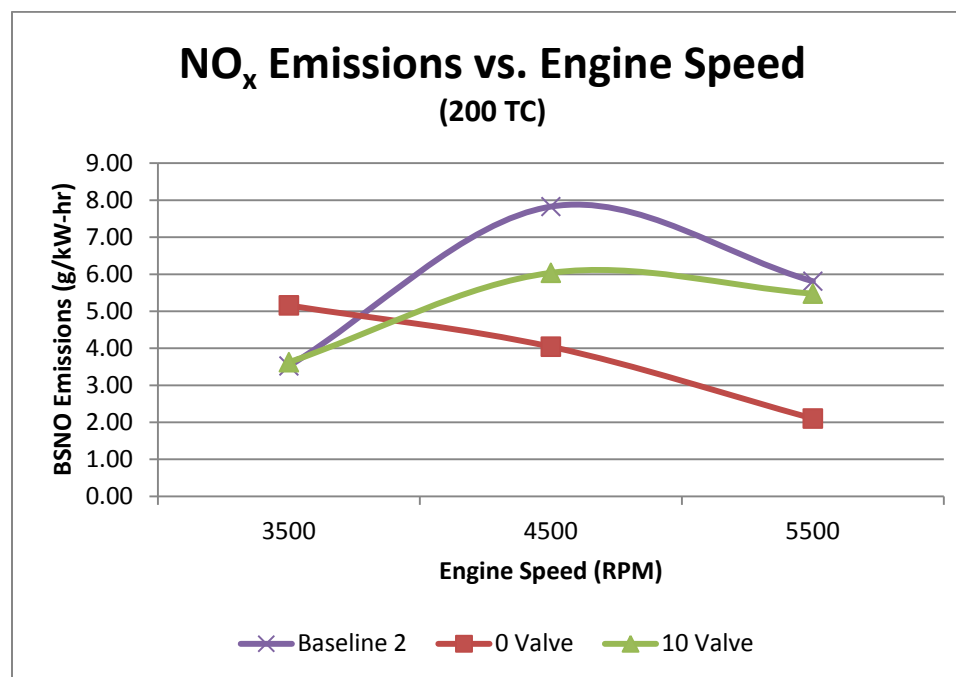


Figure 44: Oxides of Nitrogen Formation vs. Engine Speed

Figure 43 shows the brake specific NO_x (BSNO) formation at increasing engine speed. Because BSNO formation is so strongly dependent on combustion temperatures the idea that EGR is playing a significant role in many of the emissions by-products is easily seen above. For the 0° VP there is a very steady drop in BSNO as engine speed increases due a suspected increase in EGR due to the elimination of the tuned exhaust and charge trapping valve. At 3500 RPM baseline 2 and the 10° VP are too close for a clear picture to be drawn. However, the 0° VP shows a clear increase in BSNO due to a higher trapping efficiency of fresh charge that is not being diluted by EGR. As engine speed increases to 4500 RPM, baseline 2 shows the largest BSNO formation due to the elimination of the charge trapping valve and low EGR. Then as VP is decreased, more EGR is trapped in the cylinder and BSNO decreases. As engine speed increases again to 5500 RPM, the engine speed starts to affect EGR being trapped in baseline 2 which is

why baseline 2 and the 10° VP deviate very little. The 0° VP and 5500 RPM has the lowest formation of BSNO due to the high engine speeds and advance valve position.

9.0 CONCLUSIONS

- The major goals of this thesis were first and foremost to determine if synchronous charge trapping was still a viable research area.
- Second, to determine the best engine mapping process for use in further research both as a first round approach to get a base map and for fine tuning for efficiency/emissions.
- Next, to determine if the parallel rotary synchronous charge trapping system designed to replace the reciprocating style system did in fact show similar improvements in torque and brake specific fuel consumption.
- And finally, to determine the emissions characteristics of the PR-SCT system since emissions measurements had not yet been performed on a charge trapping system.

9.1 ENGINE MAPPING CONCLUSIONS

A systematic approach is needed when mapping a DI engine because of the sensitivity of the manipulated variables and their inherent interaction. In order to save time, a first round approximation for injection angle can be made using a wide band oxygen sensor. This method is much faster but slightly less accurate than using an exhaust emission analyzer. By holding lambda constant and sweeping injection angle, the minimum brake specific fuel consumption can be established. This represents the angle, for a specific calibration point, that is most efficient at converting the chemical energy in the fuel to mechanical power. Once this angle is established, the more time intensive emissions method can be implemented to fine tune the injection angle and quantity. By holding the % carbon monoxide constant, a more accurate representation of the combustion mixture is maintained at the expense of time.

9.2 PR-SCT CONCLUSIONS

The PR-SCT system had several distinct advantages over a similar test engine that did not include a charge trapping valve. Increases in torque were seen throughout the engine speeds tested during low load conditions at every valve angle tested. However, as engine speed increased the optimum valve position did not remain constant. When the engine was held at constant speed and load was increased, again the valve showed improvements in torque over the entire load range tested. However, BSFC was not always minimized with the inclusion of the valve. If the valve closed too early at higher engine speeds and loads, a large spike in BSFC could be seen. This is thought to be due to the fact that an increase in EGR caused unstable combustion and a reduction in torque. However, this could not be definitively proven given the current measurement equipment available. in Table 5 is a graph of the valve position vs. engine speed and load that could be potentially implemented to maximize torque and minimized BSFC.

	Engine Speed (RPM)				
Throttle Position	3500	4000	4500	5000	5500
20%					
30%		0° Valve			
40%					
50%			10° Valve		
60%					

Table 5: Valve Position for Maximizing Torque and Minimizing BSFC

Although the PR-SCT system did show improvements in both UHC and NO_x emissions, the current engine mapping technique was based on increasing engine efficiency only and comparing emissions. Without specifically tuning to minimize emissions, there is

potential for a further exhaust emissions reduction but torque and efficiency may need to be sacrificed to some extent.

10.0 FUTURE WORK

There are a variety of research areas that should still be explored with the PR-SCT engine in the future. The first area is an accurate measurement of the percent of the residual exhaust gas during the combustion event due to the valve. Without knowing how much EGR is in the cylinder, the characteristics of this engine are not fully understood.

Generally, carbon dioxide is measured and compared both in the intake and exhaust streams. However, this only works when exhaust gas is pumped back into an engine's intake system. Since this is not the case with the charge trapping engine, the scavenging efficiency may have to be measured and a correlation to EGR determined.

In order to increase the scavenging efficiency that was lost, a tuned exhaust system should be reintroduced. This has several advantages. First, by reintroducing a tuned pipe, similar to the one used on the baseline 1 engine, a comparison between the PR-SCT engine and baseline 1 could be made, as base engine performance should more closely match. As shown in the data previously, even though the tuned pipe is not "tuned" for the operating range that was under investigation, the effects of not having it were still noticed at engine speeds over 4500 RPM. This leads to the final advantage. By including the tuned pipe, not only could the trapped volume be increased but potentially the mistimed pressure pulse could be captured as well. This would lead to an even greater increase in engine torque and efficiency at low speed low load conditions.

In order to increase the confidence interval of the emissions measurements a repeatability study should be performed and more accurate exhaust analysis equipment obtained. If the error on the exhaust measurement system was improved by a factor of ten the percent error would drop by an average of 80% between measured exhaust species. If more accurate equipment is not attainable, the repeatability analysis would be useful to make sure the equipment is in fact showing a change in harmful emissions with the inclusion of the valve.

REFERENCES

- [1] A. Findlay and et.al., "University of Idaho's Clean Snowmobile Design Using a Direct-Injection Two-Stroke Engine," Not Yet Published, Moscow, 2007.
- [2] A. Bolland, I. Lootens, G. Hilbert and E. & Buddrius, "Muffler Deisgn and Cat Integration," Not Yet Published, Moscow, 2011.
- [3] J. Nichols, N. Miller and C. Hill, "Rear Drive System," Not Yet Published, Moscow, 2012.
- [4] ISMA. [Online]. Available: http://www.snowmobile.org/pr_snowfacts.asp. [Accessed 1 March 2012].
- [5] J. E. McCarthy, "Snowmobiles: Enviromental Standards and Access to National Parks," Library of Congress, 2002.
- [6] L. C.C. and W. J.J., "Laboratory Testing of Snowmobile Emissions," Southwest Research Institute, San Antonio, 2002.
- [7] P. Britanyak, "Synchornous Charge Trapping Modification of a Two-Stroke Engine," Master's Thesis, Moscow, 2010.
- [8] "SAE Collegiate Design Series," 8th May 2007. [Online]. Available: <http://students.sae.org/competitions/snowmobile/results/>. [Accessed 3 April 2012].
- [9] M. Nuti, "Emissions form Two-Stroke Engines," Society of Automotive Engineers, Inc., Warrendale, 1998.
- [10] N. E. Bradbury, "Retrofitting Direct-Injection and a Turbocharge to a Two-Stroke Engine for Snowmobile Applications," Master's Thesis, Moscow, 2006.
- [11] D. Dixon, "Comparison of Variable Exhaust Flow Techniques in a modern Two-Stroke Engine," Master's Thesis, Moscow, 2012.

- [12] Yamaha, 15 April 2009. [Online]. Available: <http://www.yamaha-motor.eu/designcafe/en/about-design/technology/index.aspx?segment=About%20Design%20-%20Technology&view=article&id=440980>. [Accessed 16 April 2012].
- [13] "Wikipedia," August 2005. [Online]. Available: http://en.wikipedia.org/wiki/Fuel_injection. [Accessed 17 April 2012].
- [14] F. H. D. C.-L. M. Zhao, "Automotive Gasoline Direct-Injection Engines," Society of Automotive Engineers, Inc., Warrendale, 2002.
- [15] J. Johnson, "Comparison of Stratified and Homogenous Combustion in a Direct-Injected Two-Stroke Engine for Snowmobile Applications," Master's Thesis, Moscow, 2007.
- [16] J. Turner, D. W. Blundell, D. B. Larkman, P. Burke and R. J. Pearson, "Omnivore: An Automotive Flex-Fuel 2-Stroke Engine with Variable Compression Ratio, Variable Charge Trapping, and Direct Fuel Injection," Lotus Engineering, 2009.
- [17] P. Boyd, "Catalytic Plasma Torches for Optimization Studies in a Cooperative Fuels Research (CFR) Engine," Master's Thesis, Moscow , 2012.
- [18] R. Stone, "Introduction to Internal Combustion Engines," Macmillian Press LTD, Chippenham, 1999.
- [19] R. S. Figliola and D. E. Beasley, "Theory and Design for Mechanical Measurements," John Wiley and Sons, New Jersey, 2006.
- [20] M. M. F. F. Equipment, Operators Manual, 2005.
- [21] S. R. Turns, "An Introduction to Combustion Concepts and Applications," Mc-Graw Hill, New York, 2011.

- [22] P. Hooper, T. Al-Shemmeri and M. Goodwin, "Advanced Modern Low-Emission Two-Stroke Cycle Engines," Proceeding of the Institution of Mechanical Engineers, Part D: Journal of Automobile Engineering, 2011.
- [23] A. Furhman, A. Hooper, T. Lord and C. Bode, "Synchronous Charge Trapping Final Report," Not Yet Published, Moscow, 2011.
- [24] M. Tech, "Keweenaw Reseach Center," Michigan Technological University, 1998. [Online]. Available: www.mtukrc.org. [Accessed 15th April 2012].
- [25] Horiba, "Owners Manual MEXA 584L".

APPENDIX A: PR-SCT DRAWING PACKAGE

ITEM NO.	PartNo	DESCRIPTION	QTY.	Sheet
1	Assem_1	Assembly of Jug components	2	
2	Assem_2	Rotating valve assembly	1	
3	Assem_3	Belt-train Assembly	1	
4	0	600 Rotax Case	1	

DIMENSIONS ARE IN METERS

THIRD-ANGLE PROJECTION

DEFUALT TOLERANCES:

LINEAR: X, Y, Z: .25
X, Y, Z: .1
X, Y, Z: .030
X, Y, Z: .01
X, Y, Z: .002

ANGULAR: X, Y, Z: .5
X, Y, Z: .1
X, Y, Z: .030

UNIVERSITY OF IDAHO
ME DEPARTMENT

3/23/2011

Part #:

Scale: 1:6

QTY: SHEET 1 OF 23

Short Circuit

UNIVERSITY OF IDAHO
ME DEPARTMENT

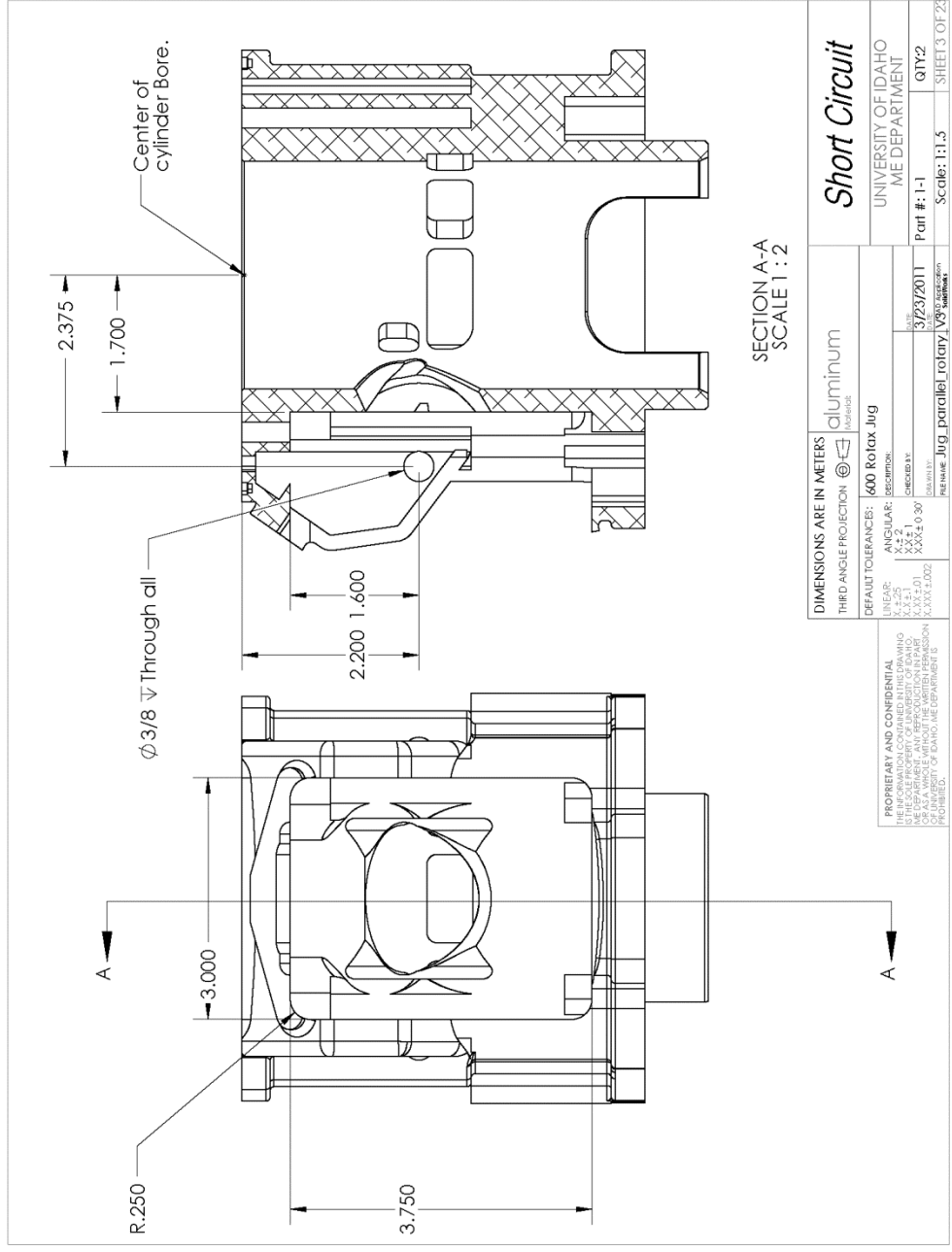
3/23/2011

Part #:

Scale: 1:6

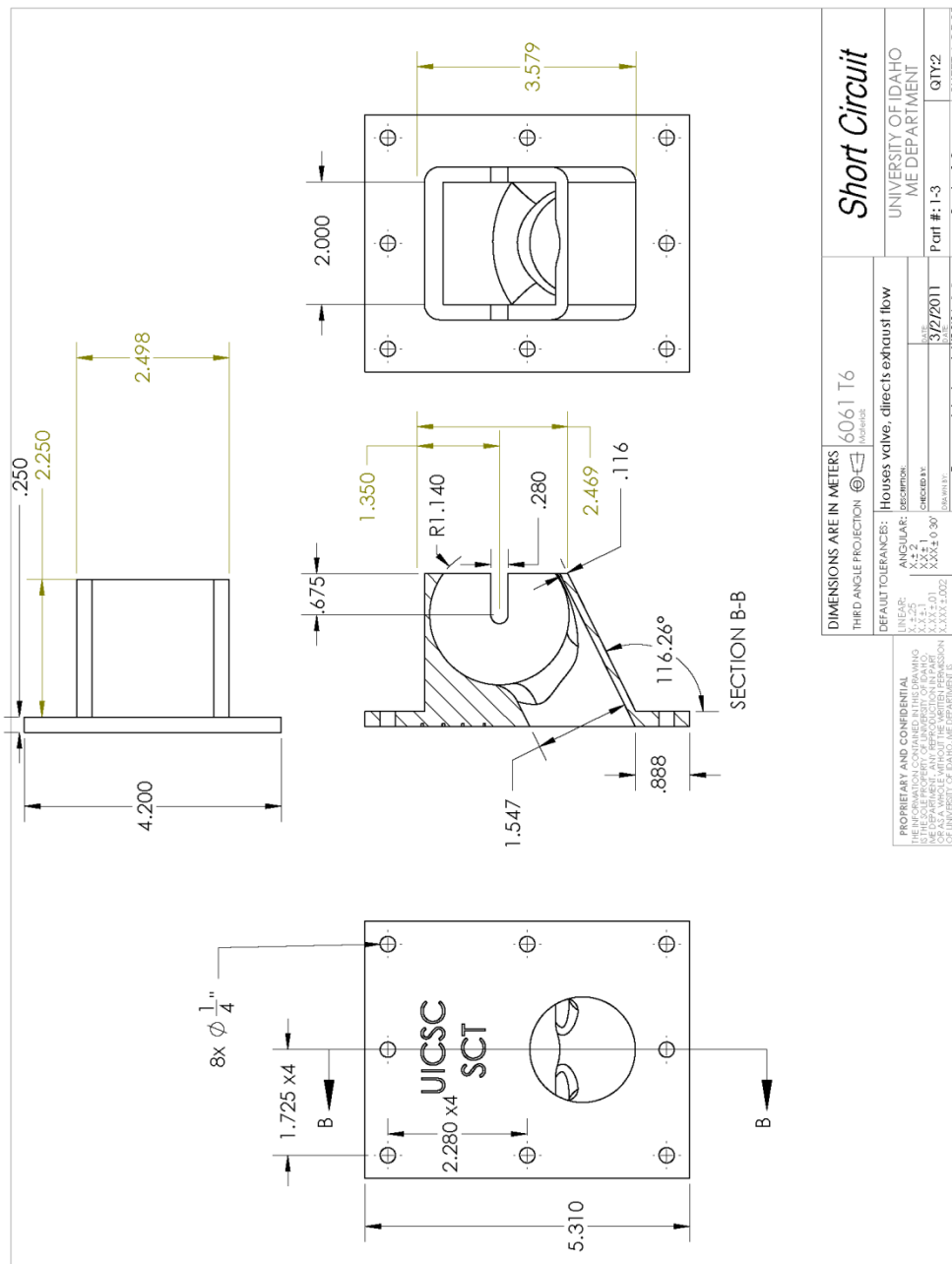
QTY: SHEET 1 OF 23

PROPRIETARY AND CONFIDENTIAL
THE INFORMATION CONTAINED IN THIS DRAWING IS THE PROPERTY OF THE UNIVERSITY OF IDAHO. IT IS TO BE USED FOR THE DESIGNATION OF A PART OR FOR IDENTIFICATION OF A PART ONLY. REPRODUCTION OR TRANSMISSION OF ANY INFORMATION CONTAINED HEREIN IS PROHIBITED.



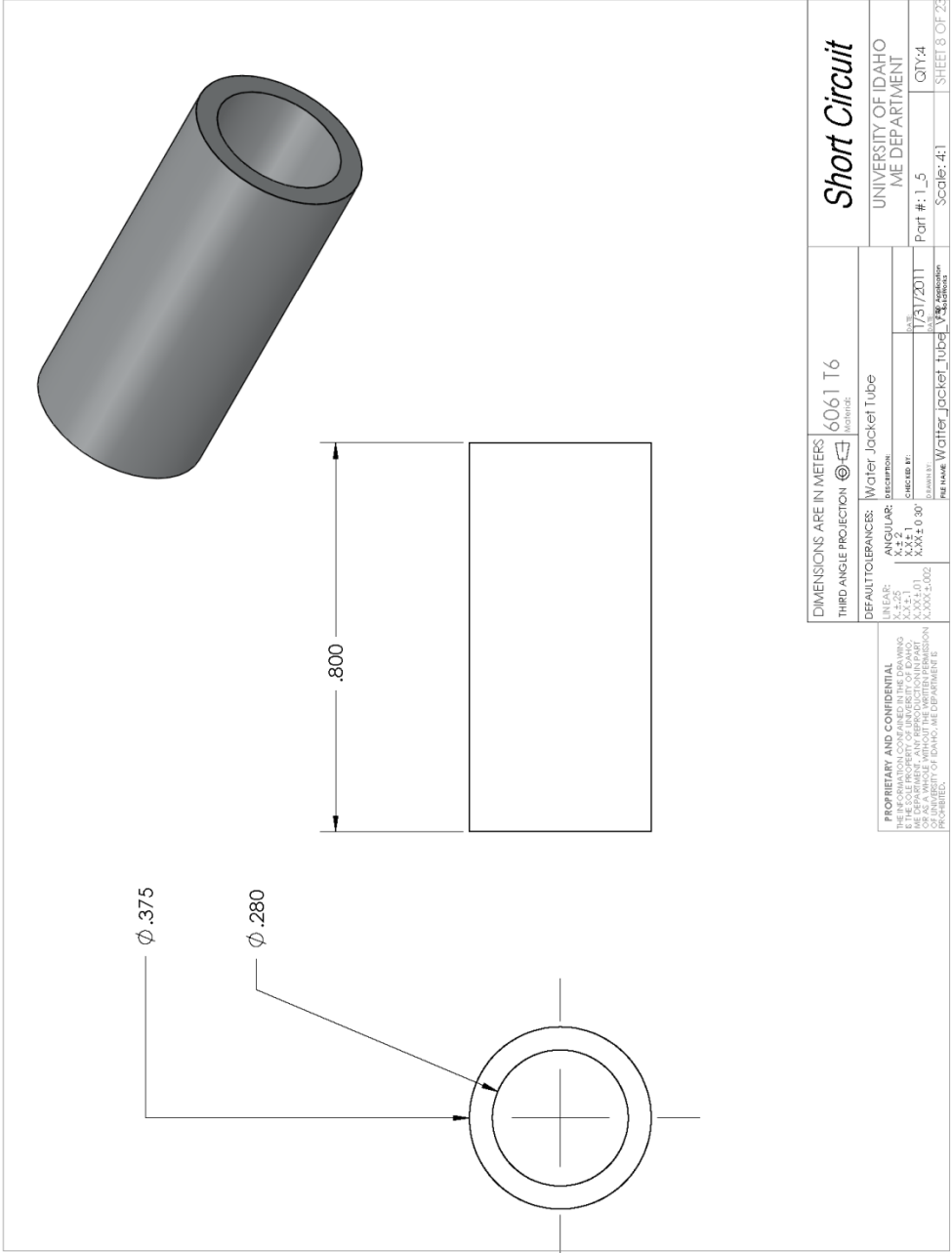
DIMENSIONS ARE IN METERS		aluminum	Short Circuit
THIRD ANGLE PROJECTION	600 Rotax Jug	UNIVERSITY OF IDAHO ME DEPARTMENT	
DEFAULT TOLERANCES:	ANGULAR:	3/23/2011	QTY2
LINEAR:	XXX.X	DATE BY:	SCALE: 1:1.5
XXX.XX	XXX.XX	PAGE NO. 30	
XXX.XXX	XXX.XXX	FILE NAME: Jug_parallel_rotary	SHEET 3 OF 23
XXX.XXXX	XXX.XXXX		

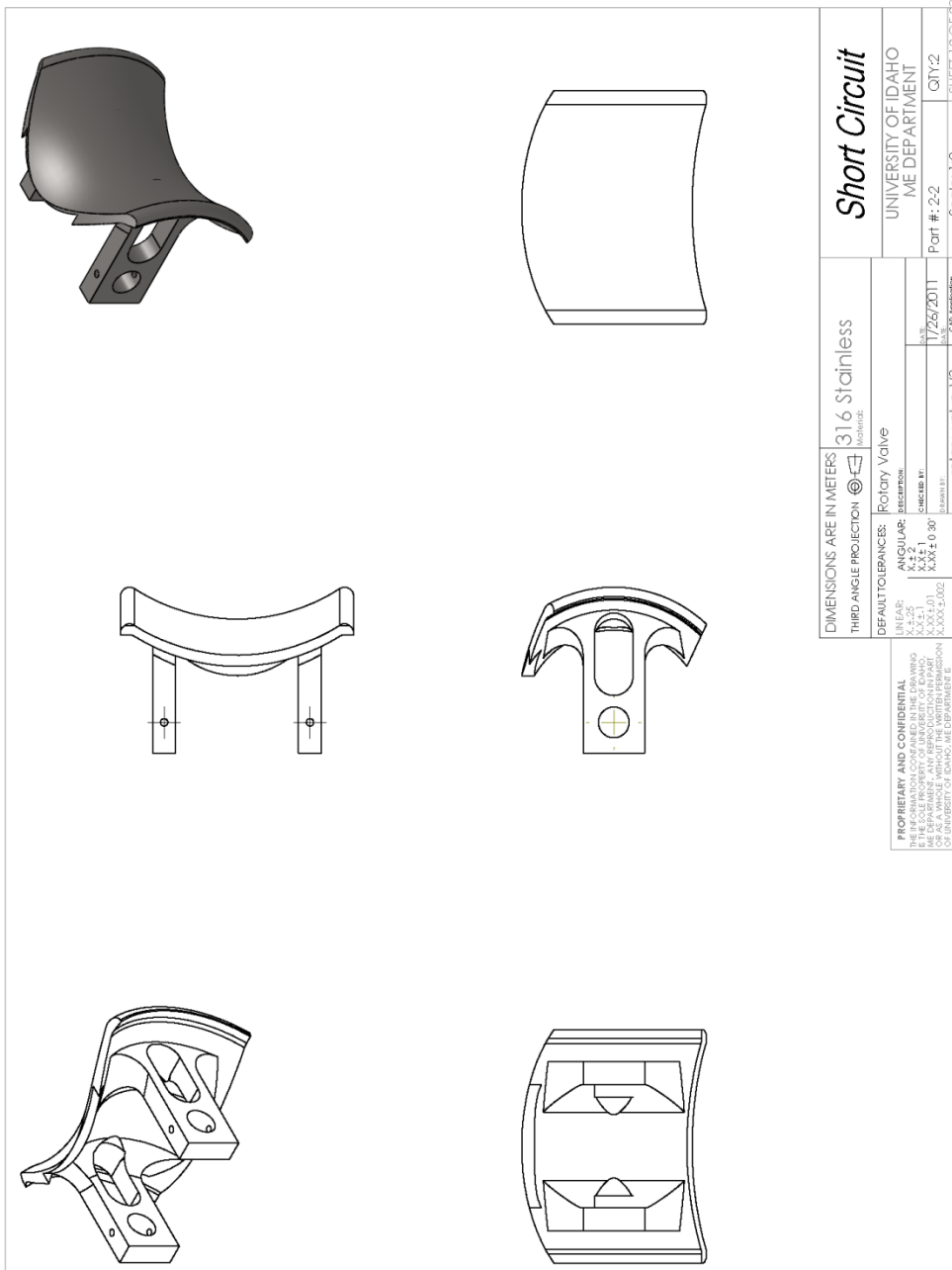
PROPRIETARY AND CONFIDENTIAL
 THE INFORMATION CONTAINED IN THIS DRAWING IS THE SOLE PROPERTY OF UNIVERSITY OF IDAHO. IT IS TO BE USED ONLY FOR THE PROJECT AND FOR A SINGLE WORK WITHOUT THE WRITTEN PERMISSION OF UNIVERSITY OF IDAHO, ME DEPARTMENT IS PROHIBITED.



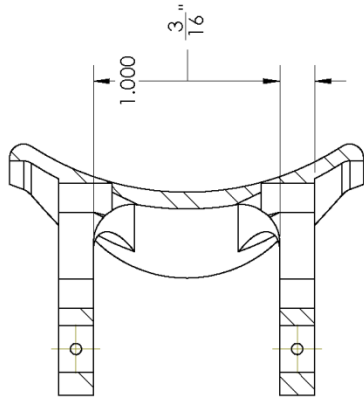
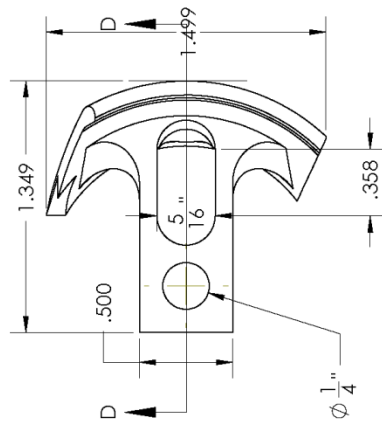
DIMENSIONS ARE IN METERS		6061 T6
THIRD ANGLE PROJECTION		Third Angle
DEFAULT TOLERANCES: Houses valve, directs exhaust flow		
LINEAR:	ANGULAR:	RESISTION:
X.XX5	X.X2	
X.XX1	X.X1	
X.XX0	XXXX.0	
X.XXX	XXXX.002	
PROPRIETARY AND CONFIDENTIAL THE INFORMATION CONTAINED IN THIS DRAWING IS THE SOLE PROPERTY OF UNIVERSITY OF IDAHO. IT IS TO BE USED FOR THE PROJECT AND NOT TO BE REPRODUCED OR TRANSMITTED IN ANY FORM OR BY ANY MEANS WITHOUT THE WRITTEN PERMISSION OF UNIVERSITY OF IDAHO, THE CORPORATION OF IDAHO.		
UNIVERSITY OF IDAHO ME DEPARTMENT		Part #: 1-3
DATE: 3/2/2011		Scale: 1:2
DRAWN BY: Removable_insert_V3		QTY: 2
SHEET 6 OF 23		

Short Circuit





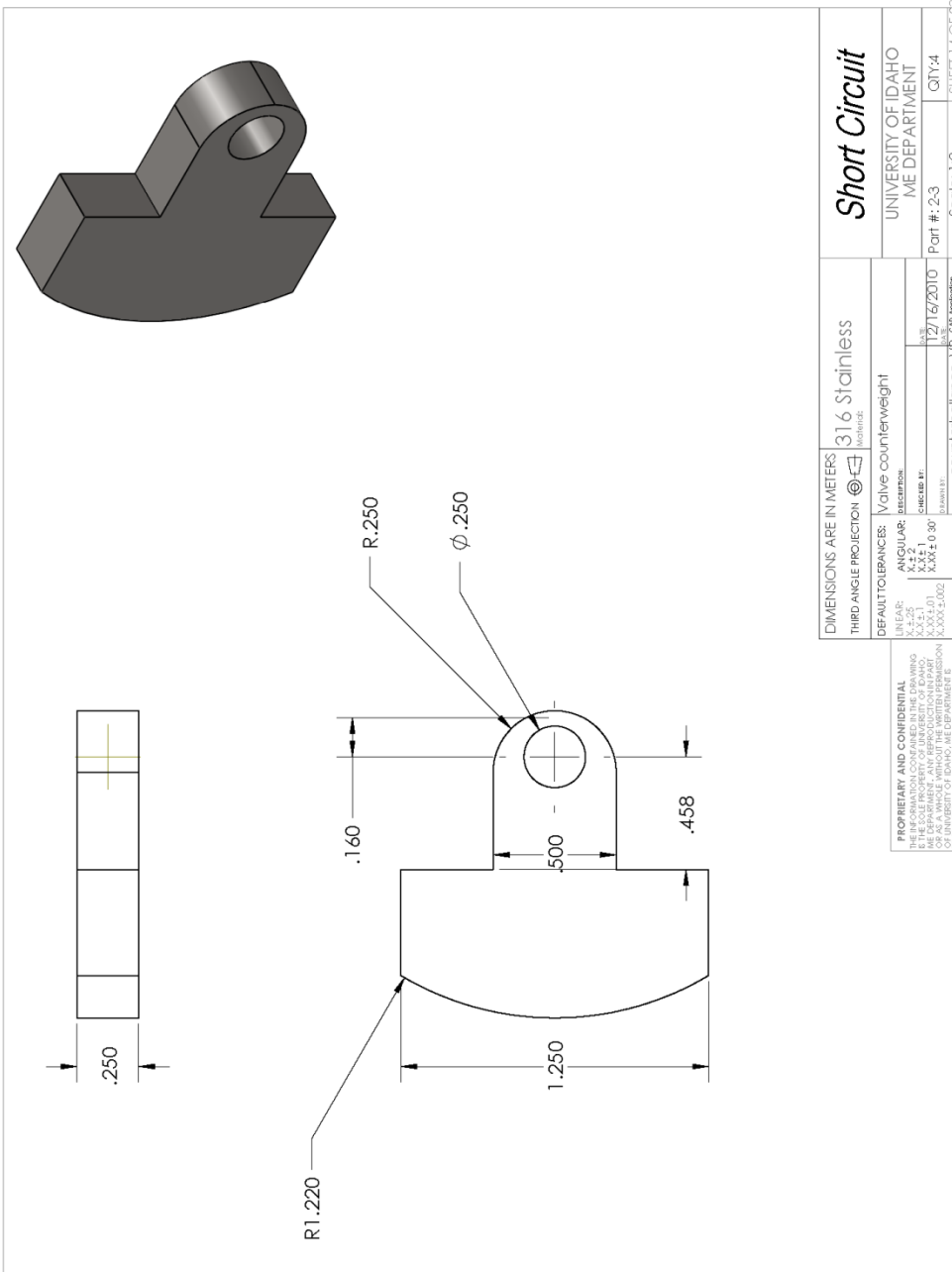
DIMENSIONS ARE IN METERS THIRD ANGLE PROJECTION		316 stainless <small>Material:</small>	Short Circuit UNIVERSITY OF IDAHO ME DEPARTMENT
DEFAULT TOLERANCES: FINISH: ANGULAR: HOLE: HOLE TO Ø: HOLE TO Ø:0.02		ROTARY VALVE <small>Description:</small> 1:1:25 1:1:25 1:1:25 1:1:25 1:1:25 1:1:25	Part #: 2-2 QTY: 2 Scale: 1:2 SHEET 12 OF 23
PROPRIETARY AND CONFIDENTIAL THE INFORMATION CONTAINED IN THIS DRAWING IS THE SOLE PROPERTY OF UNIVERSITY OF IDAHO. IT IS TO BE USED FOR THE PROJECT AND NOT TO BE REPRODUCED OR TRANSMITTED IN ANY FORM OR BY ANY MEANS, WITHOUT THE WRITTEN PERMISSION OF UNIVERSITY OF IDAHO, THE CORPORATION & PROHIBITED.		FILE NAME: TOTQTY_VALVE_V3 <small>Organization:</small>	7/26/2011 <small>Date:</small>



SECTION D-D

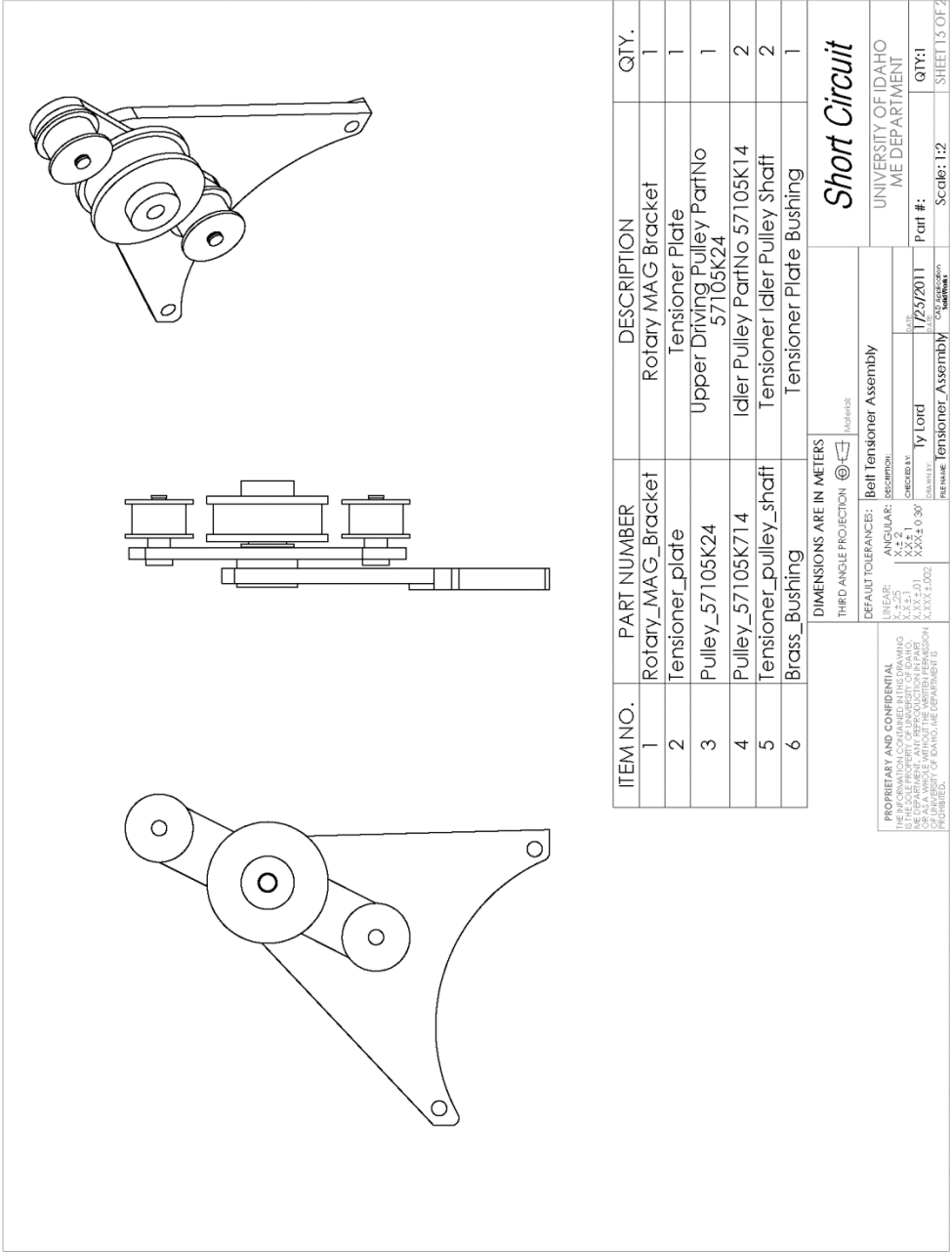
DIMENSIONS ARE IN METERS		316 stainless	Short Circuit
THIRD ANGLE PROJECTION	Rotary Valve	UNIVERSITY OF IDAHO ME DEPARTMENT	
DEFAULT TOLERANCES:	LINEAR:	ANGULAR:	Part #: 2-2
	X.XX5	X.X	Scale: 1.5:1
	X.XX2	X.XX1	QTY: 2
	X.XX1	FAVOR 0.00	DATE: 1/24/2011
	X.XX0		DESIGNED BY: [Signature]
	X.XXX ±.002		CHECKED BY: [Signature]
			DATE: 1/24/2011
			FILE NAME: ROTARY_VALVE_V3
			DATE: 1/24/2011
			SCALE: 1.5:1
			SHEET 13 OF 23

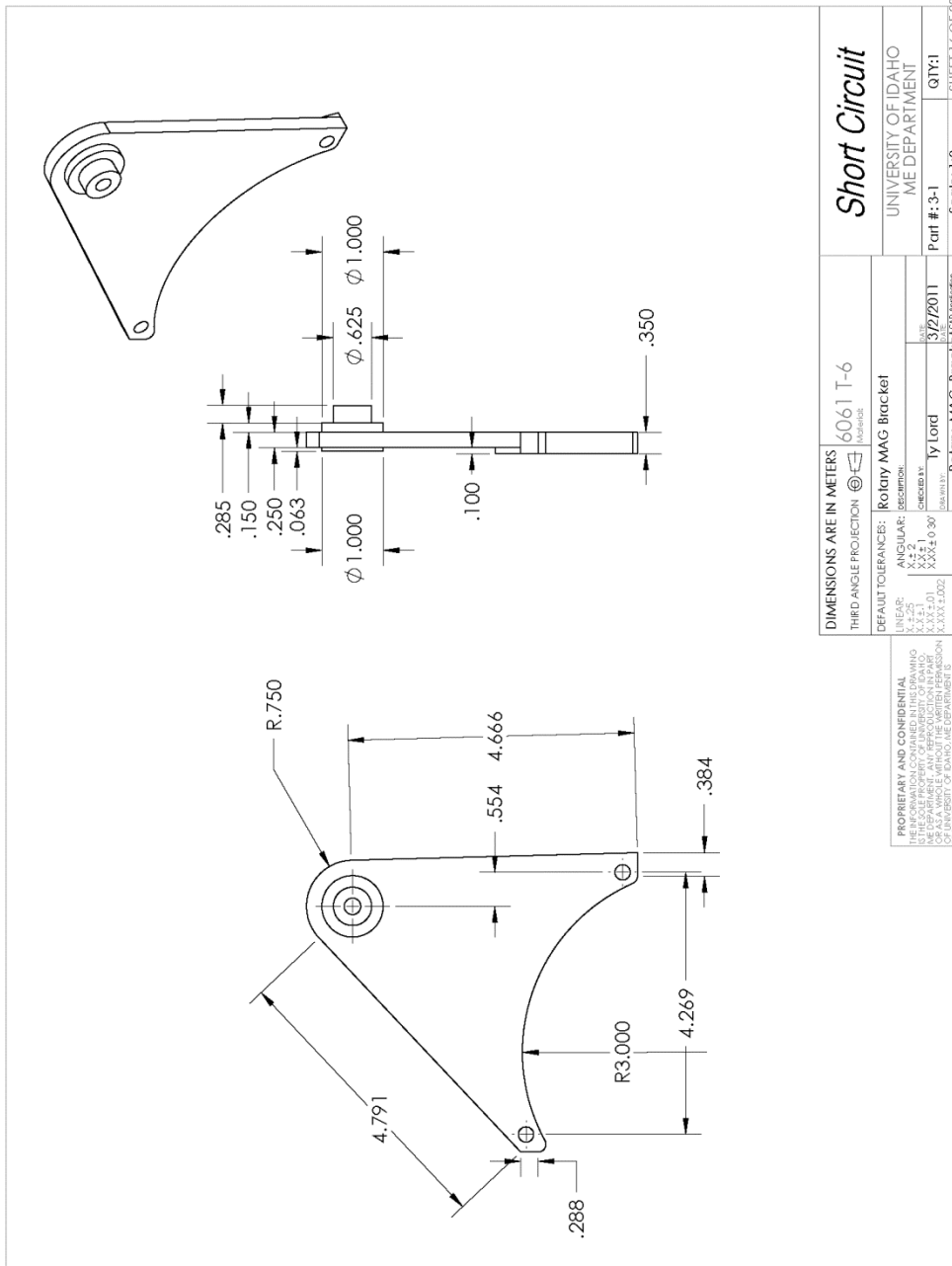
PROPRIETARY AND CONFIDENTIAL
 THE INFORMATION CONTAINED IN THIS DRAWING IS THE SOLE PROPERTY OF UNIVERSITY OF IDAHO. IT IS TO BE USED FOR THE PROJECT AND NOT TO BE REPRODUCED OR TRANSMITTED IN ANY FORM OR BY ANY MEANS, ELECTRONIC OR MECHANICAL, WITHOUT THE WRITTEN PERMISSION OF UNIVERSITY OF IDAHO, THE DEPARTMENT OF MECHANICAL ENGINEERING.



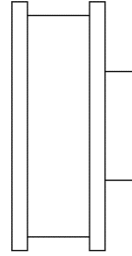
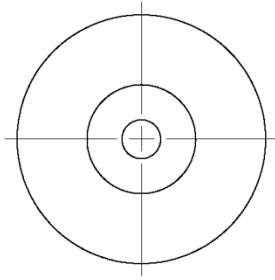
DIMENSIONS ARE IN METERS		316 stainless		Short Circuit	
THIRD ANGLE PROJECTION		Material:		UNIVERSITY OF IDAHO ME DEPARTMENT	
DEFAULT TOLERANCES: Valve counterweight		ANGLAR		Part # : 2-3	
LINEAR: X: ±.25 Y: ±.25 Z: ±.1		ANGULAR: X: ±.1 Y: ±.1 Z: ±.05		QTY: 4	
CREATED BY: [blank]		DATE: 12/16/2010		Scale: 1:2	
DRAWN BY: [blank]		FILE NAME: counterbalance_v8		SHEET 14 OF 23	

PROPRIETARY AND CONFIDENTIAL
 THE INFORMATION CONTAINED IN THIS DRAWING IS THE SOLE PROPERTY OF IDAHO STATE UNIVERSITY. IT IS TO BE USED ONLY FOR THE PROJECT AND AS A WITNESS WITHOUT THE WRITTEN PERMISSION OF IDAHO STATE UNIVERSITY. REPRODUCTION IS PROHIBITED.

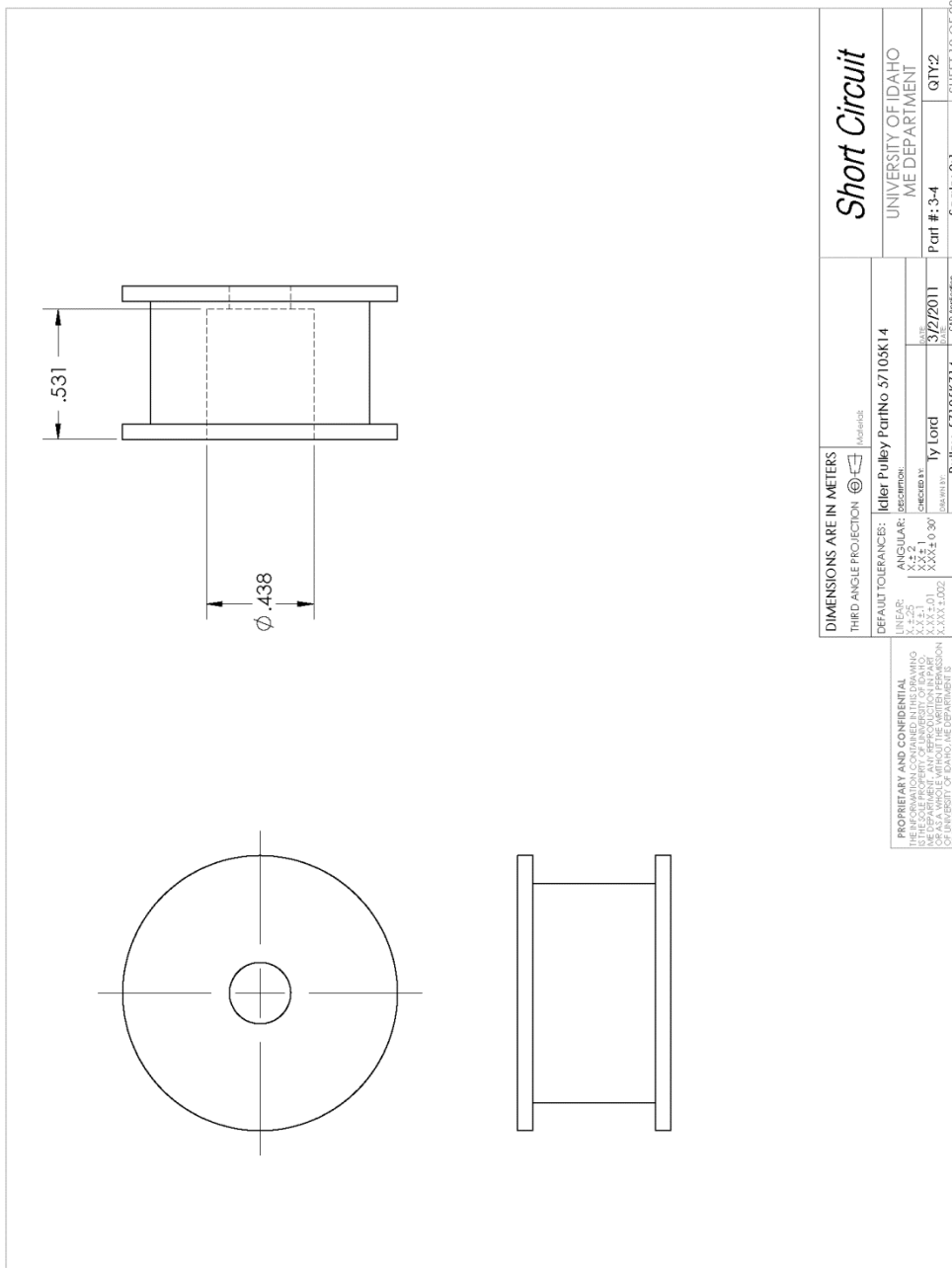




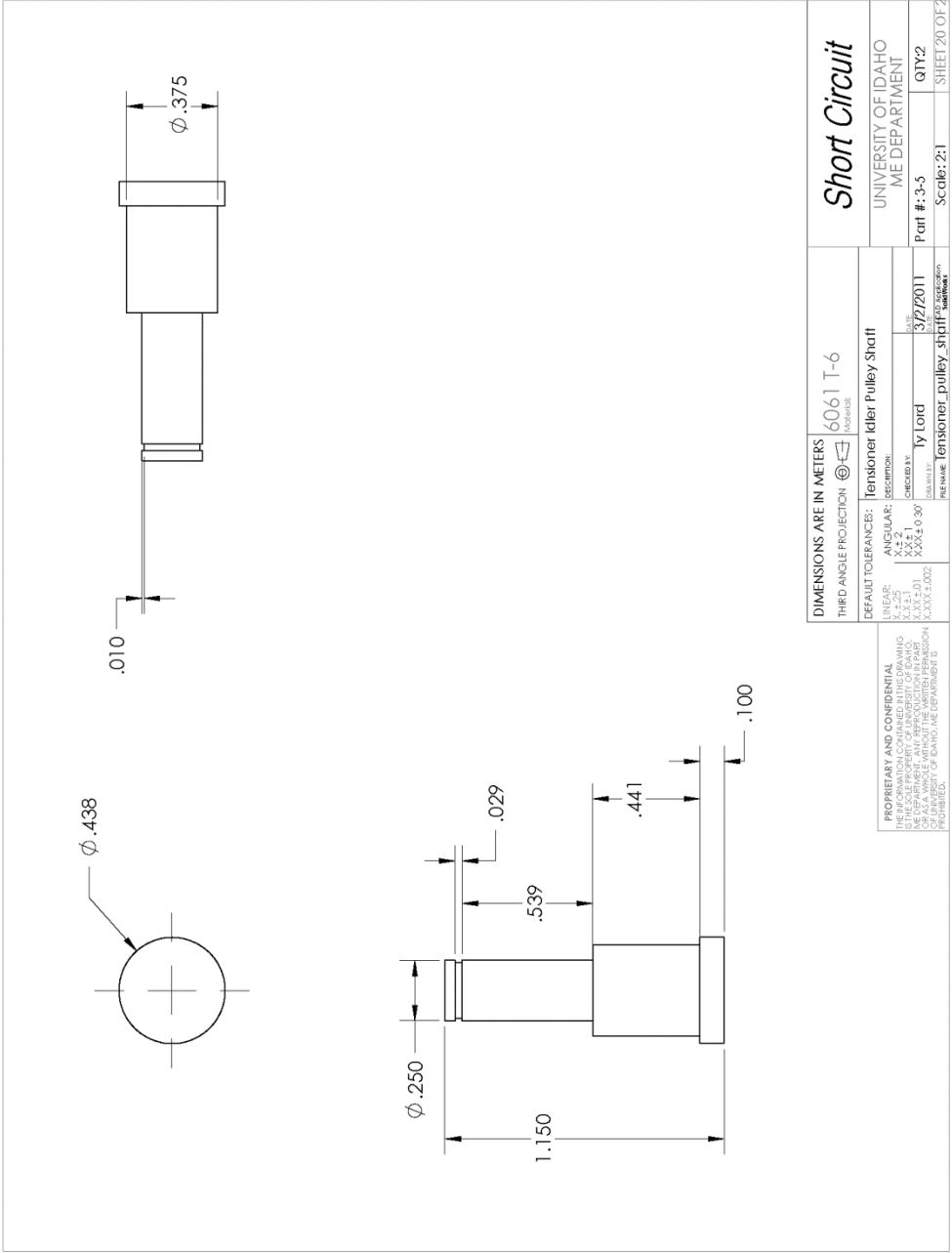
DIMENSIONS ARE IN METERS		6061 T-6	Short Circuit	
THIRD ANGLE PROJECTION		Rotary MAG Bracket	UNIVERSITY OF IDAHO ME DEPARTMENT	
DEFAULT TOLERANCES:		DESIGNED BY: Iy Lord	Part #: 3-1	
LINEAR: X.XX5		CHECKED BY: Iy Lord	Scale: 1:2	
ANGULAR: X.X		DATE: 3/2/2011	QTY: 1	
HOLE: X.XX1		DATE: 3/2/2011	SHEET 16 OF 25	
TAP: X.XX1		DATE: 3/2/2011		
THREAD: X.XXX X.002		DATE: 3/2/2011		
PROPRIETARY AND CONFIDENTIAL		DATE: 3/2/2011		
THE INFORMATION CONTAINED IN THIS DRAWING IS THE SOLE PROPERTY OF UNIVERSITY OF IDAHO AND IS TO BE USED FOR THE DESIGN AND CONSTRUCTION OF A VEHICLE WITHOUT THE WRITTEN PERMISSION OF UNIVERSITY OF IDAHO, ME DEPARTMENT IS PROHIBITED.		DATE: 3/2/2011		

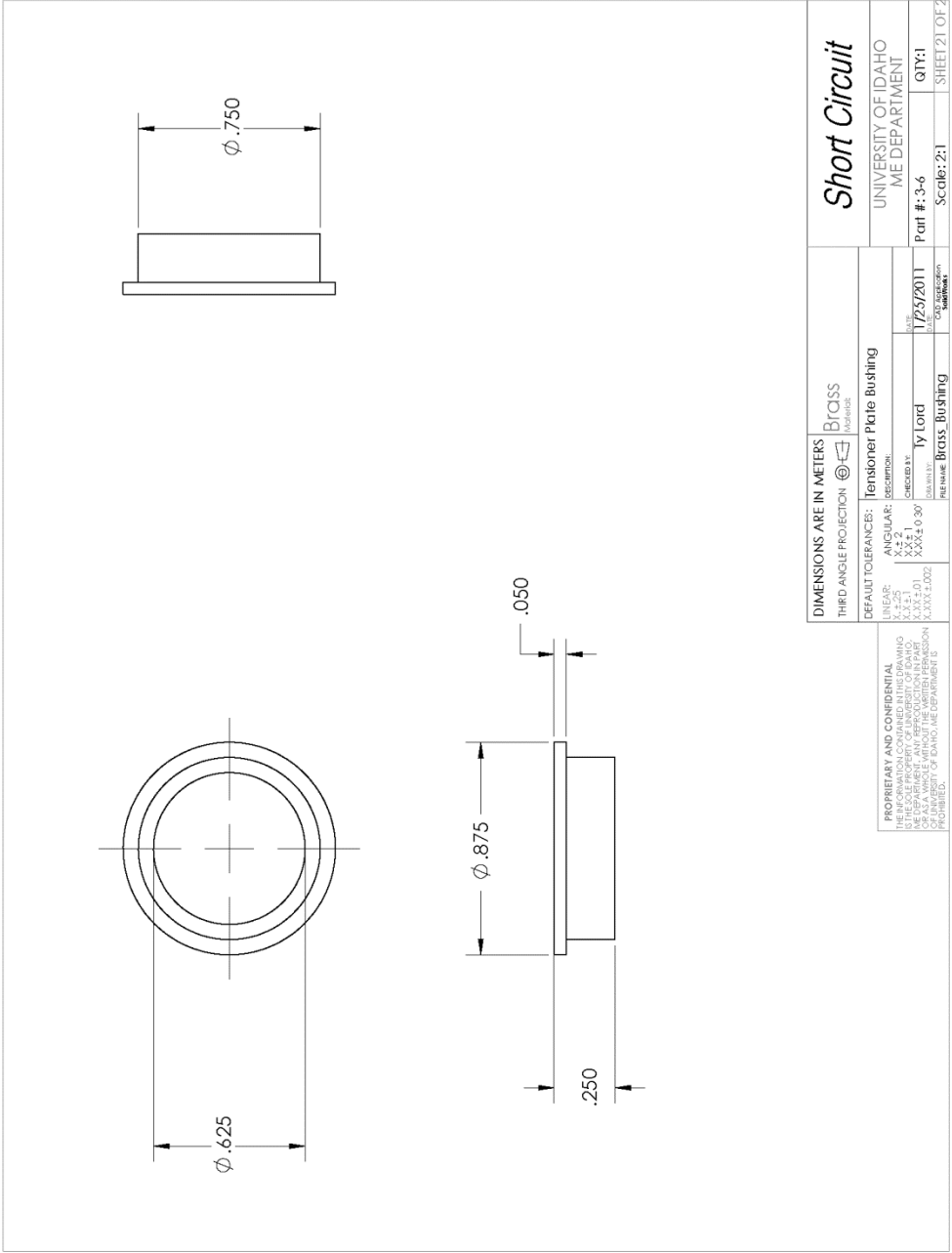


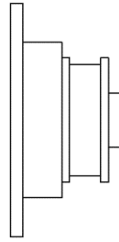
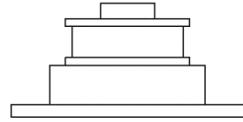
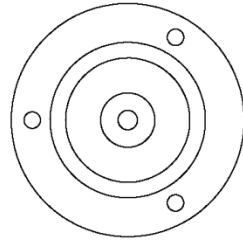
DIMENSIONS ARE IN METERS		THIRD ANGLE PROJECTION		TITLE: Upper Driving Pulley PartNo. 57105K24		Short Circuit			
PROPRIETARY AND CONFIDENTIAL THE INFORMATION CONTAINED IN THIS DRAWING IS THE SOLE PROPERTY OF UNIVERSITY OF IDAHO. IT IS TO BE USED ONLY FOR THE PROJECT AND FOR WHICH IT WAS PREPARED. ANY REUSE OR DISTRIBUTION OF THIS INFORMATION WITHOUT THE WRITTEN PERMISSION OF UNIVERSITY OF IDAHO IS STRICTLY PROHIBITED.		DEFAULT TOLERANCES: LINEAR: X.XX5 ANGULAR: X.X HOLE: X.XX TYPICAL: X.XX		REVISION: 1. X.XX 2. X.XX 3. X.XX 4. X.XX 5. X.XX 6. X.XX 7. X.XX 8. X.XX 9. X.XX 10. X.XX 11. X.XX 12. X.XX 13. X.XX 14. X.XX 15. X.XX 16. X.XX 17. X.XX 18. X.XX 19. X.XX 20. X.XX 21. X.XX 22. X.XX 23. X.XX 24. X.XX 25. X.XX 26. X.XX 27. X.XX 28. X.XX 29. X.XX 30. X.XX 31. X.XX 32. X.XX 33. X.XX 34. X.XX 35. X.XX 36. X.XX 37. X.XX 38. X.XX 39. X.XX 40. X.XX 41. X.XX 42. X.XX 43. X.XX 44. X.XX 45. X.XX 46. X.XX 47. X.XX 48. X.XX 49. X.XX 50. X.XX 51. X.XX 52. X.XX 53. X.XX 54. X.XX 55. X.XX 56. X.XX 57. X.XX 58. X.XX 59. X.XX 60. X.XX 61. X.XX 62. X.XX 63. X.XX 64. X.XX 65. X.XX 66. X.XX 67. X.XX 68. X.XX 69. X.XX 70. X.XX 71. X.XX 72. X.XX 73. X.XX 74. X.XX 75. X.XX 76. X.XX 77. X.XX 78. X.XX 79. X.XX 80. X.XX 81. X.XX 82. X.XX 83. X.XX 84. X.XX 85. X.XX 86. X.XX 87. X.XX 88. X.XX 89. X.XX 90. X.XX 91. X.XX 92. X.XX 93. X.XX 94. X.XX 95. X.XX 96. X.XX 97. X.XX 98. X.XX 99. X.XX 100. X.XX		DRAWN BY: Iy Lord CHECKED BY: Iy Lord DATE: 3/2/2011 PART NAME: Pulley_57105K24 QUANTITY: 1 SCALE: 1:1		UNIVERSITY OF IDAHO ME DEPARTMENT Part #: 3-3 QTY: 1 Scale: 1:1 SHEET 18 OF 23	



<p>DIMENSIONS ARE IN METERS</p> <p>THIRD ANGLE PROJECTION <small>Third Angle</small></p>		<p>Short Circuit</p>	
<p>DEFAULT TOLERANCES: Keller Pulley Part No 57105K14</p>		<p>UNIVERSITY OF IDAHO ME DEPARTMENT</p>	
<p>LINEAR: X.XX5 X.XX2 X.XX1 X.XX0.50</p>	<p>ANGULAR: X.X X.X2 X.X1 X.X0.50</p>	<p>DESIGNED BY: Iy Lord</p>	<p>DATE: 3/2/2011</p>
<p>PROPRIETARY AND CONFIDENTIAL THE INFORMATION CONTAINED IN THIS DRAWING IS THE SOLE PROPERTY OF UNIVERSITY OF IDAHO. IT IS TO BE USED ONLY FOR THE PROJECT AND FOR A SINGLE VEHICLE WITHOUT THE WRITTEN PERMISSION OF UNIVERSITY OF IDAHO. REPRODUCTION IS PROHIBITED.</p>		<p>PART NAME: Pulley_57105K714</p>	<p>SCALE: 2:1</p>
		<p>QUANTITY: 3-4</p>	<p>SHEET 19 OF 25</p>



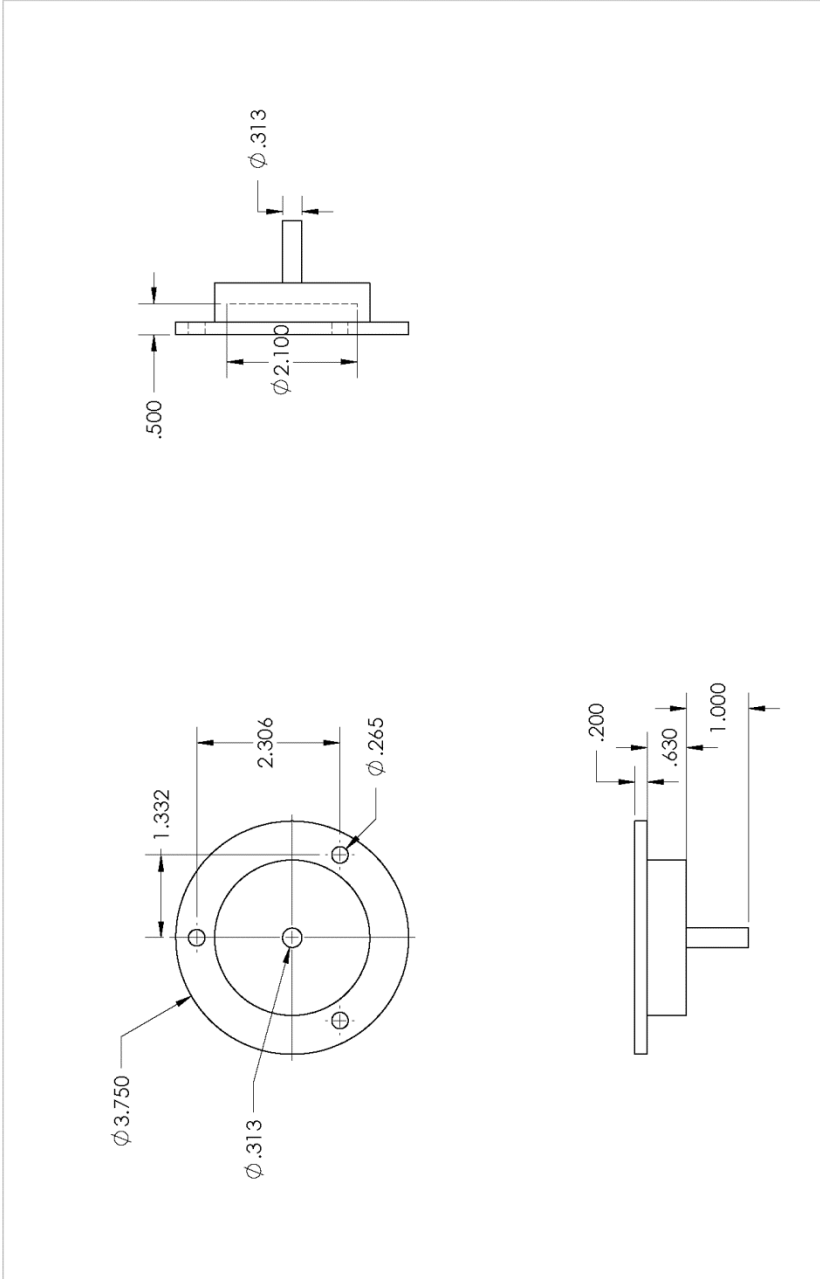




ITEM NO.	PART NUMBER	DESCRIPTION	QTY.
1	Pulley_To_crank_flang e	Pulley to Crank Flange	1
2	Pulley_57105K24	Upper Driving Pulley PartNo 57105K24	1

DIMENSIONS ARE IN METERS THIRD ANGLE PROJECTION		THIRD ANGLE PROJECTION	
DEFAULT TOLERANCES: LINEAR: X.XX ANGULAR: X.X HOLE TO FIT: X.XX		DEFAULT TOLERANCES: LINEAR: X.XX ANGULAR: X.X HOLE TO FIT: X.XX	
CREATED BY: Ty Lord DATE: 1/25/2011 DRAWN BY: Ty Lord DATE: 1/25/2011		PART NAME: Pulley_Assembly SCALE: 1:1	
PROPRIETARY AND CONFIDENTIAL THE INFORMATION CONTAINED IN THIS DRAWING IS THE SOLE PROPERTY OF UNIVERSITY OF IDAHO. IT IS TO BE USED FOR THE PROJECT AND NOT TO BE REPRODUCED OR TRANSMITTED IN ANY FORM OR BY ANY MEANS, ELECTRONIC OR MECHANICAL, WITHOUT THE WRITTEN PERMISSION OF UNIVERSITY OF IDAHO. DEPARTMENT IS PROHIBITED.		UNIVERSITY OF IDAHO ME DEPARTMENT Part #: 4 QTY: 1 Scale: 1:1 SHEET 22 OF 23	

Short Circuit



DIMENSIONS ARE IN METERS		6061 T-6	Short Circuit
THIRD ANGLE PROJECTION	Third Angle		UNIVERSITY OF IDAHO ME DEPARTMENT
DEFAULT TOLERANCES:	Pulley to Crank Frange		
LINEAR:	ANGULAR:		
X.XX	X.X		
X.XXX	X.XX		
X.XXXX	X.XXX		
		DESIGNED BY: Iy Lord	DATE: 1/25/2011
		DRAWN BY: Iy Lord	SCALE: 1:2
		PART NAME: Pulley to crank frange	QTY: 1
			SHEET 23 OF 23

PROPRIETARY AND CONFIDENTIAL
 THE INFORMATION CONTAINED IN THIS DRAWING IS THE SOLE PROPERTY OF UNIVERSITY OF IDAHO. IT IS TO BE USED ONLY FOR THE PROJECT AND FOR A SINGLE WORK WITHOUT THE WRITTEN PERMISSION OF UNIVERSITY OF IDAHO. REPRODUCTION IS PROHIBITED.

APPENDIX B: PR-SCT MODIFICATIONS

APPENDIX C: ERROR PROPAGATION BSFC

Error Propagation in Emissions Measurements

BSFC Calculation

$$\text{BSFC}(\text{fuel}, \text{power}) = \frac{\text{fuel}}{\text{power}}$$

Derivative BSFC w/ respect to fuel used

$$d\text{BSFC}d\text{Fuel}(\text{fuel}, \text{power}) := \frac{d}{d\text{fuel}} \text{BSFC}(\text{fuel}, \text{power}) \rightarrow \frac{1}{\text{power}}$$

Derivative BSFC w/respect to power made

$$d\text{BSFC}d\text{Power}(\text{fuel}, \text{power}) := \frac{d}{d\text{power}} \text{BSFC}(\text{fuel}, \text{power}) \rightarrow -\frac{\text{fuel}}{\text{power}^2}$$

$$\begin{array}{l} \text{fuel} := \begin{pmatrix} 7.937 \\ 11.11 \\ 11.64 \\ 12.96 \\ 10.58 \\ 8.13 \\ 9.78 \\ 11.64 \\ 11.64 \end{pmatrix} \quad \text{power} := \begin{pmatrix} 16.7 \\ 22.9 \\ 25.6 \\ 28.5 \\ 24 \\ 18.5 \\ 19.5 \\ 24.5 \\ 28 \end{pmatrix} \end{array} \quad \text{BSFC}(\text{fuel}, \text{power}) = \begin{pmatrix} 0.475 \\ 0.485 \\ 0.455 \\ 0.455 \\ 0.441 \\ 0.439 \\ 0.502 \\ 0.475 \\ 0.416 \end{pmatrix}$$

$$\begin{array}{l} \xrightarrow{d\text{BSFC}d\text{Fuel}(\text{fuel}, \text{power})} \begin{pmatrix} 0.06 \\ 0.044 \\ 0.039 \\ 0.035 \\ 0.042 \\ 0.054 \\ 0.051 \\ 0.041 \\ 0.036 \end{pmatrix} \quad \xrightarrow{d\text{BSFC}d\text{Power}(\text{fuel}, \text{power})} \begin{pmatrix} -0.028 \\ -0.021 \\ -0.018 \\ -0.016 \\ -0.018 \\ -0.024 \\ -0.026 \\ -0.019 \\ -0.015 \end{pmatrix} \end{array}$$

$e_{\text{fuel}} := .0075$ Error in the Fuel Measurement

$e_{\text{power}} := .02$ Error in the Power Measurement

$$e_{\text{BSFC}} := \sqrt{\left[e_{\text{fuel}} \cdot (\text{dBSFCdFuel}(\text{fuel}, \text{power})) \right]^2 + \left[e_{\text{power}} \cdot (\text{dBSFCdPower}(\text{fuel}, \text{power})) \right]^2}$$

$$e_{\text{BSFC}} = \begin{pmatrix} 7.25 \times 10^{-4} \\ 5.355 \times 10^{-4} \\ 4.605 \times 10^{-4} \\ 4.136 \times 10^{-4} \\ 4.823 \times 10^{-4} \\ 6.246 \times 10^{-4} \\ 6.423 \times 10^{-4} \\ 4.941 \times 10^{-4} \\ 3.999 \times 10^{-4} \end{pmatrix} \quad \%_{\text{error}} := e_{\text{BSFC}} \cdot 100 \quad \max(\%_{\text{error}}) = 0.073$$

APPENDIX D: ERROR PROPAGATION EMISSIONS

Error Propagation in Emissions Measurements

$$\text{BSHC}(\text{fuel}, \text{TC}, \text{power}, \%_{\text{UHC}}) := \frac{\frac{\text{fuel}}{\text{TC}} \cdot \%_{\text{UHC}}}{\text{power}} \quad \text{Brake Specific Hydrocarbon Emissions}$$

$$\text{BSCO}(\text{fuel}, \text{TC}, \text{power}, \%_{\text{CO}}) := \frac{\frac{\text{fuel}}{\text{TC}} \cdot \%_{\text{CO}}}{\text{power}} \quad \text{Brake Specific Carbon Monoxide Emissions}$$

$$\text{BSNO}(\text{fuel}, \text{TC}, \text{power}, \%_{\text{NO}}) := \frac{\frac{\text{fuel}}{\text{TC}} \cdot \%_{\text{NO}}}{\text{power}} \quad \text{Brake Specific Oxides of Nitrogen Emissions}$$

$$d\text{BSHC}d\text{Fuel}(\text{fuel}, \text{TC}, \text{power}, \%_{\text{UHC}}) := \frac{d}{d\text{fuel}} \text{BSHC}(\text{fuel}, \text{TC}, \text{power}, \%_{\text{UHC}}) \rightarrow \frac{\%_{\text{UHC}}}{\text{TC} \cdot \text{power}}$$

$$d\text{BSHC}d\text{TC}(\text{fuel}, \text{TC}, \text{power}, \%_{\text{UHC}}) := \frac{d}{d\text{TC}} \text{BSHC}(\text{fuel}, \text{TC}, \text{power}, \%_{\text{UHC}}) \rightarrow -\frac{\%_{\text{UHC}} \cdot \text{fuel}}{\text{TC}^2 \cdot \text{power}}$$

$$d\text{BSHC}d\%_{\text{UHC}}(\text{fuel}, \text{TC}, \text{power}, \%_{\text{UHC}}) := \frac{d}{d\%_{\text{UHC}}} \text{BSHC}(\text{fuel}, \text{TC}, \text{power}, \%_{\text{UHC}}) \rightarrow \frac{\text{fuel}}{\text{TC} \cdot \text{power}}$$

$$d\text{BSHC}d\text{Power}(\text{fuel}, \text{TC}, \text{power}, \%_{\text{UHC}}) := \frac{d}{d\text{power}} \text{BSHC}(\text{fuel}, \text{TC}, \text{power}, \%_{\text{UHC}}) \rightarrow -\frac{\%_{\text{UHC}} \cdot \text{fuel}}{\text{TC} \cdot \text{power}^2}$$

$$d\text{BSCOdFuel}(\text{fuel}, \text{TC}, \text{power}, \%_{\text{CO}}) := \frac{d}{d\text{fuel}} \text{BSCO}(\text{fuel}, \text{TC}, \text{power}, \%_{\text{CO}}) \rightarrow \frac{\%_{\text{CO}}}{\text{TC} \cdot \text{power}}$$

$$d\text{BSCOdTC}(\text{fuel}, \text{TC}, \text{power}, \%_{\text{CO}}) := \frac{d}{d\text{TC}} \text{BSCO}(\text{fuel}, \text{TC}, \text{power}, \%_{\text{CO}}) \rightarrow -\frac{\%_{\text{CO}} \cdot \text{fuel}}{\text{TC}^2 \cdot \text{power}}$$

$$dBSCOd\%CO(\text{fuel}, TC, \text{power}, \%CO) := \frac{d}{d\%CO} BSCO(\text{fuel}, TC, \text{power}, \%CO) \rightarrow \frac{\text{fuel}}{TC \cdot \text{power}}$$

$$dBSCOdPower(\text{fuel}, TC, \text{power}, \%CO) := \frac{d}{d\text{power}} BSCO(\text{fuel}, TC, \text{power}, \%CO) \rightarrow -\frac{\%CO \cdot \text{fuel}}{TC \cdot \text{power}^2}$$

$$dBSNOdFuel(\text{fuel}, TC, \text{power}, \%NO) := \frac{d}{d\text{fuel}} BSHC(\text{fuel}, TC, \text{power}, \%NO) \rightarrow \frac{\%NO}{TC \cdot \text{power}}$$

$$dBSNOdTC(\text{fuel}, TC, \text{power}, \%NO) := \frac{d}{dTC} BSHC(\text{fuel}, TC, \text{power}, \%NO) \rightarrow -\frac{\%NO \cdot \text{fuel}}{TC^2 \cdot \text{power}}$$

$$dBSNOd\%NO(\text{fuel}, TC, \text{power}, \%NO) := \frac{d}{d\%NO} BSHC(\text{fuel}, TC, \text{power}, \%NO) \rightarrow \frac{\text{fuel}}{TC \cdot \text{power}}$$

$$dBSNOdPower(\text{fuel}, TC, \text{power}, \%NO) := \frac{d}{d\text{power}} BSHC(\text{fuel}, TC, \text{power}, \%NO) \rightarrow -\frac{\%NO \cdot \text{fuel}}{TC \cdot \text{power}^2}$$

$$\text{fuel} := \begin{pmatrix} 3.6 \\ 5.04 \\ 5.28 \\ 4.56 \\ 5.16 \\ 5.88 \\ 4.2 \\ 5.28 \\ 5.28 \end{pmatrix} \quad \text{power} := \begin{pmatrix} 12.67 \\ 17.12 \\ 18.98 \\ 14.91 \\ 19.17 \\ 22.26 \\ 13.67 \\ 19.17 \\ 20.69 \end{pmatrix} \quad \text{TC} := \begin{pmatrix} 7.68 \\ 8.50 \\ 9.56 \\ 8.10 \\ 8.77 \\ 10.13 \\ 7.74 \\ 8.94 \\ 9.55 \end{pmatrix}$$

$$\begin{array}{l}
 \begin{pmatrix} 7800 \\ 9282 \\ 4200 \\ 7236 \\ 8640 \\ 9360 \\ 6582 \\ 6372 \\ 1980 \end{pmatrix} \cdot 10^{-4} \quad \%_{\text{UHC}} := \quad \begin{pmatrix} 389 \\ 684 \\ 604 \\ 532 \\ 399 \\ 244 \\ 387 \\ 594 \\ 620 \end{pmatrix} \cdot 10^{-4} \quad \%_{\text{NO}} := \quad \begin{pmatrix} .79 \\ .55 \\ 1.24 \\ 1.23 \\ 0.93 \\ 1.69 \\ 1.31 \\ 1.10 \\ 1.49 \end{pmatrix} \quad \%_{\text{CO}} := \\
 \\
 \text{mean} \left(\frac{25}{\%_{\text{NO}} \cdot 10^4} \right) = 0.056 \quad \xrightarrow{\text{dBShCdFuel}(\text{fuel, TC, power, \%UHC})} = \begin{pmatrix} 8.016 \times 10^{-3} \\ 6.379 \times 10^{-3} \\ 2.315 \times 10^{-3} \\ 5.992 \times 10^{-3} \\ 5.139 \times 10^{-3} \\ 4.151 \times 10^{-3} \\ 6.221 \times 10^{-3} \\ 3.718 \times 10^{-3} \\ 1.002 \times 10^{-3} \end{pmatrix} \\
 \\
 \xrightarrow{\text{dBSCOdFuel}(\text{fuel, TC, power, \%CO})} = \begin{pmatrix} 8.119 \times 10^{-3} \\ 3.78 \times 10^{-3} \\ 6.834 \times 10^{-3} \\ 0.01 \\ 5.532 \times 10^{-3} \\ 7.495 \times 10^{-3} \\ 0.012 \\ 6.418 \times 10^{-3} \\ 7.541 \times 10^{-3} \end{pmatrix} \quad \xrightarrow{\text{dBSNOdFuel}(\text{fuel, TC, power, \%NO})} = \begin{pmatrix} 3.998 \times 10^{-4} \\ 4.7 \times 10^{-4} \\ 3.329 \times 10^{-4} \\ 4.405 \times 10^{-4} \\ 2.373 \times 10^{-4} \\ 1.082 \times 10^{-4} \\ 3.658 \times 10^{-4} \\ 3.466 \times 10^{-4} \\ 3.138 \times 10^{-4} \end{pmatrix}
 \end{array}$$

$$\begin{array}{c}
 \overrightarrow{\text{dBShCd}\%_{\text{UHC}}(\text{fuel, TC, power, \%}_{\text{UHC}})} = \begin{pmatrix} 0.037 \\ 0.035 \\ 0.029 \\ 0.038 \\ 0.031 \\ 0.026 \\ 0.04 \\ 0.031 \\ 0.027 \end{pmatrix} \\
 \\
 \overrightarrow{\text{dBShCdPower}}(\text{fuel, TC, power, \%}_{\text{UHC}}) = \begin{pmatrix} -2.278 \times 10^{-3} \\ -1.878 \times 10^{-3} \\ -6.439 \times 10^{-4} \\ -1.832 \times 10^{-3} \\ -1.383 \times 10^{-3} \\ -1.096 \times 10^{-3} \\ -1.911 \times 10^{-3} \\ -1.024 \times 10^{-3} \\ -2.557 \times 10^{-4} \end{pmatrix} \\
 \\
 \overrightarrow{\text{dBShCd}\%_{\text{CO}}(\text{fuel, TC, power, \%}_{\text{CO}})} = \begin{pmatrix} 0.037 \\ 0.035 \\ 0.029 \\ 0.038 \\ 0.031 \\ 0.026 \\ 0.04 \\ 0.031 \\ 0.027 \end{pmatrix} \\
 \\
 \overrightarrow{\text{dBShCd}\%_{\text{NO}}(\text{fuel, TC, power, \%}_{\text{NO}})} = \begin{pmatrix} 0.037 \\ 0.035 \\ 0.029 \\ 0.038 \\ 0.031 \\ 0.026 \\ 0.04 \\ 0.031 \\ 0.027 \end{pmatrix} \\
 \\
 \overrightarrow{\text{dBShCdPower}}(\text{fuel, TC, power, \%}_{\text{CO}}) = \begin{pmatrix} -2.307 \times 10^{-3} \\ -1.113 \times 10^{-3} \\ -1.901 \times 10^{-3} \\ -3.115 \times 10^{-3} \\ -1.489 \times 10^{-3} \\ -1.98 \times 10^{-3} \\ -3.804 \times 10^{-3} \\ -1.768 \times 10^{-3} \\ -1.924 \times 10^{-3} \end{pmatrix}
 \end{array}$$

$$\begin{aligned}
 \overrightarrow{dBSNOdPower(\text{fuel}, TC, \text{power}, \%NO)} &= \begin{pmatrix} -1.136 \times 10^{-4} \\ -1.384 \times 10^{-4} \\ -9.26 \times 10^{-5} \\ -1.347 \times 10^{-4} \\ -6.388 \times 10^{-5} \\ -2.858 \times 10^{-5} \\ -1.124 \times 10^{-4} \\ -9.546 \times 10^{-5} \\ -8.008 \times 10^{-5} \end{pmatrix} \\
 \overrightarrow{dBSHCdTC(\text{fuel}, TC, \text{power}, \%UHC)} &= \begin{pmatrix} -3.757 \times 10^{-3} \\ -3.782 \times 10^{-3} \\ -1.278 \times 10^{-3} \\ -3.373 \times 10^{-3} \\ -3.024 \times 10^{-3} \\ -2.409 \times 10^{-3} \\ -3.376 \times 10^{-3} \\ -2.196 \times 10^{-3} \\ -5.54 \times 10^{-4} \end{pmatrix} \\
 \overrightarrow{dBSNOdTC(\text{fuel}, TC, \text{power}, \%NO)} &= \begin{pmatrix} -1.874 \times 10^{-4} \\ -2.787 \times 10^{-4} \\ -1.838 \times 10^{-4} \\ -2.48 \times 10^{-4} \\ -1.396 \times 10^{-4} \\ -6.281 \times 10^{-5} \\ -1.985 \times 10^{-4} \\ -2.047 \times 10^{-4} \\ -1.735 \times 10^{-4} \end{pmatrix} \\
 \overrightarrow{dBSCdTC(\text{fuel}, TC, \text{power}, \%CO)} &= \begin{pmatrix} -3.806 \times 10^{-3} \\ -2.241 \times 10^{-3} \\ -3.774 \times 10^{-3} \\ -5.734 \times 10^{-3} \\ -3.255 \times 10^{-3} \\ -4.35 \times 10^{-3} \\ -6.718 \times 10^{-3} \\ -3.791 \times 10^{-3} \\ -4.169 \times 10^{-3} \end{pmatrix} \\
 e_{\%CO_2} &:= .05 & e_{\%CO} &:= .03 \\
 e_{\text{fuel}} &:= .0075 & e_{\%UHC} &:= .05 \\
 e_{\text{power}} &:= .02 & e_{\%NO} &:= .056 \\
 e_{TC} &:= \sqrt{e_{\%CO}^2 + e_{\%CO_2}^2 + e_{\%UHC}^2} \\
 e_{TC} &= 0.077
 \end{aligned}$$

$$e_{\text{BSHC}} := \sqrt{\begin{matrix} \left[e_{\text{TC}} \cdot (\text{dBSHCdTC}(\text{fuel}, \text{TC}, \text{power}, \% \text{UHC})) \right]^2 \dots \\ + \left[e_{\text{fuel}} \cdot (\text{dBSHCdFuel}(\text{fuel}, \text{TC}, \text{power}, \% \text{UHC})) \right]^2 \dots \\ + \left[e_{\text{power}} \cdot (\text{dBSHCdPower}(\text{fuel}, \text{TC}, \text{power}, \% \text{UHC})) \right]^2 \dots \\ + \left[e_{\% \text{UHC}} \cdot (\text{dBSHCd}\% \text{UHC}(\text{fuel}, \text{TC}, \text{power}, \% \text{UHC})) \right]^2 \end{matrix}}$$

$$e_{\text{BSHC}} = \begin{pmatrix} 1.874 \times 10^{-3} \\ 1.757 \times 10^{-3} \\ 1.458 \times 10^{-3} \\ 1.906 \times 10^{-3} \\ 1.553 \times 10^{-3} \\ 1.317 \times 10^{-3} \\ 2.003 \times 10^{-3} \\ 1.55 \times 10^{-3} \\ 1.337 \times 10^{-3} \end{pmatrix}$$

$$\% \text{error}_{\text{BSHC}} := \text{mean}(e_{\text{BSHC}}) \cdot 100$$

$$\% \text{error}_{\text{BSHC}} = 0.164$$

$$e_{\text{BSCO}} := \sqrt{\begin{matrix} \left[e_{\text{TC}} \cdot (\text{dBSCOdTC}(\text{fuel}, \text{TC}, \text{power}, \% \text{CO})) \right]^2 \dots \\ + \left[e_{\text{fuel}} \cdot (\text{dBSCOdFuel}(\text{fuel}, \text{TC}, \text{power}, \% \text{CO})) \right]^2 \dots \\ + \left[e_{\text{power}} \cdot (\text{dBSCOdPower}(\text{fuel}, \text{TC}, \text{power}, \% \text{CO})) \right]^2 \dots \\ + \left[e_{\% \text{CO}} \cdot (\text{dBSCOd}\% \text{CO}(\text{fuel}, \text{TC}, \text{power}, \% \text{CO})) \right]^2 \end{matrix}}$$

$$e_{\text{BSCO}} = \begin{pmatrix} 1.15 \times 10^{-3} \\ 1.054 \times 10^{-3} \\ 9.221 \times 10^{-4} \\ 1.219 \times 10^{-3} \\ 9.555 \times 10^{-4} \\ 8.534 \times 10^{-4} \\ 1.303 \times 10^{-3} \\ 9.709 \times 10^{-4} \\ 8.66 \times 10^{-4} \end{pmatrix}$$

$$\% \text{error}_{\text{BSCO}} := \text{mean}(e_{\text{BSCO}}) \cdot 100$$

$$\% \text{error}_{\text{BSCO}} = 0.103$$

$$e_{\text{BSNO}} := \sqrt{\begin{matrix} \left[e_{\text{TC}} \cdot (\text{dBSNOdTC}(\text{fuel}, \text{TC}, \text{power}, \% \text{NO})) \right]^2 \dots \\ + \left[e_{\text{fuel}} \cdot (\text{dBSNOdFuel}(\text{fuel}, \text{TC}, \text{power}, \% \text{NO})) \right]^2 \dots \\ + \left[e_{\text{power}} \cdot (\text{dBSNOdPower}(\text{fuel}, \text{TC}, \text{power}, \% \text{NO})) \right]^2 \dots \\ + \left[e_{\% \text{NO}} \cdot (\text{dBSNOd}\% \text{NO}(\text{fuel}, \text{TC}, \text{power}, \% \text{NO})) \right]^2 \end{matrix}}$$

$$e_{\text{BSNO}} = \begin{pmatrix} 2.072 \times 10^{-3} \\ 1.94 \times 10^{-3} \\ 1.63 \times 10^{-3} \\ 2.115 \times 10^{-3} \\ 1.719 \times 10^{-3} \\ 1.46 \times 10^{-3} \\ 2.223 \times 10^{-3} \\ 1.725 \times 10^{-3} \\ 1.496 \times 10^{-3} \end{pmatrix}$$

$$\% \text{error}_{\text{BSNO}} := \text{mean}(e_{\text{BSNO}}) \cdot 100$$

$$\% \text{error}_{\text{BSNO}} = 0.182$$